

**ATOM INTERFEROMETRIC GRAVITY GRADIOMETER:
DISTURBANCE COMPENSATION AND MOBILE
GRADIOMETRY**

**A DISSERTATION
SUBMITTED TO THE DEPARTMENT OF MECHANICAL
ENGINEERING
AND THE COMMITTEE ON GRADUATE STUDIES
OF STANFORD UNIVERSITY
IN PARTIAL FULFILLMENT OF THE REQUIREMENTS
FOR THE DEGREE OF
DOCTOR OF PHILOSOPHY**

Chetan Mahadeswaraswamy

May 2009

UMI Number: 3364141

Copyright 2009 by
Mahadeswaraswamy, Chetan

INFORMATION TO USERS

The quality of this reproduction is dependent upon the quality of the copy submitted. Broken or indistinct print, colored or poor quality illustrations and photographs, print bleed-through, substandard margins, and improper alignment can adversely affect reproduction.

In the unlikely event that the author did not send a complete manuscript and there are missing pages, these will be noted. Also, if unauthorized copyright material had to be removed, a note will indicate the deletion.



UMI Microform 3364141
Copyright 2009 by ProQuest LLC
All rights reserved. This microform edition is protected against
unauthorized copying under Title 17, United States Code.

ProQuest LLC
789 East Eisenhower Parkway
P.O. Box 1346
Ann Arbor, MI 48106-1346

© Copyright by Chetan Mahadeswaraswamy 2009
All Rights Reserved

I certify that I have read this dissertation and that, in my opinion, it is fully adequate in scope and quality as a dissertation for the degree of Doctor of Philosophy.



(Mark Kasevich) Principal Advisor

I certify that I have read this dissertation and that, in my opinion, it is fully adequate in scope and quality as a dissertation for the degree of Doctor of Philosophy.



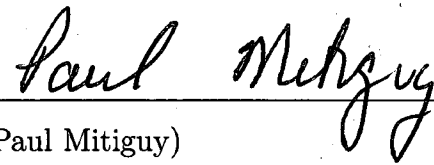
(Daniel DeBra)

I certify that I have read this dissertation and that, in my opinion, it is fully adequate in scope and quality as a dissertation for the degree of Doctor of Philosophy.



(David Beach)

I certify that I have read this dissertation and that, in my opinion, it is fully adequate in scope and quality as a dissertation for the degree of Doctor of Philosophy.



(Paul Mitiguy)

Approved for the University Committee on Graduate Studies.



To Mother and Father.

Abstract

First ever mobile gravity gradient measurement based on Atom Interferometric sensors has been demonstrated. Mobile gravity gradiometers play a significant role in high accuracy inertial navigation systems in order to distinguish inertial acceleration and acceleration due to gravity.

The gravity gradiometer consists of two atom interferometric accelerometers. In each of the accelerometer an ensemble of laser cooled Cesium atoms is dropped and using counter propagating Raman pulses ($\pi/2-\pi-\pi/2$) the ensemble is split into two states for carrying out atom interferometry. The interferometer phase is proportional to the specific force experienced by the atoms which is a combination of inertial acceleration and acceleration due to gravity.

The difference in phase between the two atom interferometric sensors is proportional to gravity gradient if the platform does not undergo any rotational motion. However, any rotational motion of the platform induces spurious gravity gradient measurements. This apparent gravity gradient due to platform rotation is considerably different for an atom interferometric sensor compared to a conventional force rebalance type sensor. The atoms are in free fall and are not influenced by the motion of the case except at the instants of Raman pulses. A model for determining apparent gravity gradient due to rotation of platform was developed and experimentally verified for different frequencies. This transfer function measurement also lead to the development of a new technique for aligning the Raman laser beams with the atom clusters to within 20 μ rad.

This gravity gradiometer is situated in a truck for the purpose of undertaking mobile surveys. A disturbance compensation system was designed and built in order

to compensate for the rotational disturbances experienced on the floor of a truck. An electric drive system was also designed specifically to be able to move the truck in a uniform motion at very low speeds of about 1cm/s. A $250 \times 10^{-9} s^{-2}$ gravity gradient signature due to an underground void at Hansen Experimental Physics Building at Stanford was successfully measured using this mobile gradiometer.

Acknowledgement

I am very grateful to my advisors Mark Kasevich and Daniel DeBra for their guidance and support throughout my thesis work. I am very thankful to both my advisors for providing this unique opportunity for a mechanical engineer to pursue research in an experimental physics group. It has been a great learning experience to pursue research in this inter-disciplinary environment through interactions with both physicists and engineers. I am thankful to Louis Deslauriers (postdoctoral researcher) for the very many discussion sessions on atom interferometry. A big thanks to fellow graduate students Xianan Wu and Sean Roy who provided assistance with the experimental setup and measurement.

I am also thankful to former graduate students and postdoctoral researchers Grant Biedermann, Ken Takase, Todd Kawakami, Jeff Fixler and Todd Gustavson for their help and valuable advice. I am also thankful to Paul Mitiguy for providing valuable suggestions on setting up of the equations of motion. I am grateful to Larry Novak and Dale Gill who provided valuable inputs during the design of the electric drive. Larry Novak was of tremendous help during the entire process of installation and testing of the electric drive and has helped us all with almost every part of this research project. I also appreciate the work that has been put into this project by former students Alwin Anbu, Apratim Dixit, Pankaj Sunkari and Matt Norcia.

I would also like to thank all my teachers from my school Kendriya Vidyalaya, CLRI (Chennai, India), Indian Institute of Technology - Madras (India) and Stanford University for cultivating scientific temper. Finally, none of this could have been achieved without the constant support and encouragement of my family and friends all through these years. A big thanks to my mother, father and sister.

Contents

Abstract	v
Acknowledgement	vii
1 Introduction	1
1.1 Gravity Gradient	1
1.2 Accelerometers	4
1.3 Applications	6
1.4 History of Gravity Gradiometry	7
1.5 Atom Interferometric Accelerometers	9
2 Overview	14
3 Atom Interferometric Accelerometer	17
3.1 Atom Interferometry	17
3.2 AI Acceleration Measurements	20
3.2.1 Measurement of acceleration due to gravity	20
3.2.2 Measurement of inertial accelerations	21
3.2.3 Presence of acceleration due to gravity and inertial acceleration	22
4 Atom Interferometric Gravity Gradiometer	23
4.1 Effect of platform motion	24
4.2 Modeling a Gravity Gradiometer	25
4.2.1 Yaw rotation	31

4.2.2	Sinusoidal Platform Motion	32
4.2.3	Comparison of atom interferometric and conventional gradiometers	33
5	Platform Actuation and Disturbance Compensation	39
5.1	Requirements	39
5.2	Design Development	46
5.2.1	Pitch and Roll motion	47
5.2.2	Yaw Motion	48
5.2.3	Gradiometer Platform	48
5.2.4	Actuation	49
5.2.5	Sensor	49
5.3	Control System	50
5.3.1	Controller	51
5.3.2	Control loop	51
5.4	Alternate Passive Isolation concept	51
6	Transfer function estimation & measurement	56
6.1	Expected Transfer Function	56
6.2	Coarse alignment by blasting atom cloud	59
6.2.1	Blasting of atom cloud	59
6.2.2	Alignment	60
6.3	Experimental Measurement Setup	61
6.3.1	Fixing atom drop phase	61
6.3.2	Measurement Setup	62
6.3.3	Synchronization	63
6.4	Insufficient alignment of Raman beam with atoms	64
6.5	Results	70
6.6	Contrast reduction	70
7	Vehicle Motion Control	74
7.1	Requirements	74

7.2	Various Design Concepts	75
7.3	Design	77
7.4	Installation	78
7.5	Positioning using differential GPS	81
8	Mobile Gravity Gradient Measurement	84
8.1	Survey Area	84
8.2	Survey Vehicle Motion and Position	86
8.3	Platform stabilization	88
8.4	Data Acquisition and synchronization	89
8.5	Static Survey	92
8.6	Mobile Survey	94
8.6.1	Sign Ambiguity	94
8.6.2	Sources of Error	97
9	Conclusion	99
A	List of Symbols	101
B	Platform actuation parameters for pitch and roll	102
C	Expressions	103
C.1	Approximate Phase Calculation	103
C.2	Gravity Gradient calculation	103
D	Disturbance Levels on Truck Floor	104
E	Control system	107
	Bibliography	113

List of Tables

A.1 List of symbols	101
B.1 Pitch actuation parameters	102

List of Figures

1.1	East-North-Up reference system for earth	3
1.2	Conventional Accelerometer	6
3.1	Schematic of Atom Interferometer	19
4.1	Schematic of Atom Interferometric Gravity Gradiometer	23
4.2	Inertial and Earth co-ordinate system	26
4.3	Platform co-ordinate system	27
4.4	The platform co-ordinate system rotated about earth's \hat{e}_z axis.	32
4.5	Simulated transfer function for a perfectly aligned gravity gradiometer	34
4.6	Light phase and propagation/separation phase of atom interferometer at various platform disturbance frequencies and phases	35
4.7	Simulated apparent gravity gradient measured by atom interferometric gravity gradiometer for a constant amplitude of angular velocity . . .	36
4.8	Simulated apparent gravity gradient measured by conventional force rebalance type gravity gradiometer for a constant amplitude of angular velocity	37
5.1	Pitch, Roll and Yaw disturbance levels on stationary truck	41
5.2	Pitch, Roll and Yaw disturbance levels on moving truck	42
5.3	Photograph of Gimbal inside the truck	47
5.4	Actuation of Pitch and Roll Motion of platform	48
5.5	Stepper Motor Actuation	50
5.6	Fiber Optic Gyro - Lytton LN250	50

5.7	Schematic of platform stabilization control system	52
5.8	Gradiometer Platform Actuation	53
5.9	Alternative Passive isolation	55
6.1	Definition of disturbance phase	57
6.2	Raman Beam Path	58
6.3	'Blasting' of the atom cloud	59
6.4	Raman Beam Path	60
6.5	Disturbance phase control	63
6.6	Data Acquisition and Synchronization	64
6.7	Response of the Gravity Gradiometer for 6 Hz platform oscillation	65
6.8	Schematic of misalignment of Raman beam with the atom clouds	66
6.9	Measuring misalignment of Raman beam with atom clouds	67
6.10	Simulated gradiometer phase at various angles of misalignment	68
6.11	Transfer function for a misaligned Gravity Gradiometer	69
6.12	Apparent gravity gradient measured by oscillating the platform at 6 Hz	71
6.13	Apparent gravity gradient measured by oscillating the platform at 12 Hz	72
6.14	Change in ellipticity due to change in phase	73
7.1	Electric Drive System	78
7.2	Installation of electric drive system	79
7.3	Split sprocket on the drive shaft	80
7.4	Custom made fixtures for holding the electric drive system	80
7.5	Electric drive system assembled on base plate	81
7.6	Electric drive after installation of all the components	81
7.7	Differential GPS system	82
7.8	Schematic of Truck electric drive and position measurement	83
8.1	Survey Area for mobile gravity gradient measurement	85
8.2	Inline Gravity Gradient T_{yy}	86
8.3	Drift of platform pitch, roll and yaw angles in 84 ms	90
8.4	Data Synchronization for mobile gradient measurement	91

8.5	Gravity Gradient measured by static surveys	93
8.6	Mobile measurement of gravity gradient	95
8.7	Gravity Gradient at the entrance of Hansen Experimental Physics Laboratory	96
8.8	Ellipse generated by plotting sinusoids with phase differences of (a) $\pi/4$ (b) $7\pi/4$	98
D.1	Truck Speed 0.4mph electric drive: Pitch, Roll and Yaw disturbance .	104
D.2	Truck Speed 1.5mph Engine Drive: Pitch, Roll and Yaw disturbance .	105
D.3	Truck Speed 1.5mph Electric Drive: Pitch, Roll and Yaw disturbance	106
E.1	Control system program implemented in xPCTarget TM for platform control	108
E.2	Control subsystem implemented in xPCTarget TM for platform control	109
E.3	Control system program implemented in xPCTarget TM for truck control	110
E.4	Control subsystems implemented in xPCTarget TM for truck control .	111
E.5	Timing truck motion implemented in xPCTarget TM using a stateflow chart	112

Chapter 1

Introduction

Gravity gradient is a spatial measure of rate of change of acceleration due to gravity at any point with displacement. Gravity gradient measurement is typically achieved by finding the difference in components of gravitational accelerations experienced by two proof masses separated by a small distance. This chapter will discuss in detail about the various methods that have been adopted to measure gravity gradient in the past and also the applications of gravity gradient.

1.1 Gravity Gradient

Gravitational potential field is a conservative field given by:

$$\phi(\mathbf{r}) = -G \int \frac{\rho(\mathbf{r}')}{|\mathbf{r} - \mathbf{r}'|} dV \quad (1.1)$$

where G is the gravitational constant and ρ is the mass density. The time dependence is small and neglected.

Acceleration due to gravity denoted by vector \mathbf{g} is given by:

$$\mathbf{g} = \nabla\phi(\mathbf{r}) \quad (1.2)$$

In many cases the vector is written out in a matrix form without indicating the

unit vectors:

$$\mathbf{g} = \begin{bmatrix} \frac{\delta\phi}{\delta x} \\ \frac{\delta\phi}{\delta y} \\ \frac{\delta\phi}{\delta z} \end{bmatrix} \quad (1.3)$$

Gravity gradient is the derivative of acceleration due to gravity with respect to position. Gravity gradient is a tensor and is commonly denoted by a 3x3 matrix of the form:

$$\nabla \mathbf{g} = \begin{bmatrix} \frac{\delta^2\phi}{\delta x^2} & \frac{\delta^2\phi}{\delta x\delta y} & \frac{\delta^2\phi}{\delta x\delta z} \\ \frac{\delta^2\phi}{\delta y\delta x} & \frac{\delta^2\phi}{\delta y^2} & \frac{\delta^2\phi}{\delta y\delta z} \\ \frac{\delta^2\phi}{\delta z\delta x} & \frac{\delta^2\phi}{\delta z\delta y} & \frac{\delta^2\phi}{\delta z^2} \end{bmatrix} \quad (1.4)$$

The components of the gravity gradient tensor are represented as:

$$\Gamma = \begin{bmatrix} T_{xx} & T_{xy} & T_{xz} \\ T_{yz} & T_{yy} & T_{yz} \\ T_{zx} & T_{zy} & T_{zz} \end{bmatrix} \quad (1.5)$$

Since gravitational field is conservative:

$$\nabla \times \mathbf{g} = 0 \quad (1.6)$$

This implies $T_{xy} = T_{yx}$, $T_{xz} = T_{zx}$, $T_{yz} = T_{zy}$

Also, since the Laplace's equation requires that at a source free point $\nabla^2\phi = \rho = 0$:

$$\nabla \cdot \mathbf{g} = 0 \quad (1.7)$$

Hence the trace of the gravity gradient vanishes, $T_{xx} + T_{yy} + T_{zz} = 0$.

Now there are only 5 independent components for a gravity gradient matrix. Hence

by default the gravity gradient tensor matrix is written as a symmetric matrix:

$$\Gamma = \begin{bmatrix} T_{xx} & T_{xy} & T_{xz} \\ T_{xy} & T_{yy} & T_{yz} \\ T_{xz} & T_{yz} & T_{zz} \end{bmatrix} \quad (1.8)$$

On the surface of the earth the inline gravity gradient in vertical direction (T_{zz}) is about 3000 E and inline horizontal gradient ($T_{xx} = T_{yy}$) is about 1500 E (Refer to Figure 1.1 for the East-North-Up reference system used on surface of the earth). The gradient varies from place to place depending on the density of material underground.

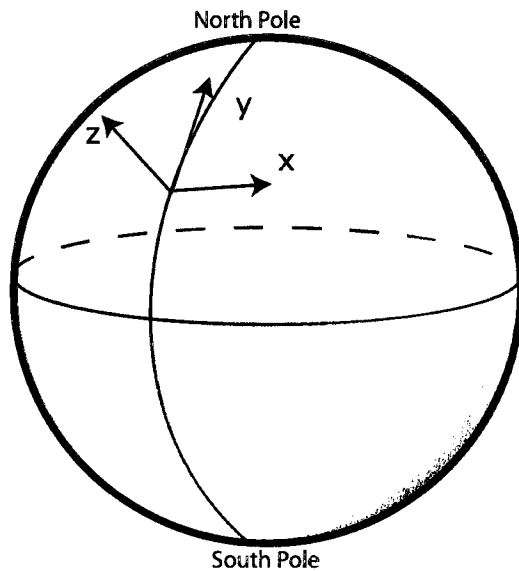


Figure 1.1: East-North-Up reference system for earth

Measurement of Gravity Gradient has been gaining importance over the years mainly for locating gravity anomalies to detect voids or mineral sources and for inertial navigation. The density of the earth is not homogeneous. It varies from one place to another due to variation of the shape of the surface and/or variation of density of the materials under the surface. A large void under the surface of the earth causes a reduction in the gravitational attraction to a body directly above the void whereas presence of very dense material under the surface causes an increase in the

gravitational attraction.

Inertial navigation systems can improve their accuracy by making use of gravity measurements. Inertial navigation systems make use of very precise accelerometers and gyroscopes to deduce the inertial acceleration and angular velocities of the vehicle. In order to deduce the inertial acceleration, one has to subtract the acceleration due to gravity from the specific force measured by the accelerometer. Currently the bottleneck in this process is the accuracy of measurement of acceleration due to gravity. A more precise measurement of acceleration due to gravity will improve the accuracy of the inertial navigation systems. Due to the equivalence principle it is not possible to measure the acceleration due to gravity and the inertial acceleration simultaneously. However it is possible to estimate the acceleration due to gravity from measurements of specific force by making use of more than one accelerometer.

1.2 Accelerometers

The most important part of the gradiometer is the accelerometer. Accelerometers measure specific forces which is a sum of inertial accelerations and acceleration due to gravity. Even though in most cases only either inertial acceleration or the acceleration due to gravity is required to be measured, it is not possible to distinguish inertial acceleration and acceleration due to gravity using the measurement of a single accelerometer.

Typically an accelerometer has a proof mass connected to a case through a spring or a feedback forcing. Any acceleration of the case with respect to the inertial frame causes the inertial mass to move with respect to the case or one can measure the force required to prevent this. The relative motion of the proof mass with respect to the case or the force to prevent it is measured and the inertial acceleration / acceleration due to gravity experienced by the case is interpreted using this measurement. It is important to note that accelerometers can not violate the Equivalence Principle and hence can not distinguish inertial acceleration and gravitational acceleration. Hence accelerometers can measure only specific forces.

Consider the accelerometer shown in the figure 1.2. Assume that the accelerometer

can move only in the n_x direction. x is extension of the spring from its natural length due to the motion of the proof mass with respect to the case.

$$m \frac{^N d}{dt^2} \mathbf{r}^{M/N_0} = -kx \quad (1.9)$$

$$m \left(\frac{^N d}{dt^2} (\mathbf{r}^{M/C} + \mathbf{r}^{C/N_0}) \right) = -kx \quad (1.10)$$

$$m(\ddot{x} + a) = -kx \quad (1.11)$$

With the initial conditions of $x(t = 0) = 0$ and $\dot{x}(t = 0) = 0$,

$$x = -\frac{ma}{k} \left[1 - \cos \left(t \sqrt{\frac{k}{m}} \right) \right] \quad (1.12)$$

Equation 1.12 shows the position of the proof mass with respect to the accelerometer case for an accelerometer with no damping. However many accelerometers are built with damping or with feedback systems that apply force on the mass to prevent the motion of the proof mass with respect to the case. In case of a well damped system, the steady state value of x is proportional to a .

$$x \Big|_{\text{steady state}} = -\frac{ma}{k} \quad (1.13)$$

$$\propto a \quad (1.14)$$

However, it is not possible to distinguish between inertial acceleration and acceleration due to gravity. Consider an accelerometer with its measurement axis oriented in the vertical direction. In that case $x \propto (a - g)$ where a is the inertial acceleration of the accelerometer case with respect to the inertial frame and g is the acceleration due to gravity. It is not possible to distinguish a and g using accelerometers.

Gradiometer that measures one component of gravity gradient tensor, requires at least two accelerometers separated by a small distance. If the platform on which the accelerometers are situated is stationary, then the difference in the specific force

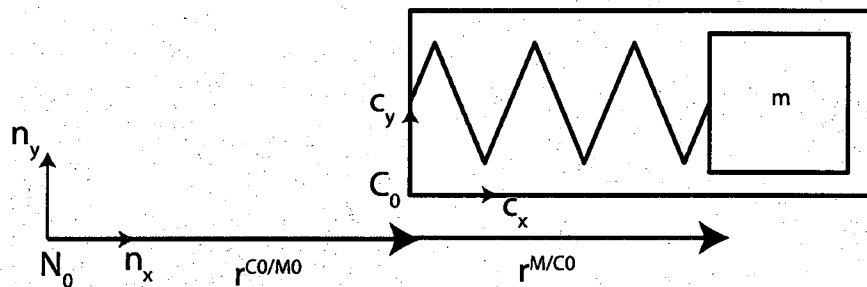


Figure 1.2: Conventional Accelerometers make use of proof masses attached to a case through a spring or feedback forcing system

measured by the accelerometers over the distance between the accelerometers gives us the gravity gradient. Even if there is any linear acceleration of the platform, the common mode inertial acceleration cancels out when the difference is taken and only the difference in the acceleration due to gravity is measured.

1.3 Applications

Gravity Gradient measurement is useful in improving the accuracy of inertial navigation systems. Inertial navigation systems use accelerometers to find inertial accelerations by subtracting acceleration due to gravity. This inertial acceleration is integrated to find the velocity and position of the vehicle. If the acceleration due to gravity is not known accurately, then errors start accumulating in the navigation solution. Gravity gradiometers play an important role in improving the accuracy of inertial navigation systems[1, 2, 3, 4, 5].

Exploring the earth, moon and other planets for mass concentrations is possible by gravity gradiometry. In the past, lunar gravity gradient measurement was carried out by measuring velocity changes of a satellite orbiting the moon. Since this method requires Doppler tracking of the velocity of the satellite, this is possible only when the satellite is in direct line of sight with the tracking station. Hence it was not possible to measure the gravity gradients of the far side of the moon. Several gravity gradiometers

were proposed for the moon and also for other planets [6, 7, 8, 9]. European Space Agency recently launched (March, 2009) a satellite called 'Gravity Field and Steady-State Ocean Circulation Explorer' to map the gravity gradients of the earth. GOCE consists of tri-axial electrostatic gravity gradiometer and is scheduled to launch in 2009 [10]. In 2002 a pair of satellites were launched to study the gravitational field of the earth (Gravity Recovery and Climate Experiment- GRACE) [11]. Using the gravitational data obtained from these satellites, variations in hydrological cycles in vast areas such as the Amazon basin have been studied. Apart from these global measurements using instruments in satellites, local measurements are also of great significance for exploring minerals and resources. In the early part of the 20th century gravity gradient measurements using torsion-balance type instruments were helpful in discovering oil deposits [12]. Many gradiometers were built in the later part of the 20th century specifically for the purpose of mineral exploration [13, 14, 15, 16]. It could also be used for locating underground structures or buildings [17].

It is also possible to use gravity data to locate very dense masses. It has been proposed that a gravity gradiometer could be used for arms control treaty monitoring purposes to distinguish conventional and nuclear missiles [18].

1.4 History of Gravity Gradiometry

Baron Lorand von Eötvös, a Hungarian physicist, was the first person to measure gravity gradients. The first ever gravity gradiometer was designed by him at the end of 19th century after his investigations on equivalence of inertial and gravitational masses [19, 20, 21, 22, 1, 23]. The gradiometer was based on a torsion balance design and had a resolution of 10^{-9} s^{-2} . It is now common to quote gravity gradient measurements in units of Eotvos ($1 \text{ E} = 10^{-9} \text{ s}^{-2}$). Measurement at each station took a long time typically an entire night [24] as the system could not be used in the day time due to large temperature fluctuations. By 1926, the instrument was improved so that it could be used during day and night and typically four stations could be covered in 24 hours. This instrument lead to the discovery of oil domes in Texas [12]. But at the end of 1930's the use of gravity gradiometers reduced and

gravimeters were used more commonly due to the ease of use and interpretation of data [12].

Until, 1960's, the gravity gradiometer did not go through much development. During 1960's improvement in inertial navigation was possible by measuring and mapping gravity gradients [25]. This lead to development of a number of mobile gravity gradiometers. Bell Aerospace (now Lockheed Martin) started developing a full tensor gravity gradiometer (FTG) with accelerometers on rotating disks. Initially this gravity gradiometer was used only in submarines, but later were developed to be used in vans and airplanes for mapping on land [26, 27, 28]. In 1990s, after the end of Cold War, the gravity gradiometer programs were declassified and were developed for surveying on airborne platforms [29].

Other gradiometers were also designed based accelerometers which use Superconducting Quantum Interface Devices (SQUID) [30, 31, 32]. SQUID accelerometers used magnetic field to levitate a proof mass and the restoring force required to retain the mass in its position was proportional to the specific force. This system has not been used for survey on mobile platform extensively. A few tests have been conducted [33] but significant progress has not been made in mobile gradiometry using SQUID sensors.

In all the above types of gradiometers, the force-rebalance type accelerometers were used [34]. There is a need for estimating the stiffness of the force-rebalance mechanism and also to know the proof mass accurately. It is possible to overcome these challenges if it is possible to avoid the spring that holds the proof mass and if it were possible to minimize any interactions between the case and the proof mass. Some gravity meters were built with this concept where a cube corner which acts as a proof mass is dropped within a case. By measuring location of the proof mass at various instances of time using laser interferometry, one could calculate the acceleration due to gravity. Many gravimeters (accelerometers built for the specific purpose of measuring variation in the acceleration due to gravity) were built [35] and even commercial versions developed for measurement of acceleration due to gravity. The disadvantage of such sensors however is that these sensors have to be built with high stiffness in order to reduce strains due to the impulse force resulting when the cube corner is

dropped. Hence it is of great advantage to use a proof mass that is as small as possible.

Atom interferometric sensors which make use of atoms as proof masses also made use of atom's wave properties for measuring the position of the atoms. Atom interferometric sensors have certain unique advantages over the conventional restoring force mechanism based gradiometer. Interferometric techniques were first used on neutrons to demonstrate measurement of acceleration due to gravity [36] and rotation of earth[37]. However the development of atom interferometric sensors involved the development of techniques for trapping atoms using optical forces. First such technique was proposed in 1970s [38, 39] followed by experimental demonstration of trapping of neutral atoms using optical molasses and magneto optical traps (MOT) [40, 41]. Atom interferometry was demonstrated using neutral atoms in 1991 [42, 43, 44, 45]. Soon after atom interferometry was used for measurement of precision measurement of acceleration due to gravity [46, 47], gravity gradient [48], angular velocity [49, 50, 51, 52] and gravitational constant [53, 54, 55, 56].

1.5 Atom Interferometric Accelerometers

Since atoms exhibit both mass and wave properties, it is possible to make use of the particle properties for measurement of inertial acceleration and acceleration due to gravity. At the same time, since atoms also exhibit wave properties, interferometers consisting of these matter waves is also possible. This wave property is the basis of atom interferometry. Wave fronts of the light pulse act as tick marks on ruler. The phase of the light pulses are imprinted on the atoms and at the end of the interferometer sequence the net phase from the atoms can be extracted through well established atom interferometric techniques which consist of a separation pulse and detection pulse. This light phase measured from the atom interferometer is directly proportional to the acceleration due to gravity along the direction of the laser pulses. The system is extremely stable and in fact very similar atom fountains are used for atomic clocks which are used as time standards.

Cesium atoms are trapped at the top of the vacuum chamber using a magneto-optical trap (MOT). The Magneto Optical Trap is switched off after enough atoms have been trapped. The atoms are in free fall by either dropping them or by launching them at a particular speed. Once the atoms are in free fall the atoms are subjected to counter propagating Raman laser pulses which imprint the atoms with their light phase. After a short time a first pulse of laser ($\pi/2$) splits the atoms into two different states. This pulse also provides a momentum kick to one of the states through stimulated emission of photons. The atoms then travel in two different trajectories and after a time period T, a second pulse of laser (π) provides momentum kick to both the states and after which the atoms move toward each other. After another time period T, both groups of atoms are spatially located together. At this instance, a third pulse of Raman laser ($\pi/2$) is applied to both states. This pulse removes all the horizontal momentum. After these three pulses the phase is extracted from the atoms through separation and detection pulses. The separation pulse splits the atoms again into two different states and spatially separates them. The phase is a function of ratio of the atoms in one state to the other state. (The light phase imprinted on the atoms is directly proportional to the distance of the atoms from a reference surface attached to laser source. This is discussed in Chapter 4) The number of atoms in each of the states depends on the probability of finding the atoms in that state which is a function of the square of the amplitude of the wave function.

The number of atoms trapped in the magneto optical trap has to be as high as possible in order to reduce the shot noise. It is analogous to finding the probability of heads or tails on perfectly balanced coin: one has to flip as high a number of coins as possible to measure the probability of find either heads or tails accurately(which would be ideally fifty percent). If only one coin is tossed, it either lands up as heads or tails and hence it is highly inaccurate to estimate the probability of finding heads or tails with just one coin. However if one tossed 100 coins, it will turn out that about 50 coins will turn up heads or tails. By increasing the number of coins in the toss, the accuracy can be increased. In a very similar manner, in our case the ratio of atoms varies depending on the light phase imprinted on them and in order to extract ratio it is important to have as many atoms as possible participating in the atom

interferometry process. The shot noise is inversely proportional to the square root of the number of atoms that participate in the atom interferometer process. About a billion atoms are trapped in the Magneto Optical Trap in our sensor.

Advantages:

- **Stability** The major advantage of atom interferometric sensors is that the lasers used to imprint phase on atoms (Raman pulse) and the lasers used for interrogating the atoms for the net phase are all very stable. The stability is not affected by the motion of the platform as long as the optics are mounted on stiff mounts. This allows for the gradiometer to be in a mobile environment where platform disturbances are high. In the current gradiometer most of the optic mounts have been custom designed and the systems for laser generation and the corresponding optics are all very stable.
- **Scale factor** The measurement of acceleration due to gravity is independent of the proof mass in an atom interferometer. In case of conventional gravity gradiometers specific forces are measured using a proof mass and a restoring force mechanism. Hence in a conventional gradiometer, there is a need for extensive calibration in order to determine the mass to stiffness ratio since the acceleration due to gravity measurement depends on this ratio. In case of an atom interferometer there is no need to know the actual mass of the atoms themselves (The attraction of the earth to the proof mass can be neglected since the proof mass is several orders of magnitude smaller compared to the mass of the earth). In an atom interferometer the acceleration due to gravity measurement does not depend on measuring the reaction force, but instead purely on the trajectory of the atoms during the free fall in the platform reference frame. Since the atoms are in free fall there is no possibility of spurious forces from the case of the sensor affecting the measurement. The only forces acting on the atoms after the atoms have been dropped from the Magneto Optical Trap are from the momentum kick from the Raman pulses (at the same time when the phase from the Raman pulses are being imprinted on the atoms). The sensor is not acted upon by any other forces other than Raman pulses which also leads to a

very stable scale factor that depends only on the following factors:

1. Time duration between the Raman pulses

Time duration between the Raman pulses can be very easily controlled to very high accuracy with currently existing technologies such as quartz oscillators.

2. Propagation vector of the Raman laser

The gravity gradient measurement depends on the magnitude as well as direction of the propagation vector of the Raman pulses. The magnitude of the Raman pulses depends on the stability of the frequency of the laser used. Frequency stability can be easily achieved using cavities.

3. Distance between the two atom interferometric accelerometers

When the distance between the sensors is discussed it is the optical distance between the sensors that is pertinent to this measurement. Even though the physical distance between the sensors can be a constant , the optical distance can be changed by either increasing or decreasing either the dimensions or the refractive indices of the optical elements in the path of the laser beam. If the thickness of the walls of the zerodur cells (through which the Raman beams pass through) is changed then the time taken by the Raman pulse from one sensor to the other sensor is changed and hence compared to an ideal sensor with only pure vacuum between the sensors, the distances now is higher. The optical distance between the atom interferometric sensors can be determined accurately by measuring the change in the differential phase when either the magnitude of propagation vector is changed (by changing the frequency) or by changing the time duration between the Raman pulses.

- Susceptible to platform motion only at instances of atom drop and laser pulses

Since the atoms are in free fall, the sensor is not susceptible to platform motion during the free fall of the atoms. The only instances at which the sensor is

susceptible to the platform disturbances are at the of drop of atoms from the magneto optical trap and the Raman pulses. Any platform motion during the free fall does not affect the sensor measurement at all. This is vastly different from conventional gravity gradiometers. In a conventional gravity gradiometer, the proof mass is connected to the case through a spring or some other form of restoring force mechanism and hence any motion of the case affects the motion of the proof mass. Conventional gradiometers are highly susceptible to platform motions as well as variations in the restoring force mechanisms of the accelerometers. However since the atom interferometer measurements are only a function of the distances of the atoms at specific instances of the laser pulses they are immune to platform motion at all the other times.

Chapter 2

Overview

The first part of the thesis work is aimed at the development of methods to understand the relation between the atom interferometric gravity gradient sensor measurement and the disturbances experienced by the gradiometer platform. The phase difference between two atom interferometric accelerometers is proportional to the gravity gradient on a stationary platform. Rotational motion of the platform however introduces significant noise into the gradient measurement. All of the noise introduced into the gradient measurement by platform disturbance can be understood through the light phase imprinted by the Raman beam on the atoms. The propagation phase and the separation phase do not contribute to the noise in the gradient measurement.

Programs were developed to calculate all three phases: light, propagation and separation phases for rotational disturbances on the platform. With such a program the apparent gravity gradient due to the platform noise could be calculated for either a simulated platform motion or an actual platform motion by making use of measurement of the angles of the platform using a fiber optic gyroscope. Using such a program, the apparent gravity gradient due to sinusoidal platform motion at various frequencies were computed. In case of an atom interferometric sensor, the apparent gravity gradient not only depends on the amplitude and frequency of the sinusoidal rotational motion, but it also depends on the phase (phase in this case is defined by making use of the time delay of drop of atoms with respect to the zero crossing of the sine). Chapter 3 describes the atom interferometric accelerometer. Chapter 4

describes the gradiometer which makes use of two atom interferometric accelerometers and the evaluation of the apparent gravity gradient due to platform motion. With such a program the apparent gravity gradient due to the platform noise could be calculated for either a simulated platform motion or an actual platform motion by making use of measurement of the angles of the platform using a fiber optic gyroscope. Using such a program, the apparent gravity gradient due to sinusoidal platform motion at various frequencies were computed. In case of an atom interferometric sensor, the apparent gravity gradient not only depends on the amplitude and frequency of the sinusoidal rotational motion, but it also depends on the phase (phase in this case is defined by making use of the time delay of drop of atoms with respect to the zero crossing of the sine). Chapter 3 describes the atom interferometric accelerometer. Chapter 4 describes the gradiometer which makes use of two atom interferometric accelerometers and the evaluation of the apparent gravity gradient due to platform motion.

The apparent gravity gradient due to platform motion were experimentally measured by actuating a platform to a sinusoidal rotational motion and measuring the phase difference of the atom interferometer. The platform angle was controlled by making use of a negative feedback control that uses the angles measured by a fiber optic gyroscope and actuated by stepper motors. Chapter 5 describes the design of the platform and the feedback control to control used to control the motion of the platform. Chapter 6 describes the experimental measurement of the transfer function of the platform disturbance to the apparent gravity gradient.

The ultimate goal of this thesis work was to measure the gravity gradient using atom interferometric sensors on a mobile platform. The atom interferometric gravity gradiometer is housed in a truck for making mobile measurements. However mobile systems also pose a significant challenge due to the increased rotational disturbances on the platform. To compensate for the disturbances, feedback of platform angle and feedforward of the angular velocity of the platform was used.

In order to reduce the disturbances on the floor of the truck while the truck was moving, an electric drive was designed and built to run the truck. The internal combustion engine of the truck would be unable to reach low speeds of 1 cm/s that is

required for mobile gravity gradient measurement of gradient signatures that occur in a very small distance. Chapter 7 describes the design and construction of the electric drive which was used to run the truck. This electric drive also allowed us to drive the truck with no one present in the truck and hence further reducing disturbances on the truck floor. In order to accurately locate the truck, a global positioning system (GPS) was used. Since a single GPS receiver can only position to within about a few meters, a pair of GPS receivers were used in a kinematic positioning mode which one receiver on a stationary base station and another on the truck. This system allows the positioning of the truck to within about 1 cm.

Chapter 8 describes the mobile measurement of the gravity gradient signature at the entrance of Hansen Experimental Physics Laboratory. The mobile measurement was carried out by moving the truck using the electric drive while the platform was actively controlled using feedback and feedforward control. This is the first ever measurement of gravity gradient on a mobile platform using an atom interferometric sensor. The experimental measurement closely followed the expected gradient computed using the dimensions of the void of the Hansen Experimental Physics Laboratory. This measurement was possible only after understanding the apparent gravity gradient due to the platform disturbances and minimizing the platform disturbances by actively compensating for the disturbances on the platform. The control of the speed of the truck also allowed for reducing the disturbances entering the truck.

Chapter 3

Atom Interferometric Accelerometer

Atom interferometry makes use of both the atom's particle and wave properties for inertial measurements using interference. The atom can be put into a superposition of two different states and the states are spatially separated by momentum kicks received from counter-propagating Raman lasers. Quantum mechanical phase terms are associated with each of the states. These states interfere with each other if they are brought together. This is very similar to laser interferometry where the light taking two different paths of different lengths have a phase difference and hence when brought together will interfere. In the case of atom interferometry, since the phase is attributed to the atoms which also have mass, it is possible to measure inertial acceleration and acceleration due to gravity.

3.1 Atom Interferometry

To begin the process of interference, the atoms need to be set in a superposition of two states which would be spatially separated. After a time t_1 after the drop (or launch), the atoms are exposed to optical pulse of light $\pi/2$. This puts the atoms which were initially in the ground into an equal superposition of ground state and an excited state. Also laser pulse imparts a momentum of $\hbar k$ to only one of the states

$|e\rangle$. Hence the two states follow different trajectories (see Figure 3.1).

At time $t_2 = t_1 + T$, a second pulse of laser called π pulse causes the two states of atoms to change their states. Now $|g\rangle$ state transforms to $|e\rangle$ and also gets a $\hbar k$ momentum kick in the positive direction. At the same time $|e\rangle$ state transforms to $|g\rangle$ and receives a $\hbar k$ momentum kick in the negative direction and hence the velocity of the atoms in the horizontal direction is now zero. Now the two atoms are in paths that would bring them to the same point at time $t_3 = t_1 + 2T$.

At time $t_3 = t_1 + 2T$ both states come back together and now a $\pi/2$ pulse applies a negative momentum kick to the $|e\rangle$ and hence both states do not possess any horizontal velocity. Now both states travel along the same trajectory together and are ready to be interrogated to measure the phase difference.

At the end of this interference sequence, the net phase measured by the sensor is a sum of three components given by:

$$\phi^{\text{sensor}} = \phi_{\text{light}} + \phi_{\text{prop}} + \phi_{\text{sep}} \quad (3.1)$$

- Light Phase: ϕ_{light}

ϕ_{light} is a linear combination of phases imprinted by the Raman laser on the atoms (ϕ_1 at t_1 , ϕ_{2a} and ϕ_{2b} at t_2 and ϕ_3 at t_3) and is given by:

$$\phi_{\text{light}} = \phi_1 - \phi_{2a} - \phi_{2b} + \phi_3 \quad (3.2)$$

- Propagation Phase: ϕ_{prop}

ϕ_{prop} is due to the free evolution of the atomic wave packets in between the laser pulses and is given by:

$$\phi_{\text{prop}} = \frac{1}{\hbar} \int_{\text{path}} L dt \quad (3.3)$$

ϕ_{prop} is zero in a constant and uniform gravitational field ([45]).

- Separation Phase: ϕ_{sep}

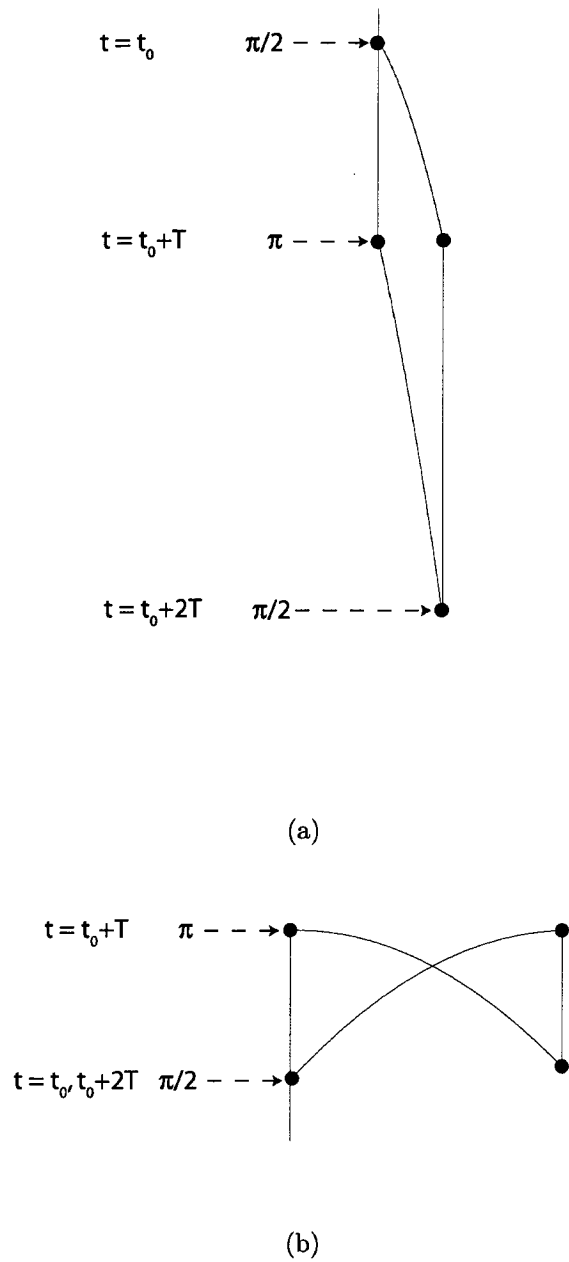


Figure 3.1: Schematic of Atom Interferometer: (a) Drop configuration (b) Launch configuration

ϕ_{sep} is the phase shift due to non-overlap of the classical positions of the wave-packets at the end of the interference sequence. This is also zero in cases where there is a uniform gravitational field and the paths overlap at the end ([57]).

$$\phi_{sep} = \mathbf{p} \cdot \Delta\mathbf{r}/\hbar \quad (3.4)$$

where \mathbf{p} is the average momentum of the atoms at the end of the interference and $\Delta\mathbf{r}$ is the spatial separation between the wavepackets at the end of the third pulse.

3.2 AI Acceleration Measurements

Using the above concept of atom interferometry, inertial acceleration or acceleration due to gravity can be measured. In the following sections different cases will be considered to highlight the measurement of inertial acceleration and acceleration due to gravity.

3.2.1 Measurement of acceleration due to gravity

Consider an atom interferometer on a platform which is not undergoing any inertial accelerations. An atom interferometer similar to the one introduced in the previous section could be used to measure the horizontal component of acceleration due to gravity. The acceleration due to gravity would be given by:

$$g_x = (x_1 - x_{2a} - x_{2b} + x_3)/T^2 \quad (3.5)$$

where x_i is the distance of the center of the cloud from a vertical reference surface.

In Equation 3.2, phase of light which is imprinted at the i^{th} pulse is related to x_i and is given by:

$$\phi_i = \mathbf{k}_{eff} \cdot \mathbf{x}_i \quad (3.6)$$

where \mathbf{k}_{eff} is the wave vector of the Raman laser.

Hence ϕ_{sensor} can be expressed in terms of the distances of the center of the atom clouds from the reference surface.

$$\phi^{sensor} = k_{eff}(x_1 - x_{2a} - x_{2b} + x_3) \quad (3.7)$$

Hence g_x can be expressed in terms of $\Delta\phi$ by using Equation 3.5.

$$g_x = \frac{\phi^{sensor}}{k_{eff}T^2} \quad (3.8)$$

3.2.2 Measurement of inertial accelerations

If the platform accelerated to the right with an acceleration a_x , then the same atom interferometer setup would measure the inertial acceleration a_x . Since the atoms do not experience the acceleration after the drop, only the platform accelerates with respect to the atoms. This is very similar to the platform not accelerating but subjected to an acceleration due to gravity of $-a_x$.

$$-a_x = \frac{\Delta\phi}{k_{eff}T^2} \quad (3.9)$$

The phase difference is entirely dependent on the position of atoms (x_1, x_{2a}, x_{2b}, x_3) at three instants of the Raman pulses ($t = t_1, t_2, t_3$). Hence the only times at which the platform motion affects the measurement is at the instance of drop ($t = 0$) of atoms which fixes the initial position and velocity for the atom's trajectory and at the three Raman pulses ($t = t_1, t_2, t_3$). Theoretically the platform is free to undergo any linear motion at all other times and will not affect the measurement of acceleration. But in reality, the geometrical constraints such as the size of cell in which the interference takes place pose some constraints on the platform motion.

3.2.3 Presence of acceleration due to gravity and inertial acceleration

In this case the platform is subjected to inertial acceleration a_x and acceleration due to gravity g_x . Then:

$$g_x - a_x = \frac{\Delta\phi}{k_{eff}T^2} \quad (3.10)$$

The atom interferometer acts like any conventional accelerometer and can only measure specific forces. It is not possible to distinguish inertial accelerations and acceleration due to gravity using one sensor. For the measurement of gravity gradients, we require at least two sensors to measure the difference in the specific forces to be able to measure the difference in the acceleration due to gravity while rejecting the common inertial acceleration. However rotation of the platform introduces components of inertial accelerations that are not common to both sensors and hence the gradient measurement includes the non-common inertial acceleration terms. The gravity gradient measurement and apparent gravity gradient due to rotation of platform is discussed in the next chapter.

Chapter 4

Atom Interferometric Gravity Gradiometer

Atom Interferometric Gravity Gradiometer consists of two accelerometers separated by a baseline distance L . The accelerometers are uniaxial and measure specific forces along the platform as shown in the Figure 4.1.

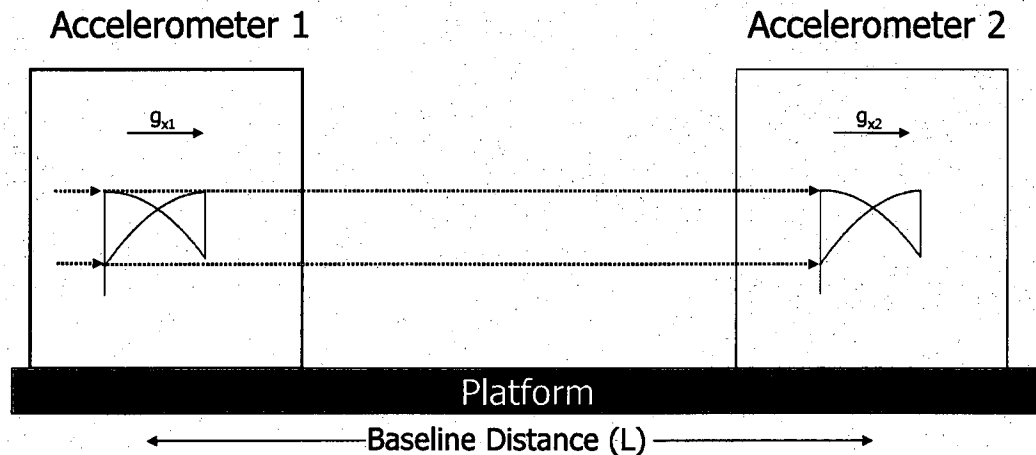


Figure 4.1: Schematic of Atom Interferometric Gravity Gradiometer

If the platform is not undergoing any motion at all, then the difference of the two phases measured ($\Delta\phi = \phi^B - \phi^A$) is proportional to the difference in the horizontal components of acceleration due to gravity ($g_{x_B} - g_{x_A}$). Hence gravity gradient is given

by:

$$\begin{aligned}
 T_{xx} &= g_{x_B} - g_{x_A}/L \\
 &= (\phi^B - \phi^A)/T^2 k_{eff} T^2 L \\
 &= (\Delta\Phi)/k_{eff} T^2 L
 \end{aligned} \tag{4.1}$$

In the following sections, the effect of motion of platform on the interferometer phase is discussed.

4.1 Effect of platform motion

- **Effect of Linear Velocity** A constant linear velocity of the platform will not introduce any relative motion between the atoms and the platform. Hence in this case the acceleration measured by the atom interferometric accelerometer will be zero. However if the linear velocity of the platform is so large as to introduce a Doppler shift in the frequency then the efficiency of the Raman pulses decreases and hence the contrast of the interference decreases. The Doppler shifts that were observed during truck motion were quite small ($\pm 1\text{kHz}$).

- **Effect of Linear Acceleration**

Any linear acceleration of the platform in any direction affects both accelerometers equally. Hence the phase change due to the linear acceleration is common for both accelerometers. Hence the linear acceleration does not affect the gravity gradient measurement. However again in this case if the linear velocity is high enough to introduce Doppler shift then again the efficiency of the Raman pulses decreases and will cause a reduction in contrast.

- **Effect of Angular motion of platform**

Any angular motion of the platform affects the measurement of gravity gradient significantly. To understand the effect of rotational motion we need to know the

direction of Raman Laser and the location of atoms at the instances of $\pi/2-\pi-\pi/2$ pulses. However the position of the atoms at these times depends directly on the position and linear velocity at the instant the atoms are dropped. The phase due to the angular motion of the platform is calculated using a model developed in the next section. However, since the atoms are not coupled to the platform after the atoms have been dropped from the magneto-optic trap any platform motion does not affect the atoms and hence the measurement. The platform motion affects the atom trajectories at only at the instant of drop of atoms from magneto-optic trap and at the instant of Raman pulse. This is quite different from a conventional gradiometer where the proof mass is attached to the case through a spring / restoring force mechanism which means that any motion of the case will also affect the proof mass.

4.2 Modeling a Gravity Gradiometer

To consider the effect of platform motion , the gravity gradiometer was modeled and simulated using MatlabTM. Figure 4.3 shows the schematic of the model and the reference frames associated with the platform and earth.

Two Atom interferometric accelerometers (S_1 and S_2) are rigidly attached to platform (P). The net phase from each sensor is a sum of three phases as shown in equation 3.1. In order to calculate the three components light, propagation and separation phases, the trajectory of the atoms need to be calculated. However, only the light phase is the predominant component that contributes to the net phase. The sum of propagation and separation phases are orders of magnitude smaller than light phase which is verified using numerical simulation. In this section, the method used to calculate the net sensor phase described.

In this model, the Raman lasers are for now assumed to be following the platform and k_{eff} vector is along \hat{p}_y . The atom clouds are treated as particles (represented by A_1 and A_2). The atoms do not interact with each other since the density of the atoms is quite low and also the velocity of the atoms is also very low due to the laser cooling.

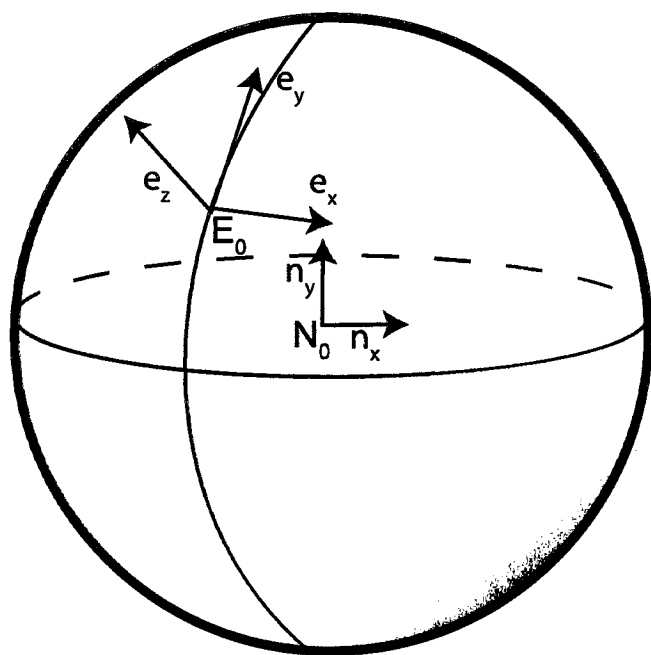


Figure 4.2: The origin of Earth's co-ordinate is at the location of the truck on the surface of earth. The unit vectors of the reference system are oriented toward east, north and radially outwards. The origin of the Inertial co-ordinate system is located at the center of the earth.

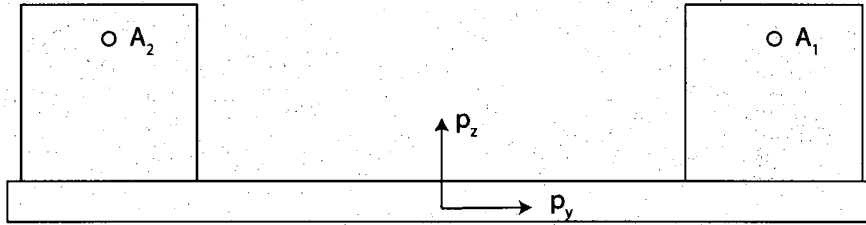


Figure 4.3: The origin of the co-ordinate system of the platform is located at the center of the platform.

P and E represent the reference frames of the platform and the earth respectively. \hat{p}_x , \hat{p}_y , \hat{p}_z and \hat{e}_x , \hat{e}_y , \hat{e}_z are right-handed sets of orthogonal unit vectors fixed in P and E respectively. The platform is considered to be rigid. The Inertial reference frame is located at the center of the earth with right-handed set of orthogonal unit vectors: \hat{n}_x , \hat{n}_y , \hat{n}_z . Latitude of the position of the truck on earth is θ . Angular velocity of the earth is given by:

$$\begin{aligned} {}^N\omega^E &= \omega \hat{n}_y \\ &= \omega \cos(\theta) \hat{e}_y + \omega \sin(\theta) \hat{e}_z \end{aligned} \quad (4.2)$$

Until the atoms are released from the Magneto Optical Trap (MOT), the atoms are fixed with respect to the platform coordinate system. After the atoms have been dropped or launched (at time $t = 0$) the atoms are in free fall in vacuum. In the sensors used in our experiments, the atoms are launched upwards at 1 m/s. After that the only force acting on the atoms is the gravitational force and the impulse force from the Raman laser. The gravitational force is from the acceleration due to gravity which is $-g\hat{e}_z$ and from gravitational attraction of the platform and the truck itself. However, the attraction from the platform and truck does not change significantly (a

small change will occur when the platform rotates with respect to the truck. In our case the platform can rotate by ± 3 degrees). The gravity gradient at the origin of the earth co-ordinate system E_0 is assumed to be Γ . Apart from the gravitational force, the trajectory of the atoms is also affected by the momentum kick on the atoms due to Raman beam at times t_0 , $t_0 + T$ and $t_0 + 2T$. The change in momentum is given by:

$$\mathbf{p}_i = \pm \hbar \mathbf{k}_{eff}(t_i) \quad (4.3)$$

The atoms receive a momentum kick from the Raman Laser due to which there is a change in the velocity of the atoms along the direction of the Raman laser. The total duration of the Raman pulses is only about $4.8 \mu s$ (π pulse is on for double the amount of time $\pi/2$ pulse is on).

$$\mathbf{r}^{A_1/E_0} = x\hat{\mathbf{e}}_x + y\hat{\mathbf{e}}_y + z\hat{\mathbf{e}}_z \quad (4.4)$$

In order to calculate the trajectory of the atoms \mathbf{r}^{A_1/E_0} the inertial acceleration term of the atoms is required.

$${}^N\omega^P = {}^N\omega^E + {}^E\omega^P \quad (4.5)$$

$${}^N\omega^E = \omega \hat{\mathbf{n}}_y \quad (4.6)$$

$$\begin{aligned} \frac{d^2x}{dt^2} &= \omega(\omega x + 2 \sin(\theta) \frac{dy}{dt} - 2 \cos(\theta) \frac{dz}{dt}) \\ &\quad + [T_{xx} \ T_{xy} \ T_{xz}] [x \ y \ z]^T \\ \frac{d^2y}{dt^2} &= \omega \sin(\theta)(\omega \sin(\theta)y - \omega \cos(\theta)(R + z)) \\ &\quad - 2 \frac{dx}{dt} [T_{yx} \ T_{yy} \ T_{yz}] [x \ y \ z]^T \\ \frac{d^2z}{dt^2} &= -\omega \cos(\theta)(\omega \sin(\theta)y - \omega \cos(\theta)(R + z)) \\ &\quad - 2 \frac{dx}{dt} - g + [T_{zx} \ T_{zy} \ T_{zz}] [x \ y \ z]^T \end{aligned} \quad (4.7)$$

The initial position and velocity of the atoms is given by

$$\begin{aligned}\mathbf{r}^{A_1/E_0}(0) &= \frac{\frac{L}{2}\hat{\mathbf{p}}_y}{\lambda} = x(0)\hat{\mathbf{e}}_x + y(0)\hat{\mathbf{e}}_y + z(0)\hat{\mathbf{e}}_z \\ {}^E\mathbf{v}^{A_1}(0) &= \frac{d}{dt}\mathbf{r}^{A_1/E_0}(0) = \frac{dx}{dt}|_{t=0}\hat{\mathbf{e}}_x + \frac{dy}{dt}|_{t=0}\hat{\mathbf{e}}_y + \frac{dz}{dt}|_{t=0}\hat{\mathbf{e}}_z\end{aligned}\quad (4.8)$$

The magnitude of the propagation vector for Raman Laser is a sum of the wave numbers of the counter propagating Raman beams. The direction of the laser is along the platform.

$$\mathbf{k}_{eff} = 2\frac{2\pi}{\lambda}\hat{\mathbf{p}}_y \quad (4.9)$$

Light Phase measured in sensor 1 is given by:

$$\begin{aligned}\phi_{light}^{S_1} &= \mathbf{k}_{eff}(t_1) \cdot \mathbf{r}^{A_1/E_0}(t_1) - 2\mathbf{k}_{eff}(t_2) \cdot \mathbf{r}^{A_1/E_0}(t_2) + \mathbf{k}_{eff}(t_3) \cdot \mathbf{r}^{A_1/E_0}(t_3) \\ &= \sum_{i=1}^3 c_i \mathbf{k}_{eff}(t_1) \cdot \mathbf{r}^{A_1/E_0}(t_i)\end{aligned}\quad (4.10)$$

where

$$c_i = 1, -2, 1$$

$$t_i = t_0, t_0 + T, t_0 + 2T$$

$\mathbf{r}^{A_1/E_0}(t)$ = position of A_1 from E_0 at time t

$\mathbf{k}_{eff}(t) = \mathbf{k}_A - \mathbf{k}_B$ = effective propagation vector of the Raman laser

The $\phi_{prop}^{S_1}$ is obtained using the Feynman path integral. This integral involves calculation of the difference between the classical actions associated with the interfering wavepacket trajectories. The actions S are obtained by integrating the Lagrangian L over the classical trajectories associated with the mean positions of each wavepacket [57].

$$\begin{aligned}\phi_{prop}^{S_1} &= \frac{1}{\hbar} \int_{path} L dt \\ &= \frac{1}{\hbar} \int_{path} m \left(\frac{1}{2} {}^N v^{A_1/N_0} \cdot {}^N v^{A_1/N_0} + \mathbf{g} \cdot \mathbf{r}^{A_1/E_0} + \frac{1}{2} \mathbf{r}^{A_1/E_0 T} \cdot \mathbf{T}_{gg} \cdot \mathbf{r}^{A_1/E_0} \right) dt\end{aligned}\quad (4.11)$$

In the MatlabTM program that is used to numerically evaluate these phases, the position and velocity of the atoms in the earth reference frame is used. Hence, the velocity of the atoms in the Newtonian (inertial) reference frame can be written as:

$${}^N v^{A_1/N_0} = {}^E v^{A_1/N_0} + {}^N \omega^E \times \mathbf{r}^{A_1/N_0} = {}^E v^{A_1/N_0} + {}^N \omega^E \times (\mathbf{r}^{A_1/E_0} + \mathbf{r}^{E_0/N_0}) \quad (4.12)$$

Further, the term ${}^N v^{A_1/N_0} \cdot {}^N v^{A_1/N_0}$ can be expanded to separate out large constant term ($\omega^2 R^2$) that depend only on angular velocity of the earth and the radius of the earth (see Equation 4.13). This helps in keeping track of the other terms which can vary and are much smaller in magnitude.

$$\begin{aligned}[{}^N \omega^E \times (\mathbf{r}^{A_1/E_0} + \mathbf{r}^{E_0/N_0})] \cdot [{}^N \omega^E \times (\mathbf{r}^{A_1/E_0} + \mathbf{r}^{E_0/N_0})] \\ = \omega^2 r^2 + \omega^2 R^2 + 2\mathbf{r} \cdot \mathbf{R} - (\omega \cdot \mathbf{r})^2 - (\omega \cdot \mathbf{R})^2 - 2(\omega \cdot \mathbf{r})(\omega \cdot \mathbf{R})\end{aligned}\quad (4.13)$$

The third phase, separation phase, arises due to the fact that the two interfering trajectories do not coincide at the end. This phase is approximated by Equation 4.14 where \mathbf{p} is the average momentum and $\Delta\mathbf{r}$ is the spatial separation between the two wavepackets at the last pulse.

$$\begin{aligned}\phi_{sep}^{S_1} &= \mathbf{p} \cdot \Delta\mathbf{r}/\hbar \\ &= \left[m \frac{({}^N v^{A_{1a}/N_0} + {}^N v^{A_{1b}/N_0})}{2} \right] \cdot ({}^N \mathbf{r}^{A_{1a}/N_0} - {}^N \mathbf{r}^{A_{1b}/N_0})/\hbar\end{aligned}\quad (4.14)$$

The net phase from sensor 1 is given by the sum of all three phases: light, propagation and separation.

$$\phi^{S1} = \phi_{light}^{S1} + \phi_{prop}^{S1} + \phi_{sep}^{S1} \quad (4.15)$$

The propagation phase ϕ_{prop}^{S1} and separation phase ϕ_{sep}^{S1} also contribute to the net phase but are very small and negligible compared to the light phase ϕ_{light}^{S1} . In the following sections all three contribution to phase were numerically calculated: light phase, propagation phase and the separation phase. The contribution of $\phi_{prop}^{S1} + \phi_{sep}^{S1}$ were found to be orders of magnitude smaller than ϕ_{light}^{S1} .

Finally, the difference in phase between the two sensors is used to measure the gravity gradient. The difference is given by:

$$\Delta\phi = \phi^{S2} - \phi^{S1} \quad (4.16)$$

The gravity gradient is given by:

$$T = \frac{\Delta\phi}{k_{eff} T^2 L} \quad (4.17)$$

4.2.1 Yaw rotation

Consider the rotation of the platform about an axis perpendicular to the plane of the platform (yaw rotation). Let the angular velocity of the platform with respect to earth is ${}^E\omega^P = \omega \hat{n}_y$. Let the angle between \hat{e}_x and \hat{p}_x be ψ as shown in Figure 4.4. To find the trajectory of the atoms, it is now required to find the initial position and initial velocity of the atoms when they are dropped. The initial position of the atoms A_1 and A_2 is given by $\mathbf{r}^{A_1/E_0}(t_0)$ and $\mathbf{r}^{A_2/E_0}(t_0)$. The initial velocity of the atoms are given by

$${}^E\mathbf{v}^{A_1}(0) = \frac{d}{dt} \mathbf{r}^{A_1/E_0}(0) \quad (4.18)$$

$$= \mathbf{r}^{A_1/E_0}(0) \times {}^E\omega^P(0) \quad (4.19)$$

Once the initial velocity and initial position are known, the trajectory of the atoms

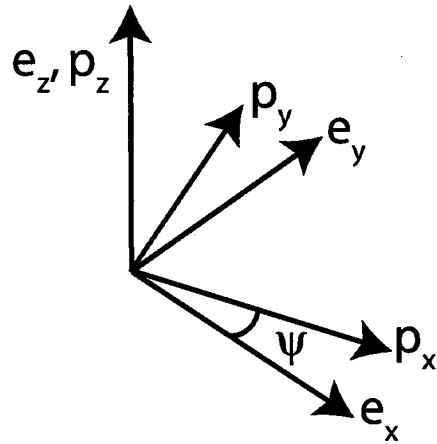


Figure 4.4: The platform co-ordinate system rotated about earth's \hat{e}_z axis.

can now be found by equating the product of mass and inertial acceleration to the forces acting on the atoms. The only forces acting on the atoms during the free fall are are the gravitational forces only. During the instances of Raman pulse the atoms receive impulse forces from the photons which produces a finite momentum change in the direction of k_{eff} .

4.2.2 Sinusoidal Platform Motion

In order to understand the response of the gradiometer at different frequencies, the system was simulated for sinusoidal platform motion at various frequencies and phases. For sinusoidal angular motion of the platform following angular velocities are used for the platform:

$${}^E\omega^P = \omega \hat{p}_z = \omega_0 \sin(2\pi ft + \phi) \hat{p}_z \quad (4.20)$$

where ω_0 is the amplitude of angular velocity and f is the frequency of the oscillations. If it is required to maintain the amplitude of the angle to be constant, then one can use

$${}^E\omega^P = \omega \hat{p}_z = \frac{\omega_0}{2\pi f} \sin(2\pi ft + \phi) \hat{p}_z \quad (4.21)$$

Using the above model the response for sinusoidal motion was simulated using a MatlabTM program. The response for constant amplitude of 1 millidegree ($17 \mu\text{rad}$) is shown in figure 4.5. The first Raman pulse was after 14 ms after the drop of atoms and the time between successive laser pulses (T) was 84 ms. The cross-section of the plot is also shown to reveal the response clearly at frequencies of $\frac{1}{2T}$ and $\frac{1}{T}$. At frequency of $\frac{1}{T}$ the apparent gravity gradient due to the platform motion is zero since the laser pulses always appear to be at the same angle. The response for a pitch motion of the platform (rotation about $\hat{\mathbf{p}}_x$) is exactly the same as that shown in figure 4.5.

All of the sensor's phase is pretty much a contribution from the light phase. The sum of propagation and separation phase do not contribute to the net phase. Figure 4.6 shows the light phase and the sum of propagation and separation phase when the platform is subjected to sinusoidal disturbance.

4.2.3 Comparison of atom interferometric and conventional gradiometers

For the sake of comparing an Atom Interferometric Gravity Gradiometer and a conventional gradiometer based on a force rebalance type (spring-mass) accelerometer a simple case is considered. Consider a platform free to rotate in about $\hat{\mathbf{p}}_z$ (yaw). Purely for the sake of comparison of these two different types of gradiometer, we will not consider the effect of earth's angular velocity or the effect of non-uniform gravitational field.

Let the platform be subject to a sinusoidal angular velocity as shown in Equation 4.20. For an atom interferometer, the apparent gravity gradient is simulated using the model described in the earlier section. Figure 4.7 shows the apparent gravity gradient normalized to the square of the amplitude of angular velocity. As the frequency increases the apparent gravity gradient decreases. This is because of the fact that in an Atom Interferometric sensor, the measurement depends on both the angular velocity of the platform at the instant of the drop of the atoms as well as the angle of the platform at the instant of the Raman pulses. At higher frequencies, the amplitude of

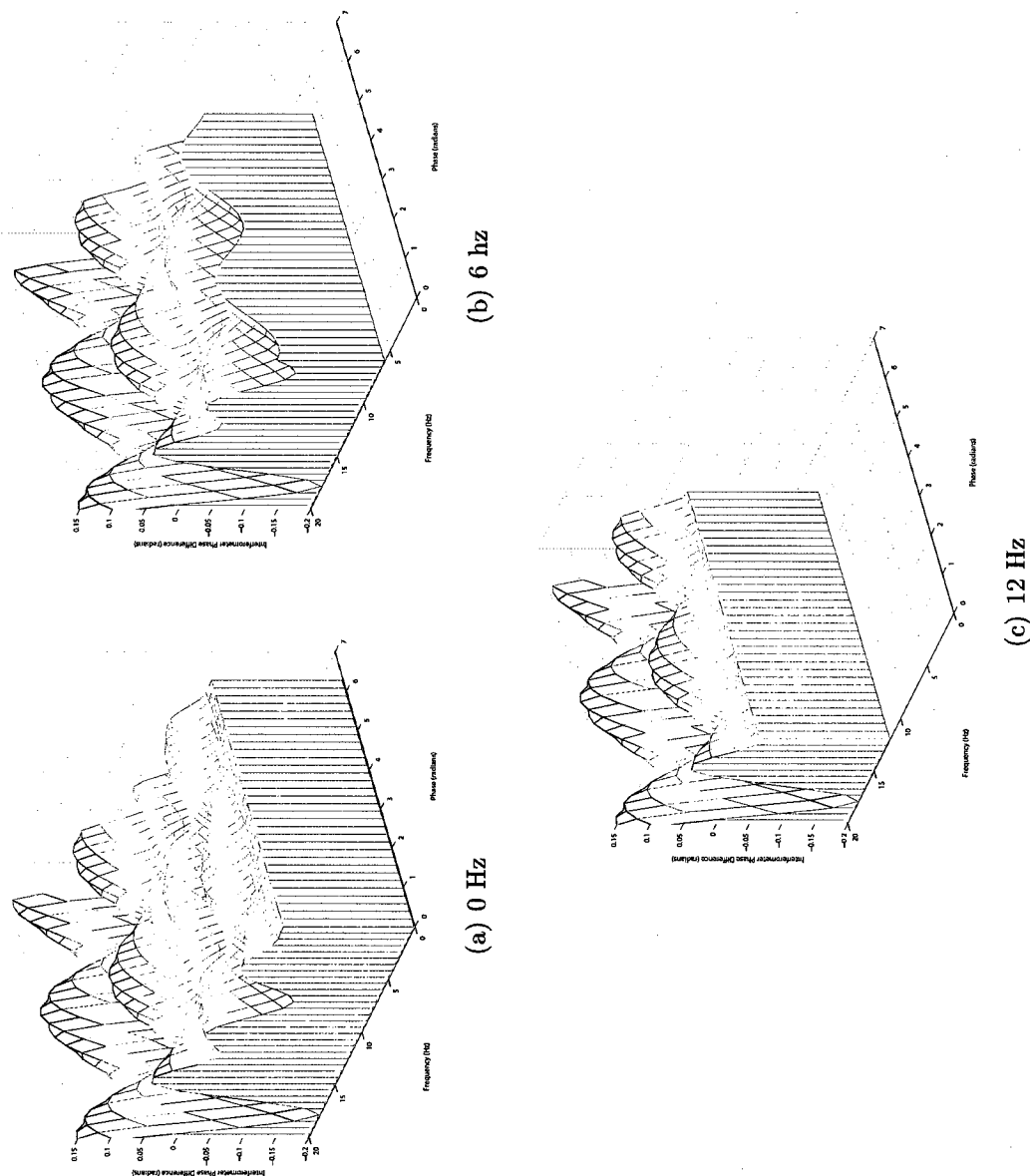
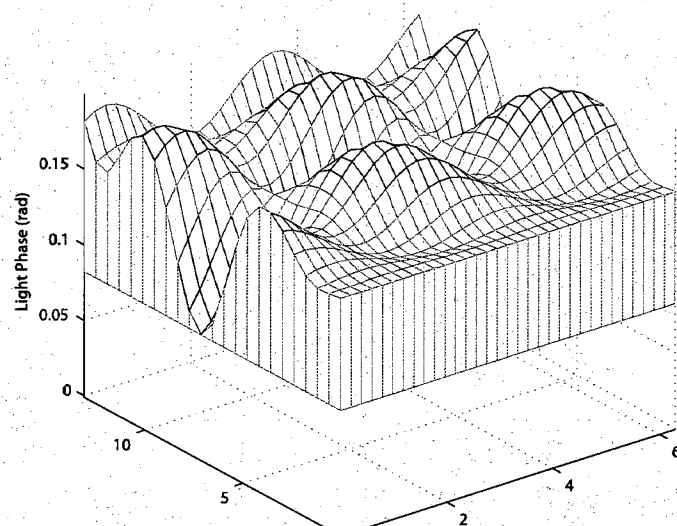
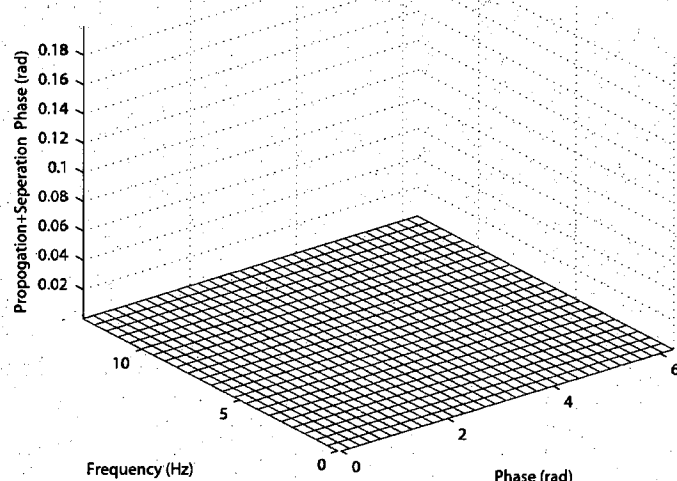


Figure 4.5: Simulated transfer function for a perfectly aligned Gravity Gradiometer. The apparent gravity gradient due to platform oscillations varies with disturbance frequency and phase. At 6 Hz there is a large variation in the apparent gravity gradient with respect to change in disturbance phase. At 12 Hz, the apparent gravity gradient due to platform oscillation is zero.



(a) Light phase



(b) Separation and Propagation phase

Figure 4.6: Interferometer phase components for platform sinusoidal disturbance of 1 milli degree amplitude ($17.5 \mu\text{rad}$). Light phase is the dominant component in the sensor phase.

the angle decreases (in order to maintain the same amplitude for angular velocity) and this contributes to the reduced apparent gravity gradient as the frequency increases.

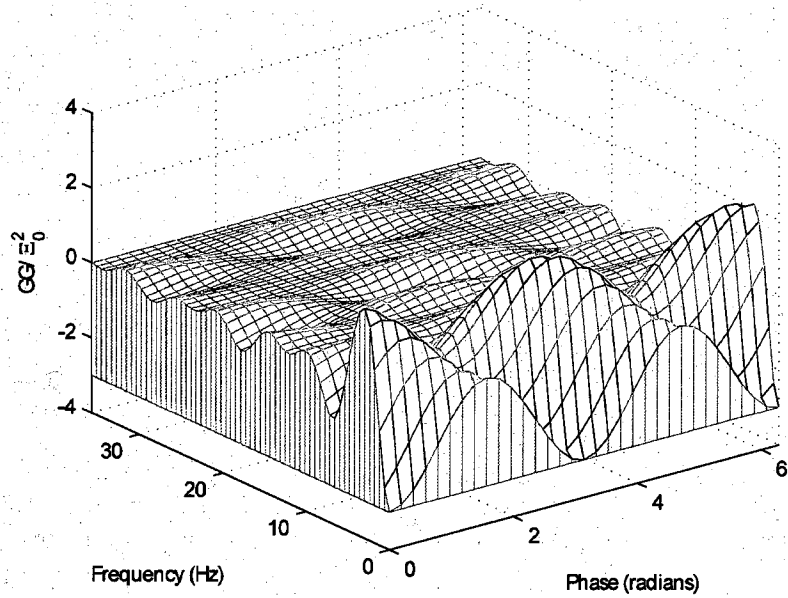


Figure 4.7: Apparent gravity gradient measured by an Atom Interferometric Gravity Gradiometer for various frequencies and disturbance phases for a constant amplitude of angular velocity of the platform yaw motion

For a conventional gravity gradiometer, the apparent gravity gradient is always the square of the angular velocity at the instant of measurement as the only force acting in the direction of measurement of the accelerometers is the centrifugal force. Figure 4.8 shows the apparent gravity gradient normalized to the square of amplitude of the angular velocity. The apparent gravity gradient does not change with respect to frequency.

However, if the platform underwent a rotation with constant angular velocity of

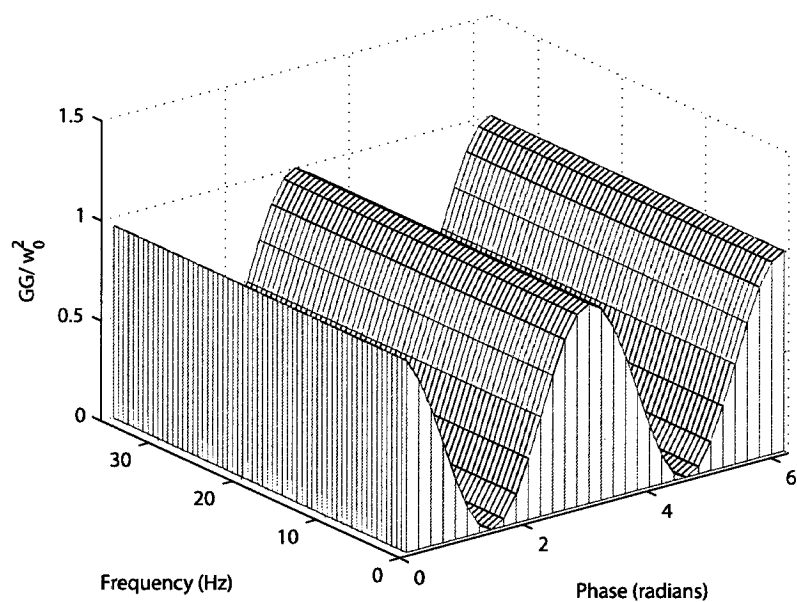


Figure 4.8: Apparent gravity gradient measured by a conventional force rebalance type gravity gradiometer for various frequencies and disturbance phases for a constant amplitude of angular velocity of the platform yaw motion

$\omega \hat{\mathbf{p}}_z$ then the approximate apparent gravity gradient measured by the atom interferometric gradiometer would be ω^2 (See Equation C.1 on page 103). This is similar to having any two accelerometers instead of atom interferometric accelerometers where the accelerometers measure the centrifugal acceleration ω^2 . The constant angular velocity case can be used to estimate the order of magnitude for apparent gravity gradient due to rotation of the platform. But in other cases, when the platform undergoes oscillatory motion, the apparent gravity gradient measured by the atom interferometric gravity gradiometer is not the square of angular velocity as the measurement depends on the location of atoms $\mathbf{r}^{A_1/E_0}(t_i)$ and the direction of propagation vector of Raman Laser ($\mathbf{k}_{eff}(t_i)$) at the instant of Raman pulses (t_1 , t_2 and t_3).

This difference exists due to the fact that in an atom interferometric sensor the atoms are in free fall and are not affected by the platform motion at all times except for at the instant of drop of atoms from the magneto optical trap and at the instant of Raman pulses. On the other hand, a conventional sensor employs a proof mass connected to the platform reference frame through a spring or some other form of restoring force mechanism. This property of atom interferometric sensor where the proof mass does not interact with the platform reference system is a unique advantage compared to conventional sensors where platform disturbances are present.

Chapter 5

Platform Actuation and Disturbance Compensation

The Atom Interferometric Gravity Gradiometer noise depends on platform rotations as seen in the previous chapter. Hence an atom interferometric gradiometer requires a platform with low angular disturbance or precise knowledge of its orientation at the time of measurement. In this chapter the design of the platform motion control is described.

5.1 Requirements

The Gradiometer platform has to be able to perform contrasting functions at various stages of the gradiometer development. During the transfer function estimation of the gravity gradiometer, the platform needs to be actuated at various frequencies. But the platform also has to be able to actively minimize the disturbances that could enter while the the gradiometer is being used for a mobile survey. To be able to achieve both these functions, the stiffness for passive isolation for the system would need to be high for use as a 'shaker' table and low for use as a disturbance isolation system. Some of the important functions and requirements of the platform are discussed below:

- **Actuation for Transfer function estimation**

The platform needs to be actuated at various frequencies in order to measure the effect of disturbances on the gravity gradiometer. From the earlier simulations for the current gravity gradiometer (see Figure 4.5), the apparent gravity gradient has zero responses at frequencies of $\frac{1}{T}$, $\frac{2}{T}$. In order to verify the theoretical model developed for the response of the gradiometer at various frequencies, it would be important to be able to actuate the platform in the band of frequencies ranging from 0 Hz to $\frac{1}{T}$ Hz (in our case $\frac{1}{T} = 1/0.084 \approx 12$ Hz).

- **Static Leveling during stationary surveys**

Leveling of platform to required Pitch, Roll and Yaw angles when the platform is static. This is required for surveys where the truck is parked at a location and gravity gradient data is measured at the same location for extended periods of time. This requires that the platform angle should not drift over time and to be able to compensate for disturbances. The disturbance during this process is minimal since the only sources of disturbances are from wind and vehicles passing by the truck. The mean square spectral density of the Pitch, Roll and Yaw angles are shown in Figure 5.1. Static gradient measurement is also described in detail in previous thesis work [58].

- **Disturbance Compensation for Mobile survey**

In order to be able to measure the gravity gradients while the truck is moving, pitch, roll and yaw angular disturbances on the platform need to be actively minimized. It is required that the platform angle be able to be controlled to minimize the apparent gravity gradient. The mean square spectral density of the Pitch, Roll and Yaw angles on the floor of the truck while the truck is moving is shown in Figure 5.2.

It is important to note that atom interferometric gravity gradiometer is significantly different from any conventional force-rebalance type gradiometers. All the gradiometers typically have worked based on a restoring force principle, for example, Eötvös torsion balance mechanism depended on the restoring force of the torsion

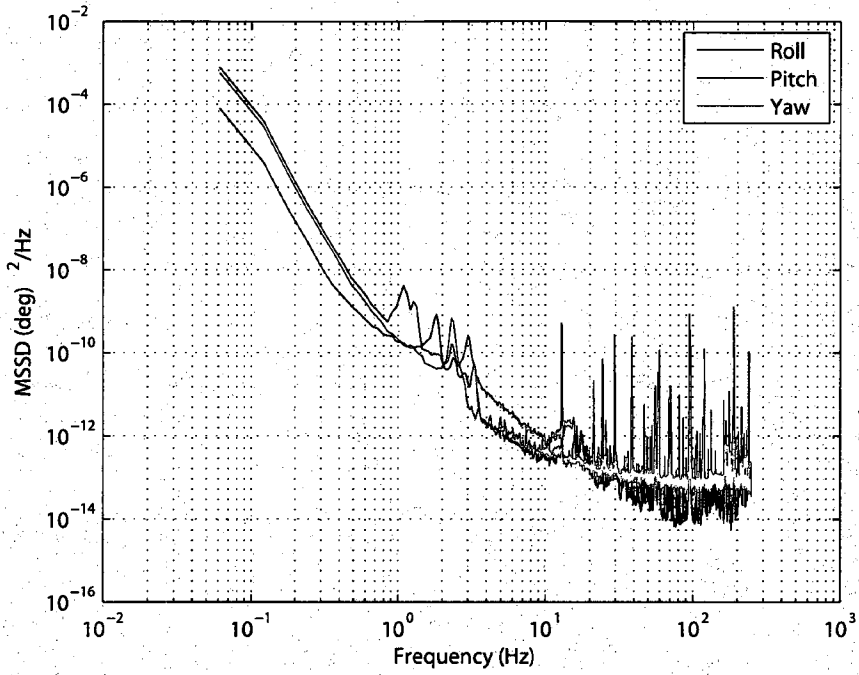


Figure 5.1: Pitch, Roll and Yaw disturbance levels on stationary truck

spring to counteract the gravitational forces on the two masses. Gradiometers developed in the later part of 20th century have made use of accelerometers to individually measure specific forces at two different points in order to identify gravity gradients. Again the accelerometers that were used for this purpose have typically depended on some kind of restoring force either directly through spring mechanisms or through counteracting magnetic forces in the case of SQUID accelerometers. By measuring the reaction force on the proof mass, the specific forces were measured.

In the above cases, it is necessary to make sure that no spurious forces enter the system through rotation of the gradiometer platform since rotation of the platform will require counteracting forces from the restoring force mechanism. This would differ

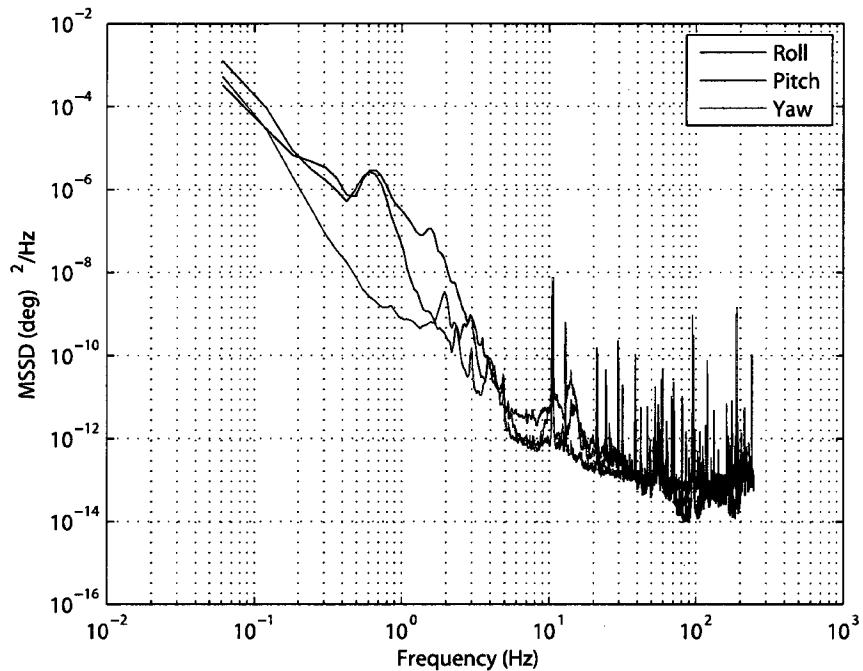


Figure 5.2: Pitch, Roll and Yaw disturbance levels on moving truck

from the measured restoring force applied by the force-rebalance mechanisms in the absence of such motion. These spurious forces may also enter purely through the motion of the platform within the inertial frame (the most troublesome being the rotational motion). For example consider a platform with two accelerometers and for the purposes of demonstration assume the platform to be in deep space where there are no measurable gravitational fields. If the platform is stationary then the accelerometers measure no specific forces. But if the platform undergoes a rotational motion, say with constant angular velocity ω , then the proof masses in the accelerometers experience forces due to this platform motion. In this condition, the difference between the two specific forces measured by the accelerometers is not zero.

In this case the apparent gravity gradient given would be:

$$T_{xx} = \frac{\rho_2 - \rho_1}{L^2} \quad (5.1)$$

From the above system it is clear that the motion of the platform significantly affects the reading of the gravity gradiometer.

However, in case of an atom interferometric gravity gradiometer, the atoms are in free fall during most of the time and do not interact with the platform. The motion of the platform affects the trajectory of atoms only at the instant the atoms are dropped when the Magneto optical trap (MOT) is switched off which sets the initial position and velocity of the atoms. Apart from the initial condition, the trajectory of the atoms are also affected by the momentum kicks that the atoms receive from the Raman pulses. Otherwise the atoms are in free fall and their motion is independent of the platform. The platform is free to undergo any motion within reason at all times other than at the instants of the drop of atoms and Raman laser pulses.

Due to these differences the apparent gravity gradient produced by the motion of platform is also significantly different for an atom interferometric gradiometer and a restoring force based gradiometer. In the case of an atom interferometric gradiometer, each measurement takes a finite amount of time during which the atoms are allowed to take up a trajectory and the Raman lasers (which are fixed to the platform) interact with the atoms for very small amounts of time during the entire free fall. In essence the atom interferometric accelerometer can be thought of measuring the distances of the atoms from a reference surface and the interferometer phase measured is proportional to the acceleration value based on these position measurements. This is analogous to throwing a steel ball from Leaning tower of Pisa and then inferring the gravitational acceleration experienced by the ball by measuring the position of the ball at three time instants.

So the output depends on position of the platform at the three instances of the Raman pulses as well as the trajectory of the atoms. The trajectory in turn is dependent on the position and velocity of the atoms when they are dropped from the MOT. The position and velocity of the atoms at the instant of drop from the MOT

in turn depends on the angular motion of the platform with respect to the inertial frame.

Due to these major differences in the way platform disturbances affect the gradiometer, there are also differences in the environmental requirements of the platform for gravity gradiometer. In the case of a conventional gravity gradiometer the angular velocity of the platform has to be as low as possible in order to reduce the apparent gravity gradient. But in case of the atom interferometric gravity gradiometer, the angular velocity of the platform matters only at the instant the atoms are dropped.

Consider a hypothetical case where the atoms are dropped and after the drop the platform undergoes any random motion, but comes back to the original position at the instant the atoms are dropped. In this case in spite of the random motions of the platform there is no effect since it only matters as to what the platform position and velocity were at the four instants of time when the atom was dropped or when the Raman pulses were on. In this case the apparent gravity gradient due to the platform motion is zero even though the platform could have undergone large motions during the free fall.

The most important requirements for the platform are:

The velocity of the atoms at the instant of drop from the magneto optical trap has to be minimized. The angular velocity of the platform with respect to the inertial frame has to be as low as possible in order to reduce the linear velocity imparted to the atoms by the platform motion. The platform angle after the atom drop has taken place should also be as small as possible in order to reduce the apparent gravity gradient.

From the simulations from earlier chapter 4.5 it is clearly seen that at frequencies near $1/T$ and integer multiples of $1/T$ (where T is the time between the laser pulses), the apparent gravity gradient due to the platform oscillations is zero. But at frequencies near $\frac{1}{2T}, \frac{3}{2T}, \dots$ etc, the apparent gravity gradient is high. Also, since the magnitude of the apparent gravity gradient is higher at higher frequencies (for a given amplitude of platform oscillation) it is imperative to prevent high frequency disturbances on the gradiometer platform. Fortunately, in most real world cases, disturbance amplitudes at higher frequencies are much lower than the low frequency

disturbances as seen in 5.2. Hence in most cases much attention needs to be focused only on the lower frequency disturbances in order to reduce the apparent gravity gradient due to platform rotation.

In order to reduce the apparent gravity gradient it is required that the disturbance frequencies near $\frac{1}{2T}, \frac{3}{2T}, \dots$ etc be suppressed. In the case of our gravity gradiometer, $T = 0.084$ s and hence some of the high amount of apparent gravity gradients is seen at frequencies of 6 Hz, 18 Hz, 30 Hz, etc. We have used drift of the platform in a time period T as a parameter that needs to be minimized. Since the disturbances that occur are not at one particular frequency, by minimizing the platform motion between the laser pulses, one can minimize the noise due to the platform motion at the laser pulses.

The basic requirement for the platform was decided as the drift of the platform to be less than a certain value in time T since that would bound the motion of the platform during the free fall and hence would bound the swing of the platform during the instances of the Raman Pulse. This requirement itself was to be tested during the first set of gradiometer tests.

A simplification could be made by assuming that the angular velocity of the platform is very low at the time of the drop so that the atom pretty much does not get any initial velocity kick with respect to the earth frame (i.e. ${}^E\mathbf{v}^A$ is small). (This assumption is based on measurements of the angular velocity of the platform when the truck was in very slow roll less than 10 cm/s). Using this assumption we can use a simplified model shown in Equation 5.2 which makes use of only the angle of the platform and assuming that the atoms just merely fall vertically downwards without being affected by the linear velocity of the magneto-optical traps at the instant of the drop.

$$\begin{aligned}\Delta\phi &= (\mathbf{k}_{eff_1} - 2\mathbf{k}_{eff_2} + \mathbf{k}_{eff_3}) \cdot \mathbf{l} \\ &\approx -\frac{1}{2}kl(\theta_1^2 - \theta_2^2 + \theta_3^2) + 2\theta_0(\theta_1 - 2\theta_2 + \theta_3)\end{aligned}\quad (5.2)$$

where θ_i is the pitch angle of the platform at the instant of the i^{th} Raman pulse.

5.2 Design Development

In order to be used as a 'shaker table' to measure the effect of disturbance on gravity gradiometer, the linkages need to be stiff enough not to resonate at these frequencies. Also this requires the use of actuators to control the pitch, roll and yaw motion. At the same time, the linkages should not be very stiff so that it transmits high frequencies from various disturbance sources into the platform while performing mobile surveys. In order to achieve both these functions a gimbal was designed and in the following sections the design development of this gimbal is described.

The disturbances that needed to be compensated from the truck floor were expected to be quite low since the truck was expected to move at very low velocities at around 1-2 cm/s (low speed is achieved by using a special purpose built electric drive for the truck which is described in Chapter 7 on page 74). The greatest disturbances were expected from occasional bumps or from wind gusts. To deal with this it was decided to build an active three degree of freedom platform actuation. After building the truck electric drive system, the disturbances on the truck floor were measured while moving on paved surface in front of Hansen Experimental Physics Laboratory, End Station 3 (at Stanford University campus).

(*** possible graph of psd at still and slow motion)

The current setup of the gimbal is shown in figure 5.8. The gimbal consists of multiple stages which successively add various degrees of freedom and also allow for passive isolation of disturbances. The first stage platform sits on a universal joint that allows the platform to pitch and roll. At two adjacent corners of the platform stiff linkages connect the platform to the truck through linear actuator which aids in the control of pitch and roll motion of the platform. The next stage consists of a platform on a slewing ring which allows for yaw motion of the platform. The third and final stage consists of a breadboard on pneumatic isolators to reject very high frequency disturbances.

The entire platform and the gimbal is enclosed inside an Aluminum framework which acts as the perimeter of the gravity gradiometer sensor system and protects the inner parts during moving the gimbal in and out of the truck. The framework was

obtained from a suspended platform tilt mechanism built by Vistek Inc. Aluminum has a relatively high coefficient of thermal expansion (about $23 \times 10^{-6}/K$) and hence temperature variation of different parts of the platform over time causes uneven expansion/contraction of the gimbal over time (very low frequency). However this does not affect the gradiometer measurement since the platform pitch/roll/yaw angles are under a closed loop feedback control with a tilt sensor (fiber optic gyro described in 5.2.5).

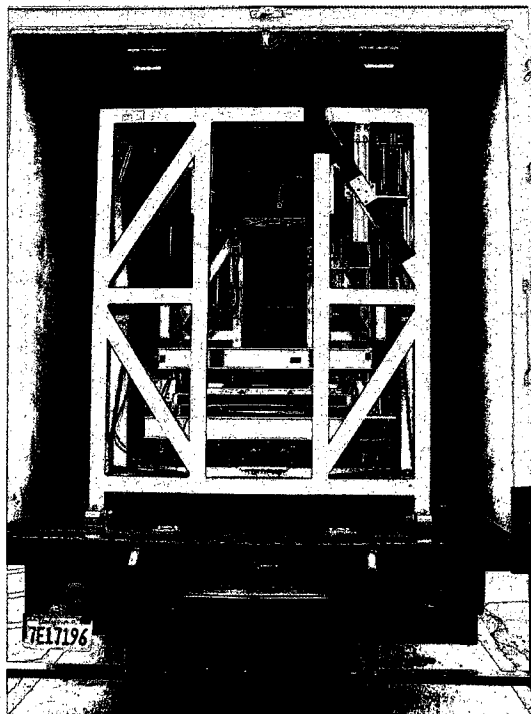


Figure 5.3: Photograph of Gimbal inside the truck

5.2.1 Pitch and Roll motion

The platform is a $1.8\text{ m} \times 1.2\text{ m}$ optical breadboard. This breadboard is seated on a universal joint at the center. This breadboard is free to pitch and roll (± 4 degrees). The actuation of pitch and roll stages are achieved by use of linear actuators that are fixed on the aluminum frame work and connected to the platform at two corners.

(The linear actuators are made of steppers motors which convert the rotary motion to linear motion through lead screws described in section 5.2.4).

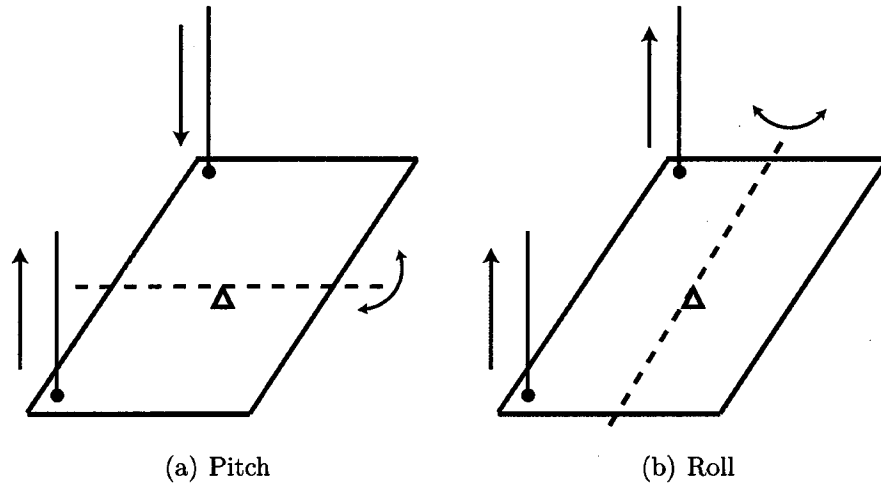


Figure 5.4: Schematic showing the actuation of Pitch and Roll Motion of platform

5.2.2 Yaw Motion

The next stage provides for a yaw degree of freedom. This stage consists of a platform on a slewing ring. In order to actuate the motion linear actuators are used which are attached to both edges of the platform. Both linear actuators have to be moved synchronously in order to achieve yaw motion. A slight pretension in one of the linkages prevents backlash. Later this setup was modified to have only one linear actuator and two sets of springs to provide pretension to prevent backlash.

5.2.3 Gradiometer Platform

The platform on which the gradiometer is seated, is on top of the yaw stage. The yaw stage and the gradiometer platform are separated by pneumatic isolators to isolate the gradiometer from high frequency vibrations. The pneumatic isolators used in this setup are Barry Control SLM 3A. Pneumatic isolators were chosen in order to be able

to maintain a constant resonance frequency of the isolators even when the isolator loads varied.

5.2.4 Actuation

The linear actuators mentioned in the above sections consist of stepper motors which turn lead screws. Each step of the stepper motor is 1.8 degrees. The rotary motion of the lead screws is converted to linear motion by using a nut which is constrained not to rotate. Relatively large rotations are converted to very small linear motions based on the number of threads per unit length in the lead screw (8 threads per inch). The stepper motors are also driven by drivers which have micro stepping enabled. The micro stepping allows each step of the motor to be further subdivided into 250 'micro' steps. This micro-stepping system allows fine control of the motor. Further, the actuation of pitch, roll and yaw is achieved by attaching this linear actuator to one edge of the platform. Each micro-step of the motor corresponds to about 69 nrad in pitch angle of the platform (see Appendix Table B.1).

The stepper motor velocity is controlled by varying frequency of the pulses sent to the motor(see Figure 5.5). Each pulse sent to the stepper driver turns the motor by one 'micro' step. Hence by varying the frequency of the pulses, one can control the speed of the motor. The direction of the motor is also controlled by another signal sent to the stepper driver.

5.2.5 Sensor

The tilt of the Platform is measured using a fiber optic gyroscope (Lytton LN 250) which outputs angular velocity as well as tilt (integrated from angular velocity). The measurements are output every 100 ms. The tilt measurements are output digitally and transmitted to the controller through RS 422 protocol. This sensor is used as a tilt sensor to measure the tilt of the platform and is used in negative feedback of tilt errors to actively control the tilt of the platform. The LN250 Fiber Optic Gyro is very small in size (about 20 cm × 15 cm × 10 cm). Another sensor of the same model is made use of as a angular velocity sensor to measure the angular velocity of

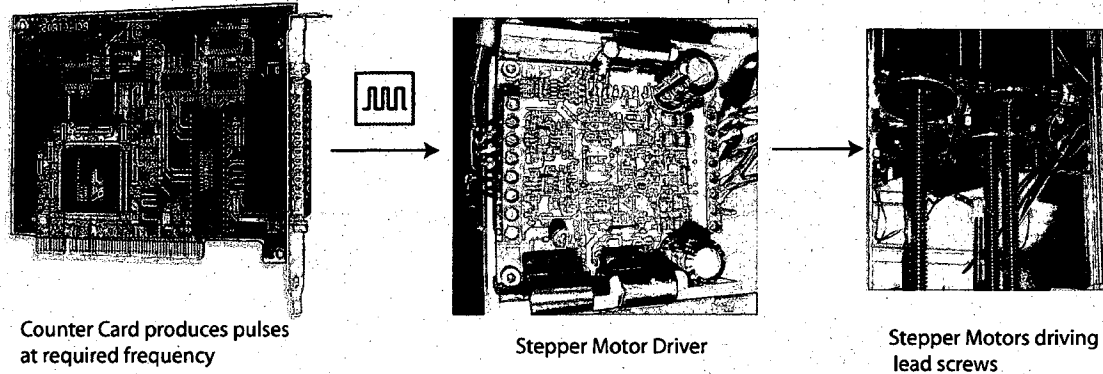


Figure 5.5: Stepper Motor actuation using variable frequency counter cards and stepper drivers

the truck floor. This angular velocity sensor forms a part of the feedforward path in the control. This sensor is made use of during mobile surveys when the mechanical disturbances are much higher than when static.

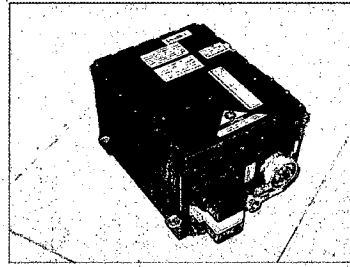


Figure 5.6: Lytton LN250 Fiber Optic Gyro: used to measure angular velocity and tilt

5.3 Control System

The angle of the platform is actively controlled by using a negative feedback loop. The schematic in Figure 5.8 shows the control loop with the fiber optic gyroscope mentioned in section 5.2.5 and the stepper motors as actuators (as described in section 5.2.4).

5.3.1 Controller

The stepper motors are controlled using computer running on xPC TargetTM operating system. This control computer is a personal computer which has a number of PCI cards that receive and send data to actuators and from sensors. All control programs are written on another host computer and transferred to the control computer (Target) through the ethernet. The programs are written in MatlabTM Simulink environment. This controller executes a negative feedback loop by measuring the error in the tilt of the platform and then actuating the stepper motors to overcome the error. This xPC Target system was used in order to be able to change the control architecture easily and be able to prototype various architectures in a very short time. The schematic of the entire system is shown in Figure 5.8.

5.3.2 Control loop

When the truck is stationary a negative feedback loop is used with a proportional gain to control the angle of the platform mainly for aligning the platform with the local level. The tilt angle is provided by integrated data of angular velocity measured by the fiber optic gyroscope (LN250). However, when the truck is in motion, the disturbances are higher (Figure 5.2) and to compensate for the higher disturbances feedforward of angular velocity of the truck is also used. For the feedforward, the controller directly makes use of the angular velocity measured by the fiber optic gyroscope (LN250) which is on the floor of the truck. A schematic of the control loop is shown in figure 5.7.

5.4 Alternate Passive Isolation concept

An alternative passive isolation concept was tested earlier which made use of very low resonance frequency passive isolator (less than 1 Hz resonance). The passive isolator made use of a 'Negative Stiffness Mechanism' which consists of a load perched on top of nearly buckled columns. Very low resonance frequencies are difficult to achieve in case of large masses. For example, in our case, the load was more than 200 kg. A

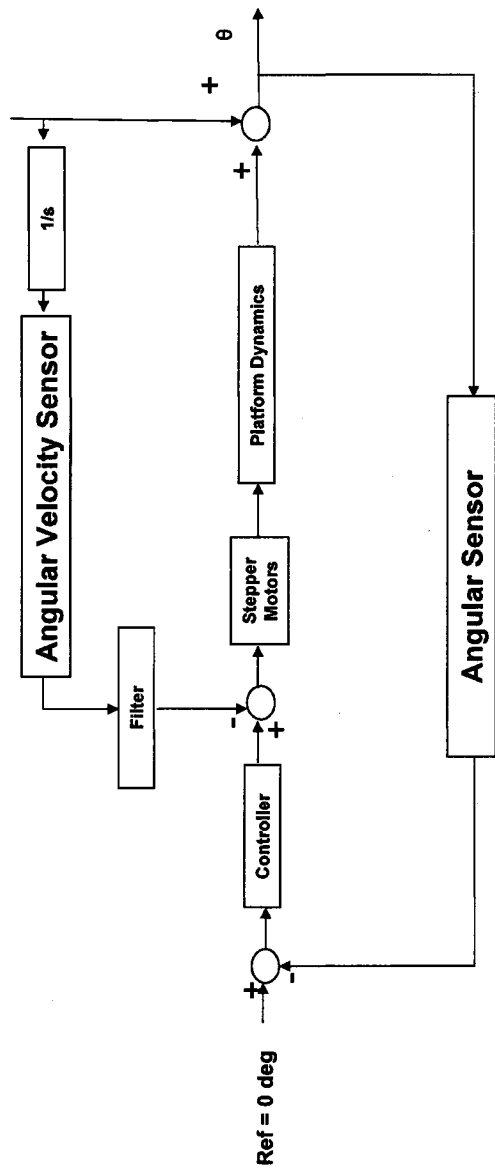


Figure 5.7: Schematic of platform stabilization control system consisting of feedback of platform angles and feed-forward of truck floor angular velocities

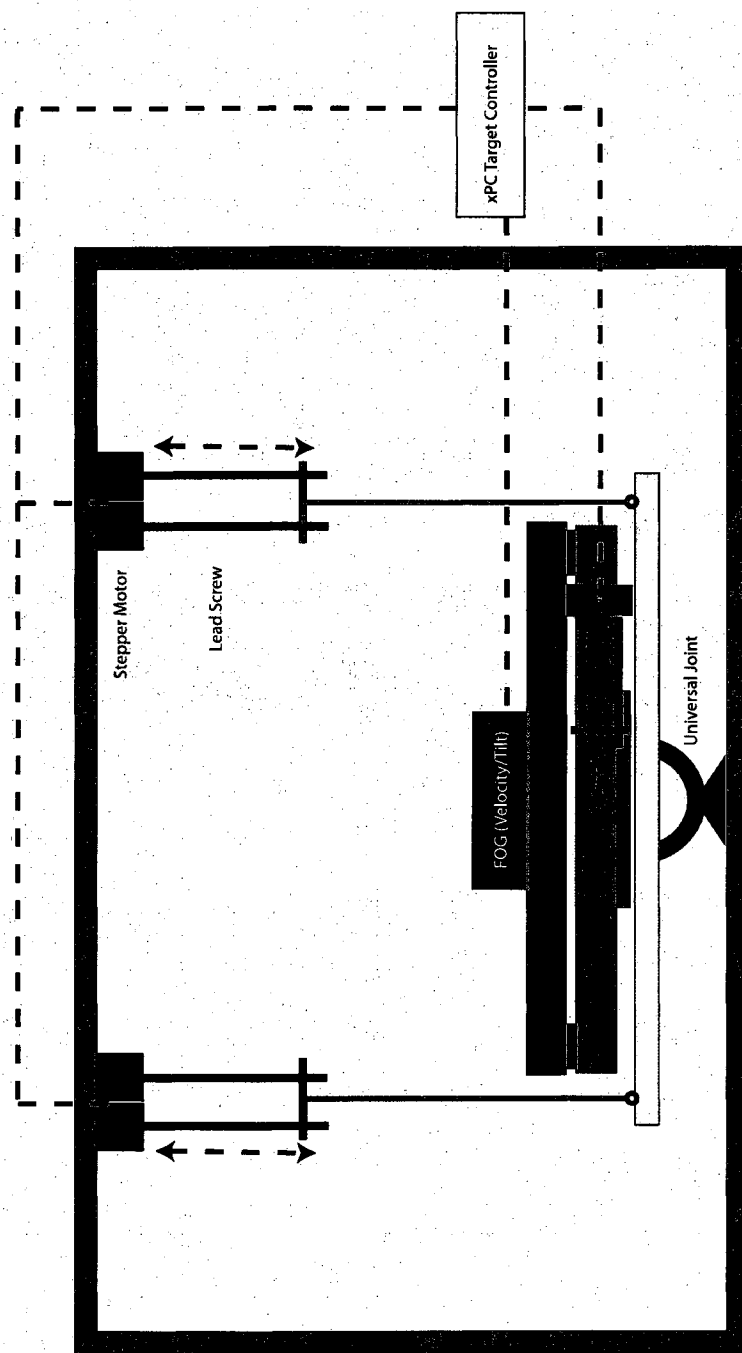


Figure 5.8: Schematic of Pitch, Roll and Yaw actuation of Gradiometer Platform

spring designed to take such a high load will need to be made with very thick wire and hence will need to be extremely long (hundreds of meters) in order to achieve low resonance frequencies as 1 Hz. However negative stiffness mechanism relies on columns in nearly buckled state. The column takes up the load in the longitudinal direction. However in the horizontal direction the buckled column offers very low stiffness which leads to a very low resonance frequency.

$$\text{Resonance Frequency} \propto \sqrt{\frac{\text{stiffness}}{\text{load}}} \quad (5.3)$$

Figure 5.9 shows the passive isolation system consisting of the negative stiffness mechanism from Minusk Technology Inc [59]. Even though this system is suitable for low disturbance situations such as a static case, it is not suitable for cases when there are large accelerations/decelerations such as in a stop-and-go mode of testing. When the truck is stopped suddenly or encounters a bump on the path, then the load undergoes large oscillations for a prolonged period of time (due to very low stiffness and very low damping).

Also the size of the atom interferometer sensors increased significantly due to the addition of large vacuum enclosures to prevent jitter in Raman beam due to the temperature induced changes in refractive index of the air in the beam path. Due to the large oscillations and due to the size constraints the negative stiffness mechanism was removed from the design. However, negative stiffness mechanisms would be of great use in cases where there are no significant sudden changes in acceleration or size constraints. A very good vehicle for the atom interferometric gravity gradiometer are Zeppelin balloons that can move at a very low speeds close to the ground and do not start/stop suddenly.

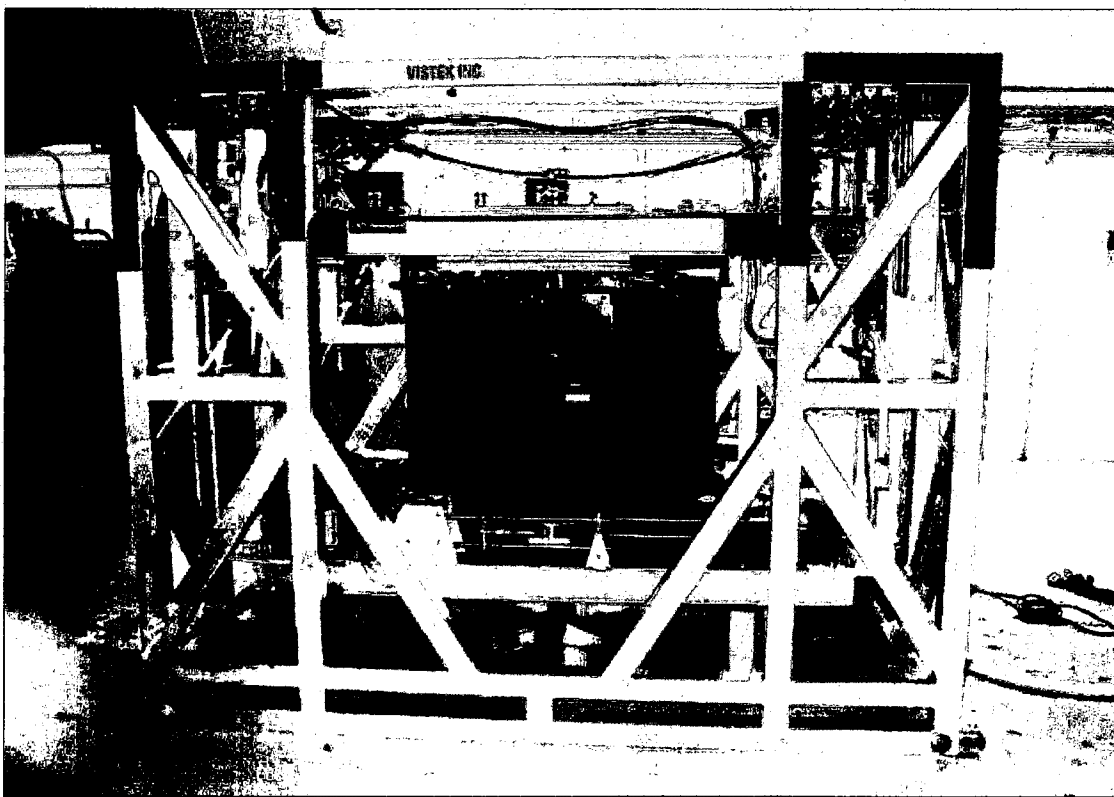


Figure 5.9: Passive isolation consisting of a negative stiffness mechanism to isolate gradiometer from disturbances on the truck floor

Chapter 6

Transfer function estimation & measurement

The atom interferometric gravity gradiometer is susceptible to platform motions especially rotations which manifest as undesirable apparent gravity gradient. In order to be able to conduct mobile gravity gradient surveys it is important to estimate and also measure the effect of rotation of platform disturbances on the gravity gradiometer. In Chapter 4 it was shown that linear accelerations of the platform do not fundamentally affect the gravity gradiometer whereas the rotations do. A model was also developed to simulate the effect of rotation on the gradiometer. The theoretical estimation of the effect of platform rotations on apparent gradient has been predicted by methods previously discussed in Chapter 4. In this chapter the experimental measurement of the transfer functions will be discussed. Discovery of deviations from expected values led to identification of misalignment of Raman Laser with atom clouds and further led to development of a new method of aligning Raman beam with the atom clouds.

6.1 Expected Transfer Function

In case of an ideal gravity gradiometer where the Raman beam is perfectly aligned with the atom clouds, the gradiometer interferometer phase (which is proportional to gravity gradient as shown in 4.1) depends on the frequency and the phase of the

platform oscillations. The phase of the platform oscillations is defined using the time interval between the rising edge zero-crossing time of the platform and the drop time of the atoms. Phase $\psi_{A/P}$ is given by:

$$\psi_{A/P} = 2\pi\Delta t/T_{osc} \quad (6.1)$$

Δt is time duration between rising edge zero-crossing of the platform oscillation and drop of atoms. T_{osc} is the time period of the sinusoidal oscillations (see Figure 6.1)

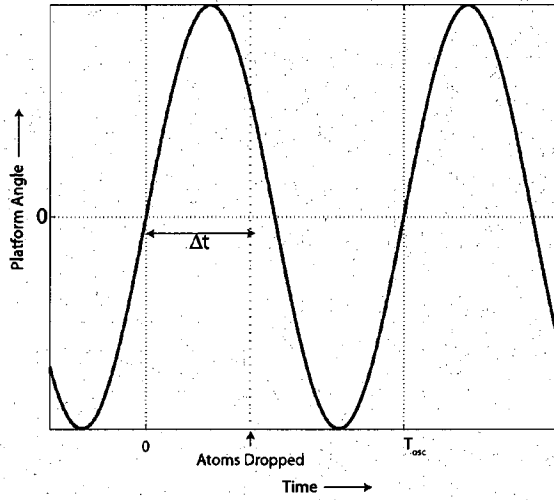


Figure 6.1: Phase is defined with respect to positive edge zero-crossing time of the platform and dropping of atoms

The phase of the gradiometer ($\psi_{A/P}$) is an important parameter since at a given frequency, the effect of the disturbance can be zero at certain phases. For example in Figure 4.5 one can observe that at certain phases the phase difference of the gravity gradiometer is not affected by platform pitch oscillations whereas at certain other disturbance phases it is quite high.

For such a gradiometer the transfer function shown in Figure 6.2 has been calculated (in Chapter 4.2).

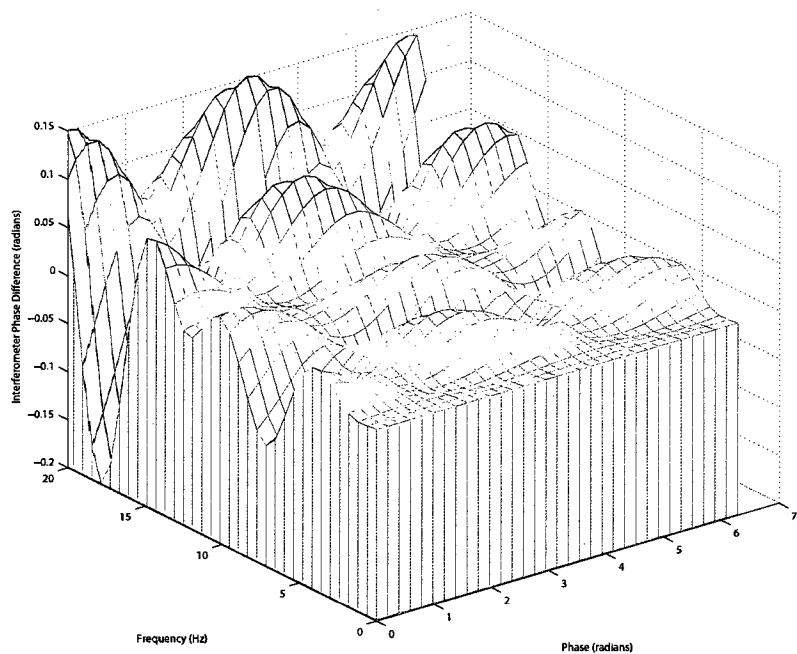


Figure 6.2: Transfer function for platform disturbance to apparent gravity gradient (Z axis is gradiometer interferometer phase in radians)

6.2 Coarse alignment by blasting atom cloud

The sensor cells are enclosed within vacuum chamber. When the vacuum chamber is evacuated the initial alignment of the Raman laser is lost due to the strains on the vacuum chamber after the evacuation. Hence it is necessary to align the Raman laser with the atom clouds after the chamber has been evacuated. This alignment is carried out by 'blasting' the atom cloud with a resonant laser beam.

6.2.1 Blasting of atom cloud

In this method, instead of using two counter propagating lasers only one beam is used. This beam takes the atom from the ground state to an intermediate unstable level. Since this is not a stable state, the electrons spontaneously decay to either $F=3$ or $F=4$ levels. But during this decay, a photon is emitted and the atom recoils in the opposite direction. However, this photon emission is in a random direction and not along any particular direction. Hence the atom recoil is also in random direction during the spontaneous decay. Due to this recoil in random direction the cluster is broken (Figure 6.3). At the end of the sequence the number of atoms is measured.

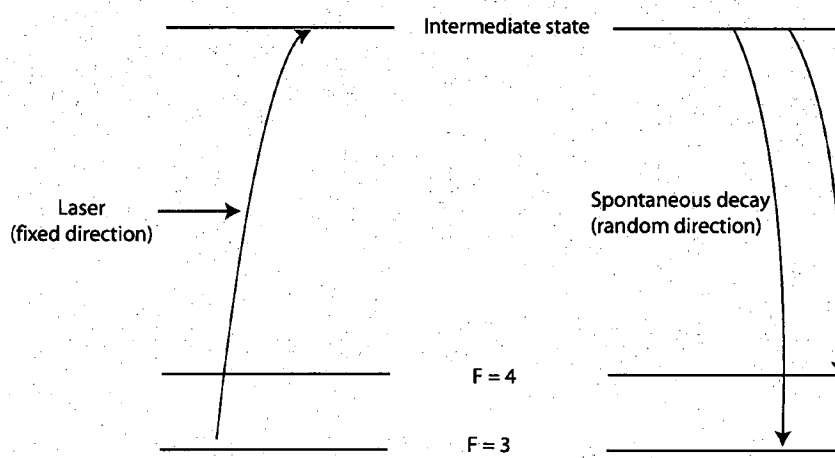


Figure 6.3: 'Blasting' of the atom cloud using spontaneous decay which emits photons in a random direction

If the laser was aligned with the cluster of atoms, then the maximum number

of atoms are subjected to this randomly directed recoil velocity and hence a large number of atoms move out of the cluster. If the beam was not aligned with the atom cluster then the number of atoms that are lost from the cluster is lower.

At the end of the fountain, the total number of atoms in F=3 and F=4 are measured. A large number of atoms present at the end of the cycle would mean the laser was not aligned well (and vice versa a small number of atoms means the laser was aligned well).

6.2.2 Alignment

The atoms in the gradiometer interferometer sequence receive momentum kicks from a counter propagating lasers. The net effective momentum kick received by the atoms depend on the direction of the effective propagation vector of the system given by Equation 6.2:

$$\mathbf{k}_{\text{eff}} = \mathbf{k}_A - \mathbf{k}_B; \quad (6.2)$$

Both \mathbf{k}_A and \mathbf{k}_B have to be aligned individually to ensure that the \mathbf{k}_{eff} is aligned with the center of the atoms. There are two sets of these beams - one at the top of the fountain for π pulse and one at the bottom for $\pi/2$ pulses. A cube corner re-routes both these laser beams to be able to reach both these positions. A schematic of the setup is shown in Figure 6.4.

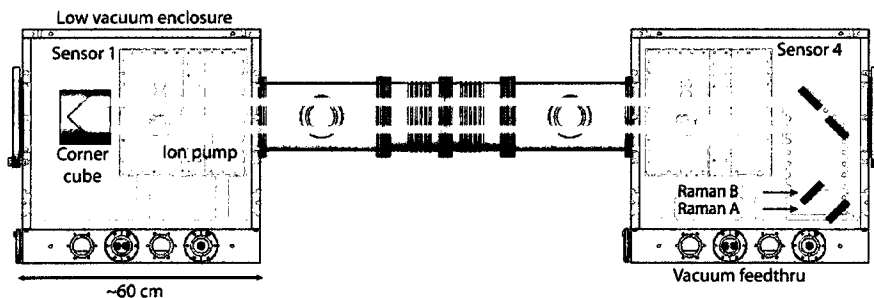


Figure 6.4: Raman Beam Path in the atom interferometric gradiometer

Atom blasting technique is used to align these lasers. Since the mirrors that control the direction of the beams are inside the vacuum enclosure, all the mirror mounts are controlled using motors remotely from outside (mounts contain PicomotorTM which actuates a piezo controlled jaw that holds a screw). Each mirror mount allows rotation in two degrees of freedom. Two such mirror mounts are used for each of the laser beams.

During the alignment process to check if the atoms are already well aligned the direction of the laser is changed by a small angle (about $250 \mu\text{rad}$) by actuating the mirror mount. Suppose the laser beam was not very well aligned initially and was at the edge of the atom cloud, then after this change in angle a large part of the beam passes through the atom cloud. So after this change in angle, more atoms get blasted and hence we observe a large decrease in the number of atoms that remain in the fountain path. This technique is used to identify if the laser beam is close to the atom clouds or not. (If the laser beam is already well aligned with the atom cloud, then the change in the number of atoms is not much.)

This technique is repeated on both beams k_A and k_B .

6.3 Experimental Measurement Setup

In order to measure the effect of platform rotations on the gravity gradiometer, the platform is actuated to oscillate in sinusoidal motion in pitch and yaw degree of freedom at various frequencies. The platform angle was controlled using negative feedback controller using a fiber optic gyro as a tilt sensor and stepper motors as actuators as described in Section 5.2. The reference sinusoid for the negative feedback was generated by xPC Target controller.

6.3.1 Fixing atom drop phase

The time of drop of atoms in the gradiometer sensor cells had to be timed accurately in order to control atom drop phase ($\psi_{A/P}$) which depends on the time delay between the instant of platform tilt zero crossing and the drop of the atoms (as shown in

Figure 6.1).

The platform oscillation lags the reference sinusoid by a fixed amount of phase ($\psi_{P/R}(f)$) for a given frequency due to the fact that the platform angle is controlled by a closed feedback loop with a tilt sensor on the platform. Hence the reference sinusoid was used to determine the time of atom drop. The atom drop was triggered by maintaining a fixed amount of delay (Δt) with respect to the zero crossing time of the reference sinusoid. Hence the phase lag between the atom drop and reference sinusoid was fixed ($\psi_{A/R}$). The parameter that affects the transfer function is the phase between the atom drop and the platform motion ($\psi_{A/P}$) given by Equation 6.3.

$$\psi_{A/P}(\Delta t, f) = \psi_{A/R}(\Delta t) - \psi_{P/R}(f) \quad (6.3)$$

However if the platform oscillation frequency changes, then the phase difference between the platform and reference ($\psi_{P/R}(f)$) changes.

6.3.2 Measurement Setup

In order to measure the transfer function the apparent gravity gradient has to be measured at various frequencies (f) and atom drop phases ($\psi_{A/P}$). The speed of measurement could be increased by either sweeping through a given range of frequencies while holding the atom drop phase constant or by sweeping through atom drop phase while holding the frequency constant.

The latter case was adopted since at a fixed frequency (f_0) the phase difference between reference sine input and the platform angle ($\psi_{P/R}(f_0)$) and hence the phase difference between atom drop and the reference is also fixed ($\psi_{A/R}$). Experimentally it is much easier to control ($\psi_{A/R}$) as it only requires delaying the drop of atoms by a fixed amount (Δt) with respect to the reference sinusoid which can all be programmed ahead of time without the need for finding the platform zero crossing time in real-time. To scan through entire 0 through 2π range of atom drop phase, the atom drop time offset (Δt) just needs to be incremented from 0 through $1/f$ (where f is the frequency of the platform disturbance). Figure 6.5 shows a schematic of the phase control setup followed during the experimental measurement of the apparent gradiometer phase

due to platform oscillations.

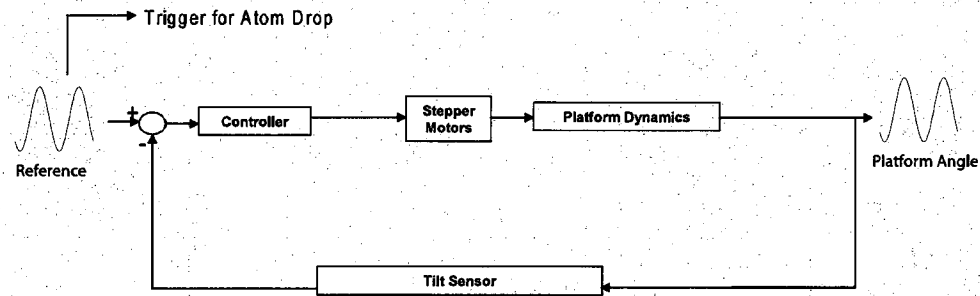


Figure 6.5: Controlling atom drop time with respect to platform zero crossing time

In contrast, it would be cumbersome to hold the atom drop phase a constant while varying the frequency of the platform oscillations since that would require prior measurement of the platform phase lag with respect to reference accurately.

6.3.3 Synchronization

In the experimental setup, the trigger to drop atoms was generated by platform control computer and was transmitted to the gradiometer controller which ultimately controls the Magneto Optical Trap that is turned off in order to drop the atoms .

The platform and the gradiometer were controlled through two different computers. But in order to be able to finally estimate the noise in the gradiometer system due to platform disturbances, it is important to synchronize the platform and gradiometer control computers. To synchronize, a separate computer was used to receive pulses from the platform and gradiometer control computers. But apart from synchronizing at one particular time instance it is also important to know if the clocks in these control computers are either running slower or faster with respect to the other.

Hence a stable frequency source slaved to an atomic clock (SRS FS725) was used to send pulses at 10 Hz to all of the computers. Finally before processing the data, all time scales recorded by the computers were either stretched or shrunk to match with the stable frequency source (see Figure 6.6).

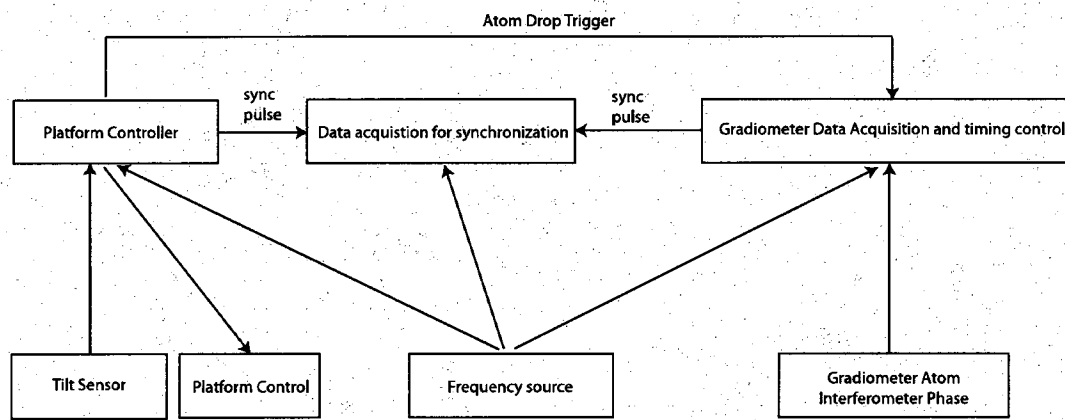


Figure 6.6: Acquisition and Synchronization of data collected by platform and gradiometer control computers

6.4 Insufficient alignment of Raman beam with atoms

With the setup described in the previous sections, the transfer function from the platform disturbance to the apparent gravity gradient were measured. The first measurements were carried out after coarse alignment using atom blasting technique described in Section 6.2. The first results showed deviation from the expected transfer function. When the atom drop phase was swept through 2π radians, while the platform pitch oscillation were set at 6 Hz the resulting apparent gravity gradient had only one peak and one valley as seen in Figure 6.7. Also the magnitude of the apparent gradiometer phase was much higher than what was expected by the simulations.

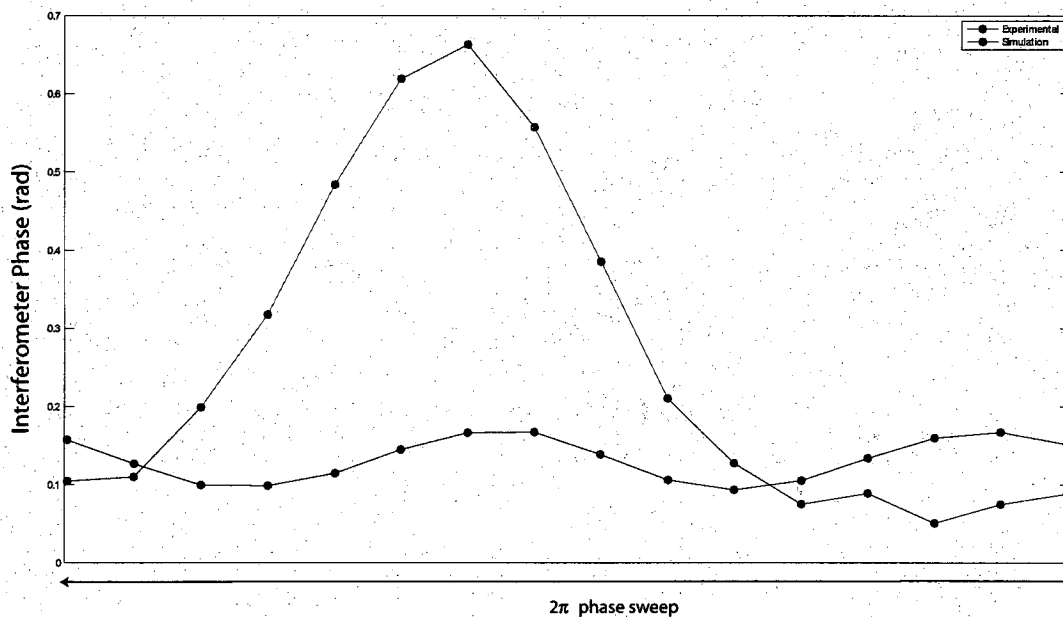


Figure 6.7: Response of the Gravity Gradiometer for 6 Hz platform oscillations shown in red. Note the deviation from the expected response based on simulations (shown in red) for a perfectly aligned gravity gradiometer

The cause of the deviation from expected simulated values was found to be due to misalignment of the Raman Laser with the atom clouds. It was found that the alignment of the laser done by the atom blasting method (discussed in section 6.2) is best only up to about $300 \mu\text{rad}$ (misalignment is denoted by α in figure 6.8). The problem is due to the fact that in a nearly aligned state the sensitivity of the atom blasting technique is very low which results in the best alignment of the laser with atom clusters to only about $300 \mu\text{rad}$.

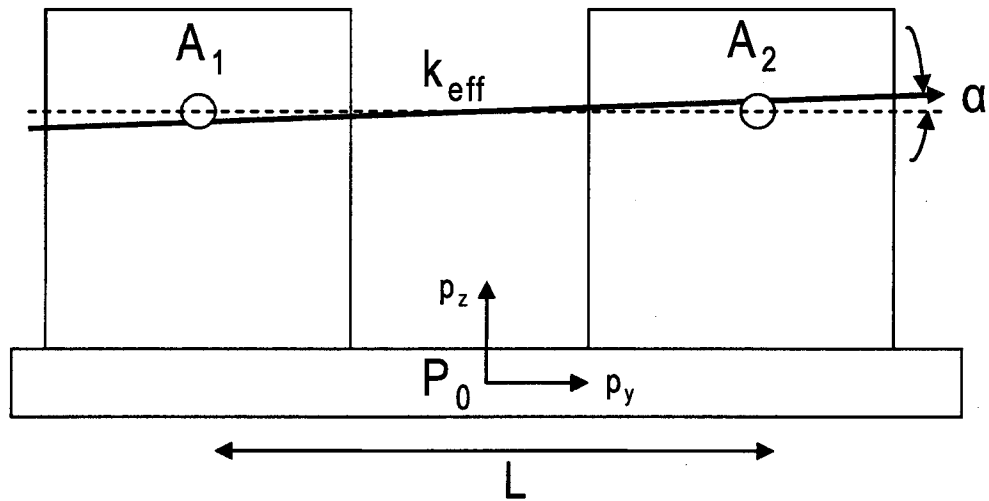


Figure 6.8: Schematic of misalignment of Raman beam with the atom clouds

The actual angle of misalignment was found by matching the simulation with experimental measurement. It is not possible to measure directly the misalignment inside the vacuum enclosure.

Figure 6.10 shows the gradiometer phase at various angles of misalignment (the

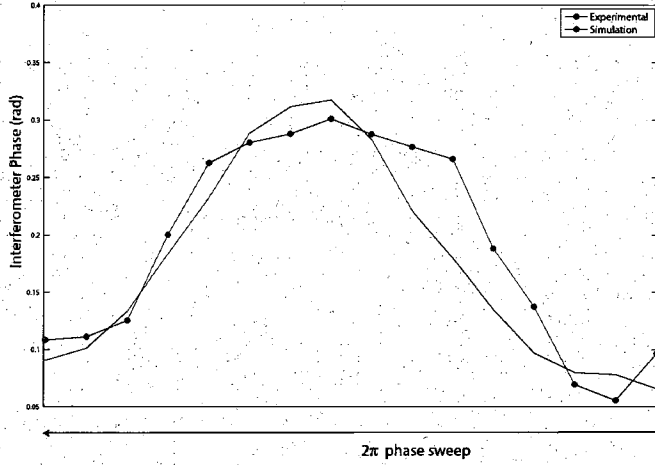


Figure 6.9: Misalignment of Raman beam with the atom clouds is measured by matching the measured gradiometer phase to platform oscillations with simulated phase.

sinusoidal oscillation of platform is at 6 Hz with an amplitude of $20 \mu\text{rad}$). Figure 6.11 shows the effect of misalignment at various frequencies of platform disturbance.

It is clear from the above simulations that this misalignment of the Raman beam with the atom clouds (α) magnifies the apparent gravity gradient due to the disturbances on the platform and is detrimental in mobile gravity gradient survey. Hence it is important to reduce the misalignment α to as close to zero as possible. The alignment process was carried out by moving the motorized mirror mounts while monitoring the apparent gravity gradient when the platform of gravity gradiometer was subjected to oscillations. The oscillations were at 6 Hz and the timing of the atom drop was changed gradually over time in order to step through disturbance phase $\psi_{A/P}$ from 0 to 2π . The platform oscillation frequency is chosen to be 6 Hz since at that frequency the apparent gradient is high since it is in between nodes of 0 Hz and 12 Hz (At 12 Hz the apparent gravity gradient is zero since it is close to $1/T$ where $T=0.084$ s is the time between the Raman pulses).

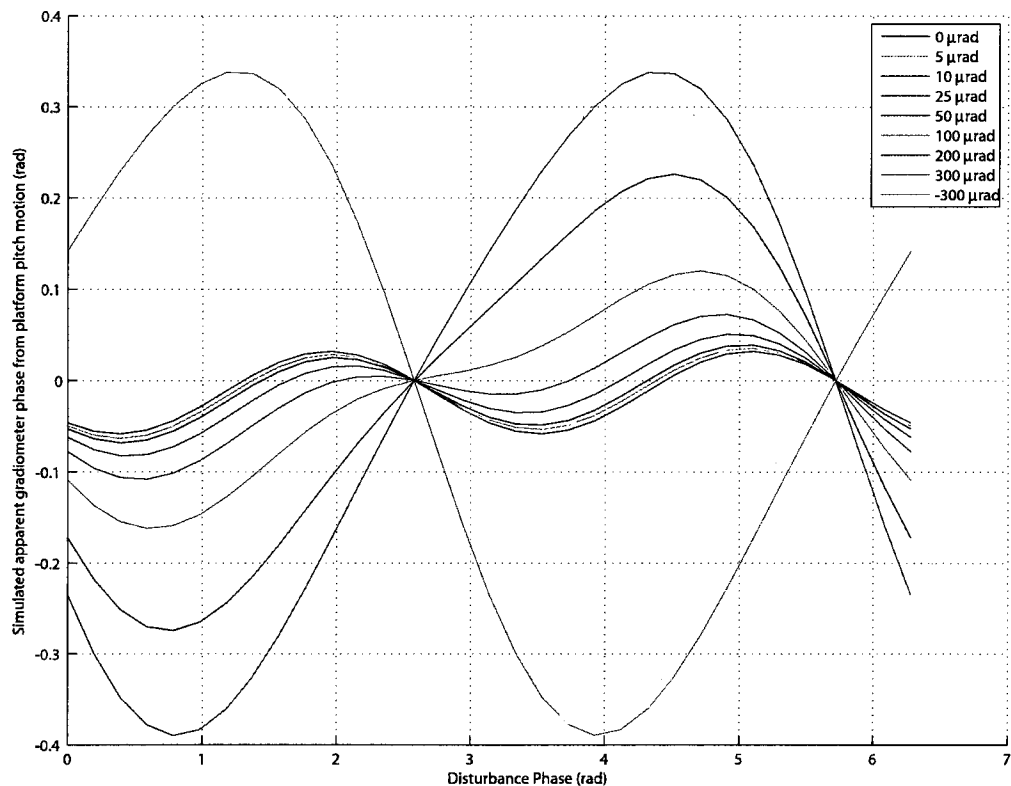


Figure 6.10: Simulated gradiometer phase at various angles of misalignment (α) of the Raman beam with the line joining center of atom clouds (the sinusoidal oscillation of platform is at 6 Hz with an amplitude of $20 \mu\text{rad}$)

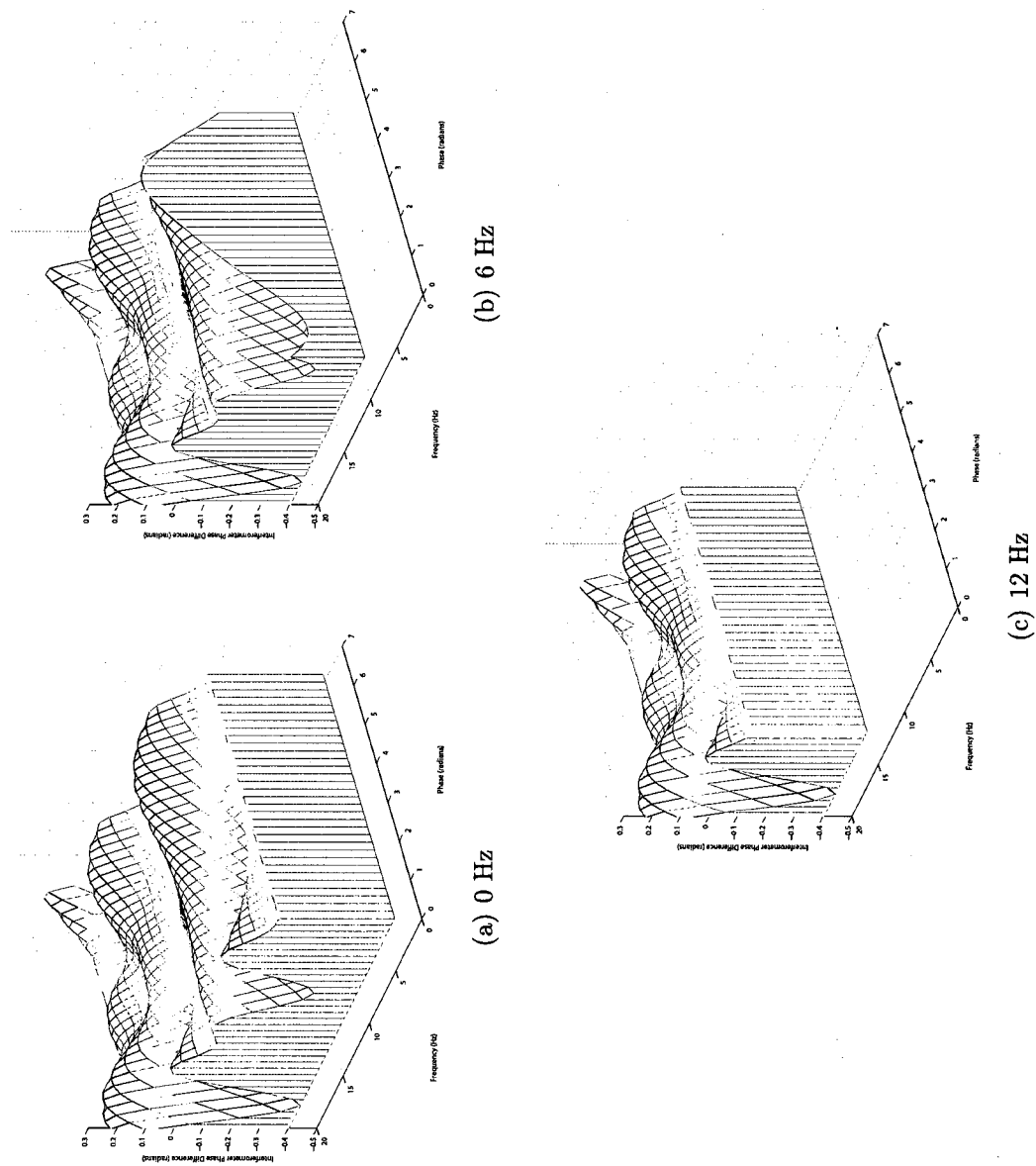


Figure 6.11: Transfer function for a misaligned Gravity Gradiometer. For a 2π disturbance phase sweep, there is only one peak in the gradiometer phase at 6 Hz (instead of two peaks for an aligned case).

The above technique has been perfected over months and now is the best way to achieve alignment such that the Raman laser is within $20 \mu\text{rad}$ to line joining the center of atom clouds (i.e. $\alpha < 20 \mu\text{rad}$).

6.5 Results

Once the Raman beam is aligned with the atom clouds, transfer functions at frequencies of $1/T$ and $1/2T$ (6 Hz and 12 Hz) were obtained to verify if the experimentally obtained apparent gradiometer phase matched with the model. Figures 6.12 and 6.13 show the experimentally measured transfer functions for platform pitch oscillation frequencies of 6 Hz and 12 Hz respectively. In the case of 6 Hz oscillations, two peaks and two valleys are clearly seen in a 0 to 2π sweep of disturbance phase.

There is no apparent gravity gradient seen at a platform pitch oscillation frequency of 12 Hz just as expected in the model. (The drift seen in the experimentally obtained transfer function is a drift due to temperature variation which was observed before and after the platform oscillation too.)

6.6 Contrast reduction

Atom interferometer phase is extracted by using an ellipse fitting method in order to overcome the issue of common phase noise in the interferometer. In each of the sensors, the ratio of atoms in $F=3$ and $F=4$ is measured. This measurement is a sinusoidal function of the common phase. Due to the presence of common phase noise, the sensor measurements can be plotted with respect to each other and since they are sinusoidal functions of common phase, the plot produces an ellipse. The differential phase is extracted from the ellipticity.

To extract phase from this ellipse fitting method, 20 shots are used. The ellipse parameters are obtained by least square fit of the ellipse [60, 61, 62].

During the actual experimental measurement of the apparent gravity gradient by oscillating the platform at a specific frequency at various disturbance phases, the ellipticity changes (since the differential phase between the sensors changes). This can

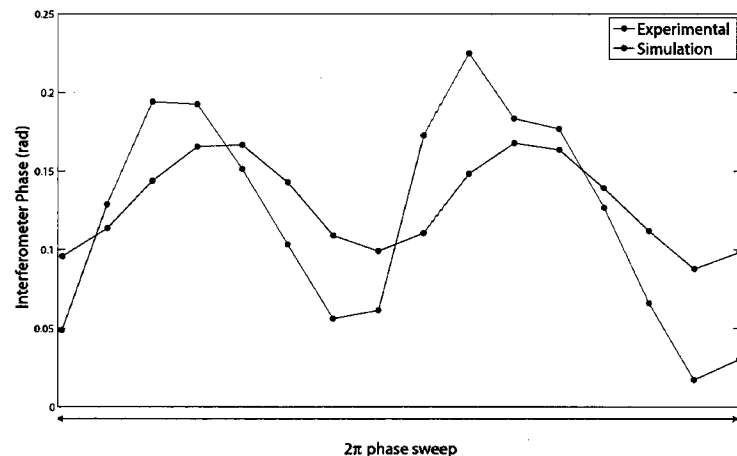


Figure 6.12: Apparent gravity gradient (red) measured by oscillating the platform at 6 Hz and changing the disturbance phase from 0 to 2π . Note there are two peaks and two valleys for a 2π phase sweep just as expected in simulations (shown in blue)

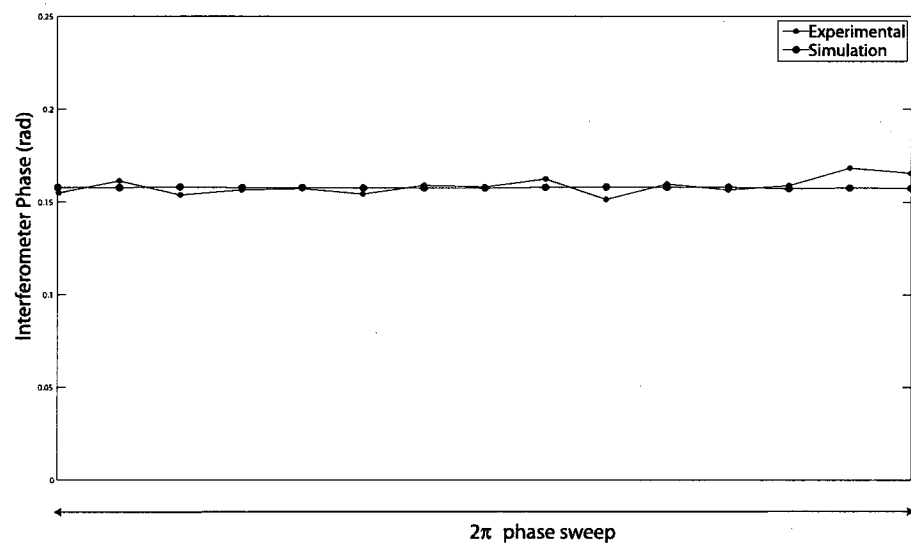


Figure 6.13: Apparent gravity gradient (shown in red) measured by oscillating the platform at 12 Hz and changing the disturbance phase from 0 to 2π . There is no effect of the platform disturbance on the apparent gravity gradient at 12 Hz since the platform is in sync with the Raman pulse timing. The simulated phase is shown in blue.

be observed in figure 6.14 clearly where the difference in ellipticity is clearly visible. However apart from the change in the ellipticity, there is also a significant change in the size of the ellipse. This is because the contrast of the sensor measurement decreases at large angular motions. In this case contrast reduction does not affect the extraction of the differential phase. This is because the amplitude of the oscillation is held constant throughout the tests and hence the contrast remains constant and hence only the size of the ellipse reduces.

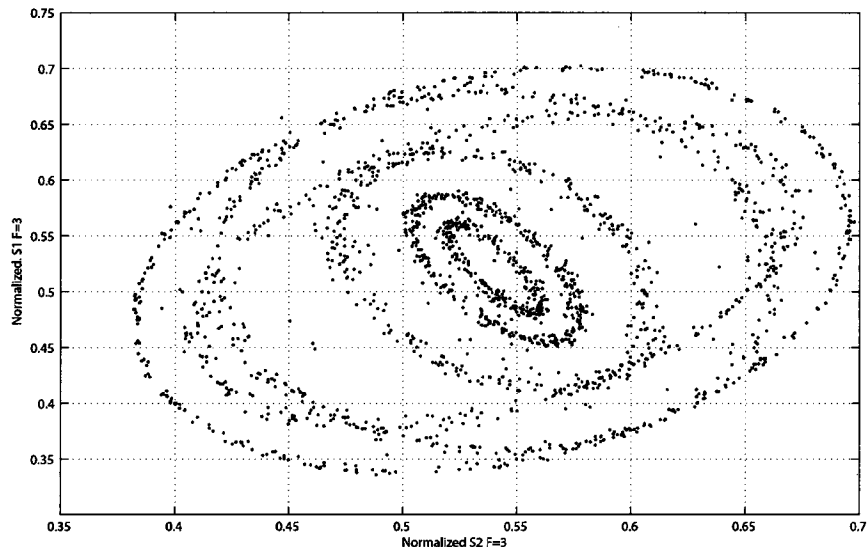


Figure 6.14: The ellipticity changes as the interferometer differential phase changes (due to change in disturbance phase while the frequency is constant). However along with interferometer differential phase change we also observe change in contrast (seen by the change in the size of the ellipses)

Chapter 7

Vehicle Motion Control

7.1 Requirements

The most important goal of this project was to measure the gravity gradients on a mobile platform. In order to reduce the disturbances on the gradiometer platform it was important to move at a uniform speed. Another requirement was to be able to move at very low speeds in order to be able to take as many measurements as possible in a very short distance. In our case we had to measure the gravity gradient of a 25 m × 68 m × 11 m which produces a prominent gravity gradient signature over a 6 m length. Each measurement takes about 8s and hence it is necessary to be able to move at as low speeds as 1 cm/s.

In order to achieve the above mentioned requirements of uniform motion and slow speed an electric drive was designed which could be used alternatively to the existing internal combustion engine drive. Some of the important requirements of the design are listed below.

- **Dual power source:** It was decided that the electric drive would be designed mainly for the uniform motion of the truck and could be aided by the internal combustion engine to overcome the static friction and start the motion of the truck. This would allow us to size the electric motor to a smaller power capacity and be able to use the limited power available from the on-board generators.

This requirement also meant that the design had to incorporate a clutch to be able to connect or disconnect the electric motor power source at any time.

- **Remote control:** To minimize the disturbances inside the truck it was required that the truck motion be able to be controlled from outside the truck. Based on this requirement it was decided to have all the controls for motor start/stop, speed of the motor, direction of rotation of motor and the clutch were all controlled through a computer. The computer in turn could be accessed through the ethernet by using a cable or through wireless connection.
- **Dismantle the electric drive from the engine drive:** In case the truck had to be transported from one area to another on city roads or highways, it was required that the electric drive be disconnected physically from any of the original transmission devices. So the design involved use of components which could be easily detached or attached from the existing transmission drive.
- **Position Measurement:** Apart from being able to move the truck with a uniform speed, it was also required to be able to locate the position of the truck accurately. The gravity gradient signatures that were expected to be measured had its entire peak structure within 6 m. Hence there was a need to position the truck with a few centimeter accuracy.

7.2 Various Design Concepts

A number of design concepts were deliberated. The most important part of the design to be chosen was the source of power. In our case, we decided to use an electric motor since the truck already had adequate electric power available which could be obtained either from the on board mobile generators or through shoreline power. There were a number of ways in which one could transfer the mechanical power from the motors to the wheels:

- **Wheel axles:** The individual wheels could be powered through use of separate motors directly driving the wheel axles. Due to the paucity of space around

the wheels, this design would require the removal of the existing axles that transmit power from the differential to be either cut or replaced to have an exclusive electric motor drive. The major disadvantages of this system were that this would allow the use of only electric motor to be used and the internal combustion engine could not be used when the truck needed to be transported long distances. Since there was very limited power available for electric drive, it could not be used for driving at required speeds on a city road or on a highway. Also this design would require the use of two separate electric motor drives for the two rear wheels increasing the complexity and possibly decreasing its reliability.

- **Differential Gear box shaft:** The other part where the electric drive could have engaged with the existing power transmission would be on a spare shaft on a differential gear box at the rear end of the truck. Since the existing gear box did not have a spare shaft, this design would require the removal of the existing differential gearbox and replacing it with a new gearbox with a spare shaft.
- **Drive shaft:** The power from the electric motor could also be transmitted to the existing drive shaft that transmits power from the front to the rear differential gear box. This would require the use of a gear, belt or a chain to transmit the power from the electric motor to the existing drive shaft. Since any of these methods of transferring power would involve applying forces on the drive shaft that would cause bending of the shaft, it was important to add any of these power transmission devices near an existing bearing that could take up the forces from the gear, belt or chain drives.

The major constraint in our case was the limited space under the truck. One had to accommodate electric motors and other components such as clutches and reduction gear boxes. Among the above different concepts the transmission of power to the drive shaft was chosen since there was sufficient space for electric motor and other components to be installed under the truck next to the drive shaft. In the next section the actual design of the electric drive is described.

7.3 Design

An AC motor was chosen to run the system. A variable frequency drive was used to change the speed of the motor. Due to the very limited availability of power inside the truck the motor had to be sized to as low power rating as possible. A large amount of power is required for starting the initial motion of the truck compared to maintain the motion of the truck once it has already started moving. Hence it was decided that the truck's motion could be started using already existing internal combustion engine and then once the truck has started moving, the power source could be shifted from the internal combustion engine to the electric motor drive. This would mean that the new design of the truck would also require a clutch system in order to be able to engage or disengage the electric motor power from the transmission.

The power sizing of the motor was now dependent only on the power required to run the truck after the truck had already started running. At very low speeds most of the power is dissipated in tires and bearings. The air resistance is negligible at low speeds at which the truck was being designed to run (less than 0.5 m/s). The estimated power required to overcome air resistance at a speed of 1 m/s is about 5.6 W. $P = \frac{1}{2}\rho v^3 A C_d = 5.58$ W assuming air density $\rho = 1.293 \text{ kg/m}^3$, speed $v = 1 \text{ m/s}$, area of the front surface of truck $A = 8.64 \text{ m}^2$, coefficient of drag $C_d = 0.5$). The power required to overcome friction is due to rolling resistance and friction in bearings in other parts are significantly higher. If the coefficient of friction (due to rolling resistance) is assumed to be 0.03, then the power required to overcome this friction at a speed of 1 m/s is about 2 kW. Since the truck was being designed to run at speeds of about 0.5 m/s or lower, a 2 kW motor would be more than sufficient. Hence a 2.2 kW (3 horse power) motor was chosen to run the drive system.

Typical motor speeds for these motors is about 1200 rpm. To transmit the power from the motor to the drive shaft at lower speeds, an appropriately sized gear box (SEW Eurodrive R97 AM213) was included in the design. In order to be able to engage and disengage the power transmission from the electric motor a clutch-brake

assembly was included. Chain drive is used to transmit the power from the electric drive to the drive shaft. The speed of the motor was to be controlled by using a variable frequency drive which changes the speed of the motor by changing the frequency of the AC power supplied to the motor.

A CAD model of the entire electric drive system design is shown in Figure 7.1.

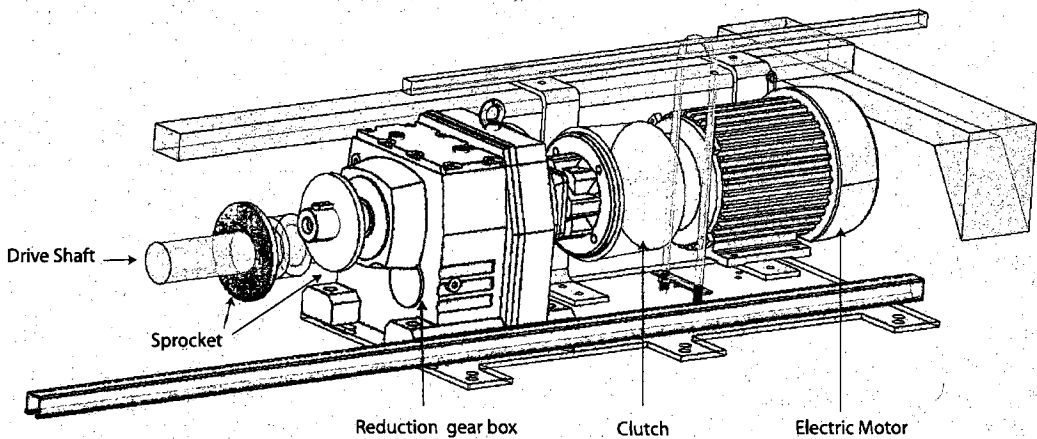


Figure 7.1: Electric Drive System for the truck used for mobile gravity gradient measurement

7.4 Installation

In order to access the area where the electric drive was to be installed the truck had to be lifted up by about 30 cm. Due to lack of space near the front of the truck to use a jack, a five U.S. tonne crane was used to lift the front axles of the truck (see 7.2). Rear of the truck was lifted using jacks. Installation of this system required the truck to be elevated by more about 30 cm on heavy wooden blocks using jacks and crane.

In order to transmit the power to the existing drive shaft of the truck a chain drive was designed. It was important that the entire electric drive be physically disengaged from the existing drive shaft so that the truck can return to its original configuration if it is required to travel long distances on a highway. Hence it was decided to not



Figure 7.2: A five Tonne crane was used to lift the front axles of the truck and place them on a 30 cm wooden blocks

to cut or bore through the existing drive shaft to install chain sprockets. A split-sprocket was used. The two halves of the sprockets were attached to the drive shaft using friction between the sprockets bore surface and the surface of the drive shaft. In case the electric drive has to be physically disengaged, then the bolts on the split sprocket just needs to be loosened to completely remove the sprocket out of the drive shaft. Figure 7.3 shows the split sprocket installed on the drive shaft just in front of the existing bearing.

Custom made brackets were installed to hold the electric drive system in place. The brackets were so designed that it would be possible to install the entire electric drive by using just 6 bolts from underneath the truck.

After the electric drive system was assembled and installed on a base plate, the entire system was lifted up using jacks and attached to the custom made fixtures that

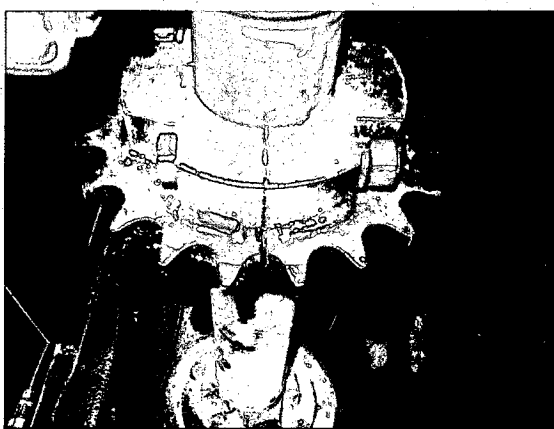


Figure 7.3: Split sprocket on the drive shaft is held by the friction between the sprocket and shaft surfaces. This split design allows for easy installation/removal

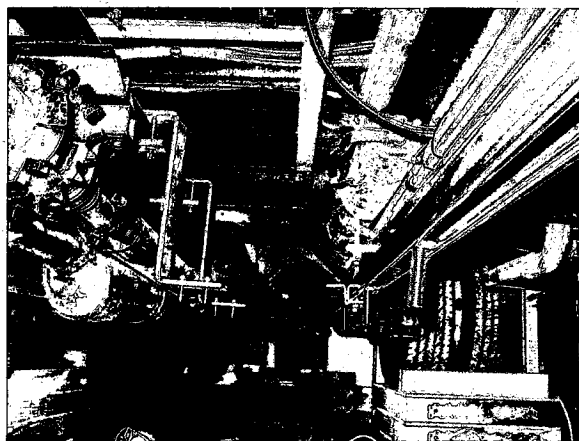


Figure 7.4: Custom made fixtures for holding the electric drive system were installed on the chassis.

were already bolted on to the truck chassis.

After securing the drive in position, the chain was installed over the sprockets. The chain had to be taut to reduce backlash in order to be able to reverse directions quickly if required.

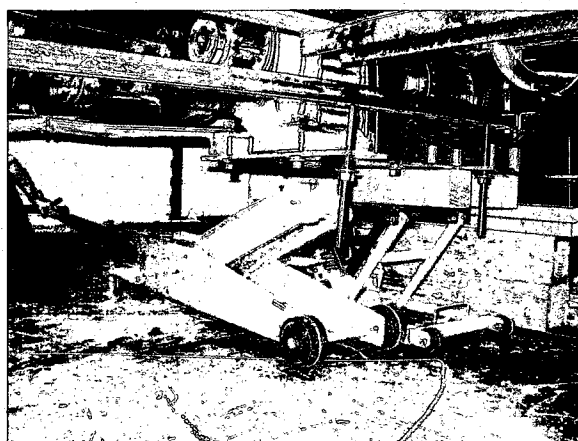


Figure 7.5: Electric drive system already assembled on a base plate was lifted using jacks for installing on the fixtures

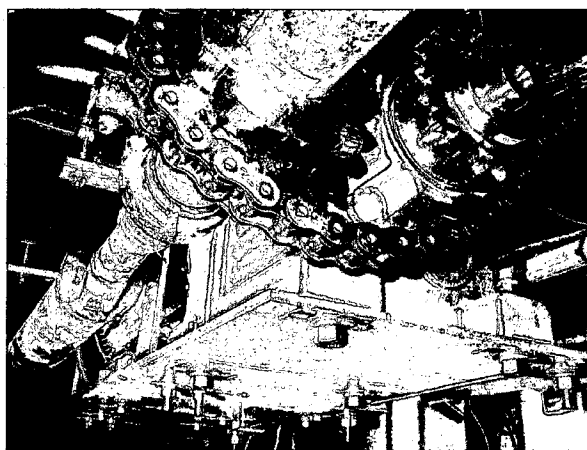


Figure 7.6: Electric drive seen from below the truck after installation of all the components

7.5 Positioning using differential GPS

Locating the position of the truck accurately within a few centimeters was very important. The expected gravity gradient signatures were found within a short distance of about 6 m. A Trimble Global Positioning System (GPS) receiver typically provides location information with an accuracy of about 2 m to 10 m depending. Inaccuracies

depend on the number of satellites visible at any given time and a number of other factors including the refraction of electromagnetic waves through the ionosphere. In order to improve the accuracy of the system a dual GPS receivers were used. One GPS receiver was located on top of a building close to the survey area. The location of this stationary GPS was measured with very high accuracy by averaging the location data over a 24 hour period. Once the location of this base station GPS was established, all the future measurements of this GPS is compared to the actual location and the error is transmitted to another GPS which is on the truck. The GPS receiver on the truck subtracts this error from its calculated position. This way the error in positioning is considerably reduced and is within about 1 cm.

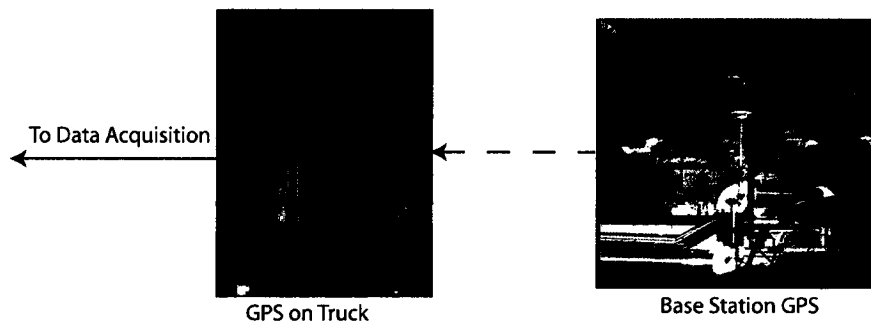


Figure 7.7: Differential GPS system installed on the base station and on the truck for achieving positioning accuracies to within 1 cm

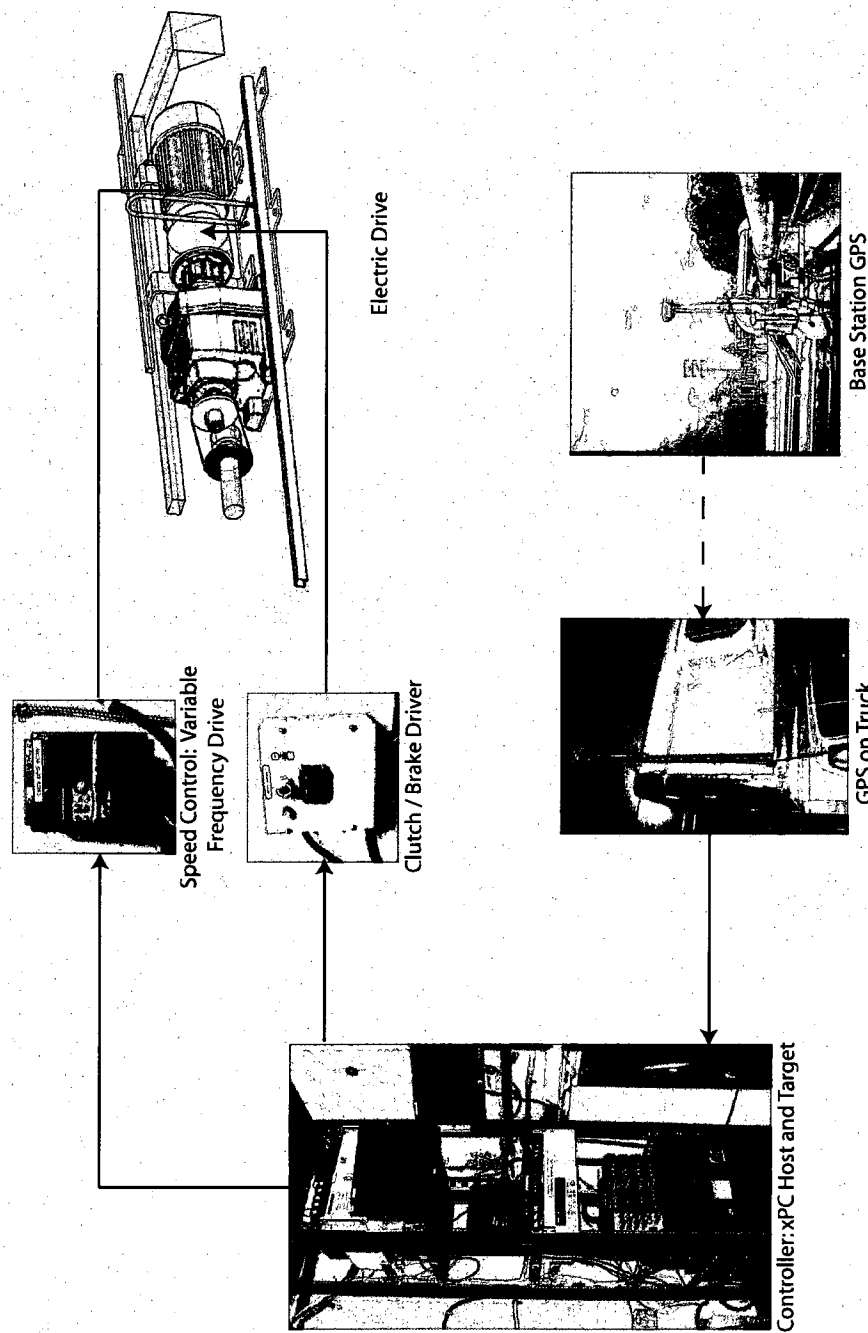


Figure 7.8: Schematic of Truck electric drive and position measurement. An xPC Target computer controls the truck electric drive system as well as receives data from GPS. This computer is controlled from outside the truck through ethernet.

Chapter 8

Mobile Gravity Gradient Measurement

Measurement of Gravity Gradient while the platform is traversing has been the ultimate goal of this project. As mentioned in Section 1.3 mobile gradiometry has a significant use in inertial navigation systems and in resource exploration for earth and even other planets and satellites of the solar system.

In this chapter, the process of measurement of the mobile gravity gradient and the survey results are described. Measurement of transfer functions (described in Chapter 6) and compensation of disturbances play a critical part in the mobile gravity gradient surveys. Estimation and Measurement of apparent gravity gradient due to platform motions also provide a means for both determining the platform requirements for mobile gradiometry as well as to estimate the net phase noise due to platform motion. The survey results are described and an estimate of the error in gravity gradient measurement due to platform motion has been described.

8.1 Survey Area

The survey location was chosen to be the entrance of our office building End Station 3 of Hansen Experimental Physics Laboratory (HEPL) (See Figure 8.1)). End Station 3 is an underground facility with about 2.25-2.5 m thick walls and ceiling. It consists

of an open void of dimensions 28 m x 65 m x 11 m . Due to this large void in the earth and due to the absence of a large part of the building wall at the entrance of the building, there is a significant amount of gravity anomaly in and around the building.



Figure 8.1: Survey Area for mobile gravity gradient measurement: Entrance of Hansen Experimental Physics Laboratory (HEPL), End Station 3 (Stanford University)

The gravity gradient at the entrance of the HEPL End Station 3 was significantly higher compared to the surroundings (inline gradient in a direction perpendicular to the boundary of the building). At the entrance, if one were to travel in and out of the building a gravity gradient anomaly of about 250 E can be measured within a distance of about 6 m. It was decided to conduct the gravity gradient survey at the entrance of the End Station 3 as shown in Figure 8.2 by the survey line. Even though there were larger gradients near the edge of the loading bay, it was not possible to

traverse over those areas since the width of the truck and protrusions on the wall would not allow the gradiometer to be above those regions.

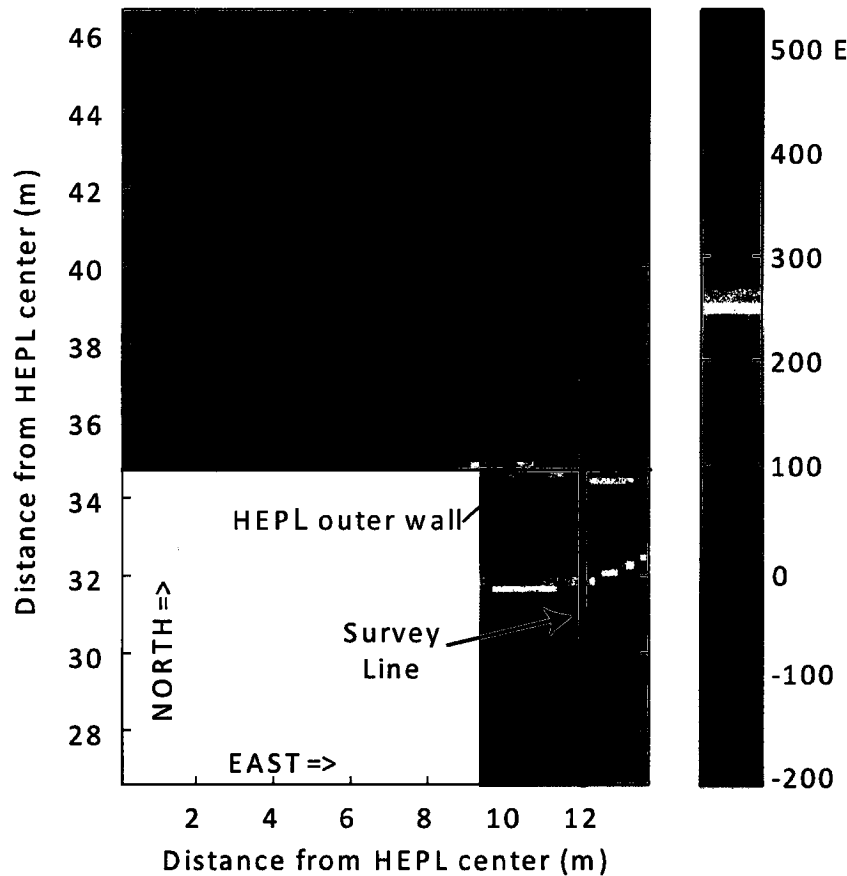


Figure 8.2: Inline Gravity Gradient T_{yy} (along north south direction) around HEPL End Station 3 where mobile gravity gradient survey was conducted

8.2 Survey Vehicle Motion and Position

The truck which carries the gravity gradiometer has to be moved in and out of the End Station 3 entrance. This motion of the truck had to be smooth so that disturbances due to the motion of the truck were minimized in order to minimize the platform motion which that in turn would minimize the resulting apparent gravity gradient

due to platform motion. This truck was retrofitted with an electric motor drive in order to move at very low speeds as well as with a constant speed. The slow speed is necessary since each of the gravity gradient measurement takes about 8 s and the entire length of the gravity gradient anomaly signature was within a short distance of about 6 m.

Under normal idling speeds of a typical truck (of about 0.75 m/s on a flat surface) would cover the entire stretch of 6 m in about 8 s which means that during the entire stretch of the gravity gradient signature only one or two measurements could be obtained. Hence the truck had to be considerably slowed down in order to be able to make multiple measurements within the small stretch. The truck was made to move at about 0.01 m/s using the electric drive and hence this system provided us the ability to make a significantly large number of measurements in the small stretch.

In order to minimize the disturbances inside the truck nobody was present inside the truck while conducting the survey. The motion of the truck was completely controlled from outside the truck. All computers used to control the gradiometer, platform motion and truck motion were all remotely operated. To position the truck precisely at the starting point (which acts as a reference) electrically operated brakes were used which were also operated through computers remotely. In order to maintain reliable communication to computers within the truck wired ethernet communication was used. Also the power to the truck motion and all the equipments inside the truck including the gradiometer was supplied from the building power supply at End Station 3.

Apart from being able to traverse the entrance at a slow speed, it was also essential to locate the position of the truck precisely in order to be able to locate the gravity gradient measurements. A pair of GPS receivers in real time kinematic positioning mode were used for this purpose. One receiver was stationed on the roof of a neighboring building while another one was on top of the cab of the truck (base station GPS: Trimble R8, Rover GPS: Trimble 5800). It was necessary to locate the GPS at the front since that was the only part of the truck which would be in direct line of sight with the GPS satellite constellation the maximum amount of time. Another GPS was used as a base station for monitoring errors in positioning. These GPS

receivers were part of a Real Time Kinematic positioning system which was able to provide centimeter level accuracy in positioning. (Chapter 7 describes in detail about the electric motor drive and the positioning system). Since the entire southern sky as well as most of northern sky close to the horizon was not in view, the positioning was possible only certain times of the day when the constellation of the satellites were such that the receiver was in the line of sight with at least 4 GPS satellites.

8.3 Platform stabilization

The disturbance levels on the platform (after active disturbance compensation with feedforward and feedback) are low enough to permit the measurement of the interferometer phase difference.

The platform motion has to be actively compensated since the atom interferometer works only in a small range of platform motion. Some of the restrictions are due to the fact that after the atoms have participated in the interferometer process, the atoms have to finally go through a narrow region that is detectable by the quad-detector which is where the number of atoms in each state is measured. Due to this restriction the platform has to be close to horizontal so that the trajectory of the atoms at the end of the fountain passes through the region detected by the quad-detector. Hence it is not possible to make measurements on this sensor in a 'strap-down' mode where the gradiometer platform can undergo any unlimited motion since that would result in atoms not going through the required region for the quad detectors. Hence there is a need for a stabilized platform in order to be able to make any measurements at all. Further by reducing the disturbance levels on the platform, we can also reduce the apparent gravity gradient.

Apart from the fact that the gradiometer currently can not be operated as a 'strap-down' sensor, any platform motions also cause spurious gravity gradients to be measured due to the fact that rotational motion of the platform cause apparent gravity gradient. This apparent gravity gradient due to the platform can not be distinguished from the actual gravity gradient unless the platform motion is also measured. In order to reduce the apparent gravity gradient the platform drifts must be reduced to a value

less than $10 \mu\text{rad}$. For example sinusoidal motion of platform with an amplitude of 1×10^{-3} degrees (17×10^{-6} rad) at 6 Hz would cause an apparent gravity gradient as large as 600 E at certain disturbance phase which in most circumstances would be much higher than the gravity gradient signature to be measured. Typical gravity gradient signature such as from the Hansen Experimental Physics Laboratory gravity signature is only about 250 E.

The platform motion is actively controlled using a feedback as well as feedforward control. The feedback control helps in maintaining the angle of the platform to the specified nominal value. The feedforward control is used to remove the disturbances by directly measuring the disturbances at the source which is the truck floor. The feedback control works by moving the platform with a speed proportional to the error in the platform angle. Hence the feedback control merely reacts to the error in the platform angle due to the disturbances that propagate from the truck floor to the platform. However, feedforward control on the other hand allows for a proactive compensation of disturbance on the platform by measuring the angular velocity of the floor of the truck. By being able to measure the disturbances at the floor of the truck at the source it is possible to control the platform almost instantaneously compensate for the disturbances that propagate to the platform.

This combination of feedback control and feedforward control suppresses the noise on the platform to less than $10 \mu\text{rad}$ in an 84 ms interval (time duration between the Raman pulses) shown in Figure 8.3. The apparent gravity gradient due to phase noise due to this platform motion is about $12 \times 10^{-9} \text{s}^{-2}$ (12 E).

8.4 Data Acquisition and synchronization

Three computers were used to control and acquire data from Gradiometer, Platform and Truck. In order to synchronize the data from all these different sources, another computer was used which received pulses from all three computers. Since the clocks of the computers were either running faster or slower with respect to the synchronization computer, a stable frequency source slaved to an atomic clock (SRS FS725) was used to send pulses at 10 Hz to all the four computers. The time scales of all the

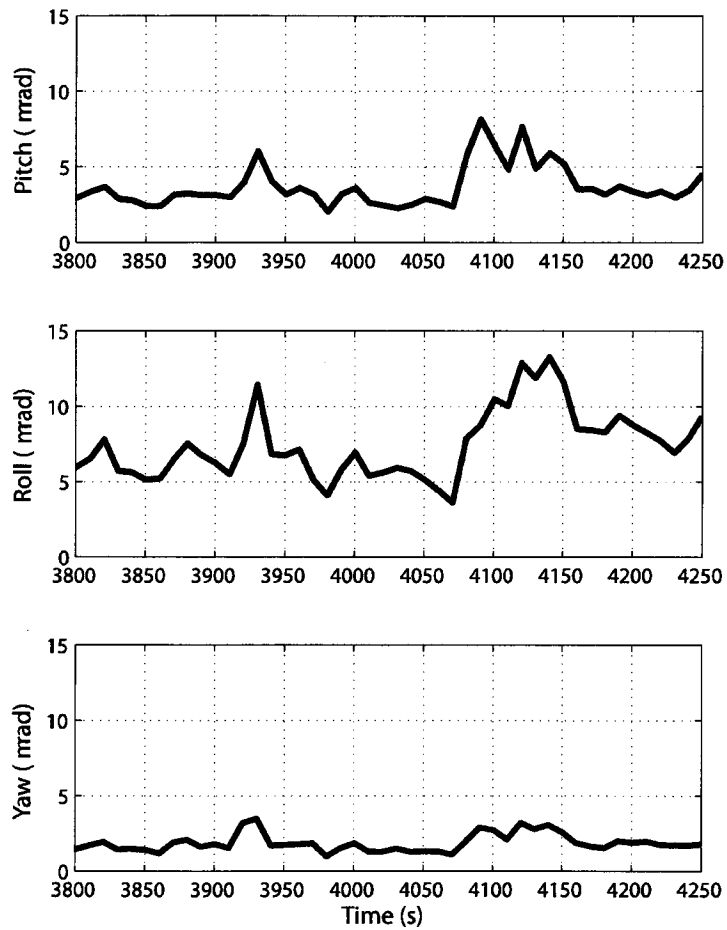


Figure 8.3: Drift of platform pitch, roll and yaw angles in 84 ms time interval during mobile gravity gradient survey

computers were either stretched or shrunk to match with the stable frequency source. A schematic of the synchronization setup is shown in Figure 8.4.

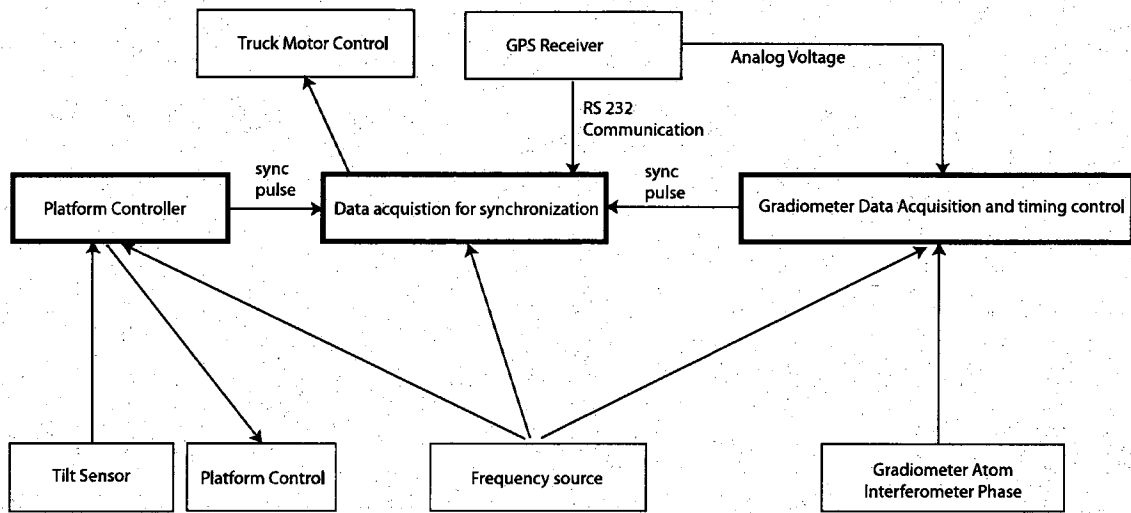


Figure 8.4: Data acquisition and synchronization of various data acquisition systems during the mobile measurement of gravity gradient. The truck control computer is used as the synchronization computer for the entire system.

Pulses were sent from the gradiometer control computer to the synchronization computer at the instance of atom drop and first Raman pulse ($\pi/2$). This information was used to determine the platform angles at the instances of the $\pi/2$ and π pulses. This is to enable the simulation of the apparent gravity gradient due to platform rotational motion. The platform angles were measured using the LN250 Fiber optic gyro and were acquired by the platform control computer.

All of the data synchronization from the various computers were carried out while post-processing and not in real-time. When there was a need for certain data to be exchanged between these systems in real time for monitoring purposes, they were transmitted to each other through analog voltage signals in real time. For example GPS signals that were acquired through the truck control computer transmitted the latitude and longitude of the truck position as an analog voltage to the gradiometer

control computer which also acquires the gradiometer phase. This latitude and longitude data was converted to a local tangent plane reference system which enabled plotting of the gradiometer phase with respect to truck position in real-time as shown in Figure 8.6.

8.5 Static Survey

In order to estimate gravity gradient accurately at the entrance of the building a static survey was conducted when the disturbance levels on the platform are minimal. It is very similar to measuring gravity gradient in a static laboratory environment. The truck remained stationary at each point for about three minutes. During this period, the platform was actively servoed to be horizontal. Since the disturbance levels are quite low when the truck is stationary, a pure feedback loop with low gain was enough to ensure a stable platform that allowed accurate gravity gradient measurements. The drift of the platform was typically less than $0.5 \mu\text{rad}$ during the static tests. The integrated sensitivity of the gradiometer was about 12E in 3 minutes. Figure 8.5 shows the gravity gradient measurements made using static tests.

Since there were drifts present in the gravity gradiometer, it was important to measure the gravity gradient with respect to a reference position and return to the reference position as often as possible in order to interpolate the drift. During the survey, the truck was positioned at a reference point 3.5 m inside the building with respect to the entrance (position referred to as -3.5 m). At the end of the survey the truck was returned to the same point. It was observed that most of the drift was linear, hence a linear fit between the reference measurements gave the baseline with respect to which the gravity gradient could be measured. This linear interpolation of the drift was effective and the gravity gradient measurements were repeatable in multiple surveys.

The GPS positioning system requires direct line of sight of the satellites to the receiver. The southern skies were blocked by the End Station 3 building. Hence most of the survey was done at night times since more GPS satellites are visible in the northern hemisphere at that time.

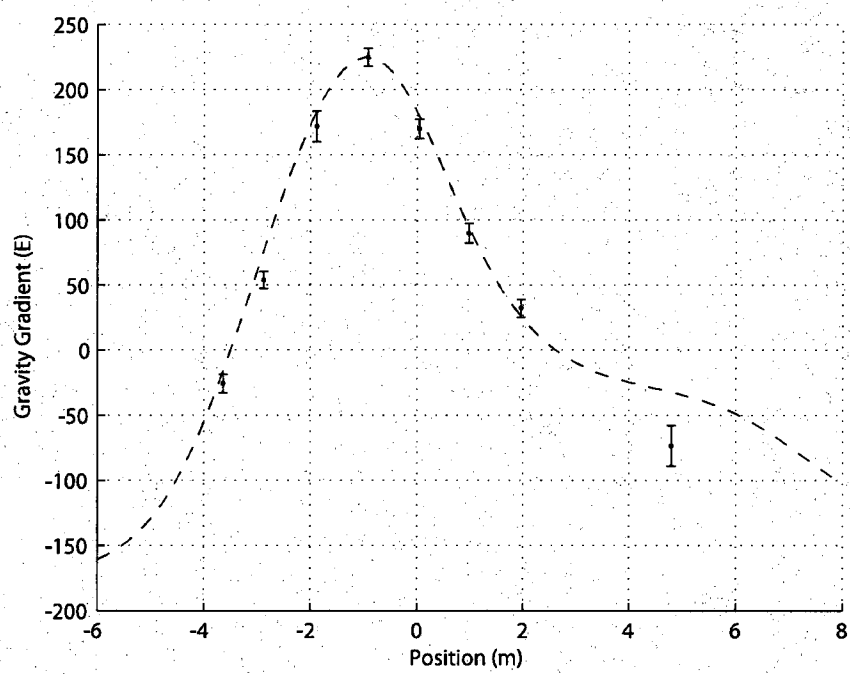


Figure 8.5: Gravity Gradient measured by static surveys (dotted lines show simulated gravity gradient expected at that location). Position 0 m refers to the location of the entrance door and positive position values are outside the building.

8.6 Mobile Survey

Mobile measurement of gravity gradient is more challenging compared to a static survey since the platform experiences large disturbances. Mobile survey for gravity gradient was carried out by moving the truck at a speed of about 1 cm/s. In order to overcome the problem of drift of the atom interferometer, the interferometer phase was measured at a specific location at two instances of time. Since the drift was linear within the short duration of time of survey, the drift was easily identified using the phase measured at the same location at two different time instances (very similar to the method adopted for static tests discussed in section 8.5). Before and after the mobile survey, the gradiometer phase was measured (for about three minutes) at the location -3.5 m. Using the phase at the same location at two different times, the linear drift was subtracted from the measured gradiometer phase.

During the mobile tests, the disturbance levels on the truck floor are higher compared to static tests. The platform stabilization control made use of feedback of the platform angles as well as feedforward of the truck floor angular velocities. The platform drifts were maintained to be less than $10 \mu\text{rad}$ during the mobile survey (as discussed in section 8.3).

The gravity gradient was measured while the truck was in motion and it was possible to identify the increase or decrease in gravity gradient while the truck moved. Figure 8.6 shows the gravity gradient that was observed in real-time and the phase difference measured by the atom-interferometer follows the expected trend.

8.6.1 Sign Ambiguity

The ellipse fitting method provides a means for overcoming the issue of common phase noise. A least square method [60, 62, 61] is used to extract the ellipse which is represented as a general conic (Eqn 8.1).

$$Ax^2 + Bxy + Cy^2 + Dx + Ey + F = 0 \quad (8.1)$$

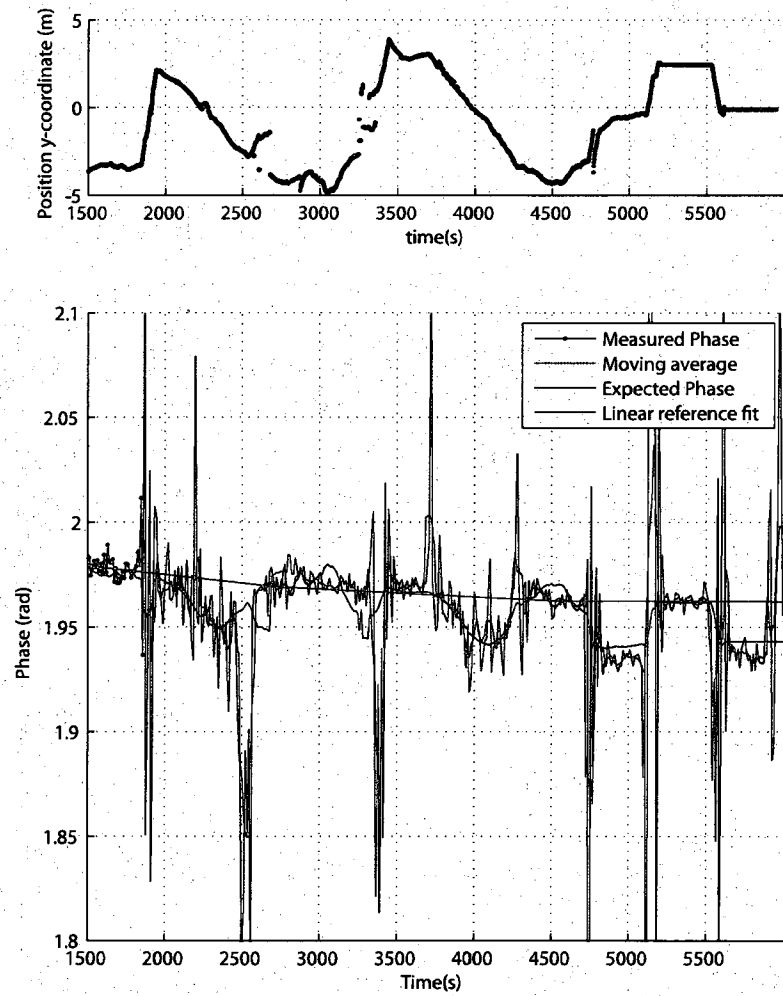


Figure 8.6: Mobile Measurement of interferometer phase which is proportional to gravity gradient is shown in blue. The expected atom interferometer phase is shown in red.

$$\Delta\phi = \cos^{-1} \left(\frac{-B}{2\sqrt{AC}} \right) \quad (8.2)$$

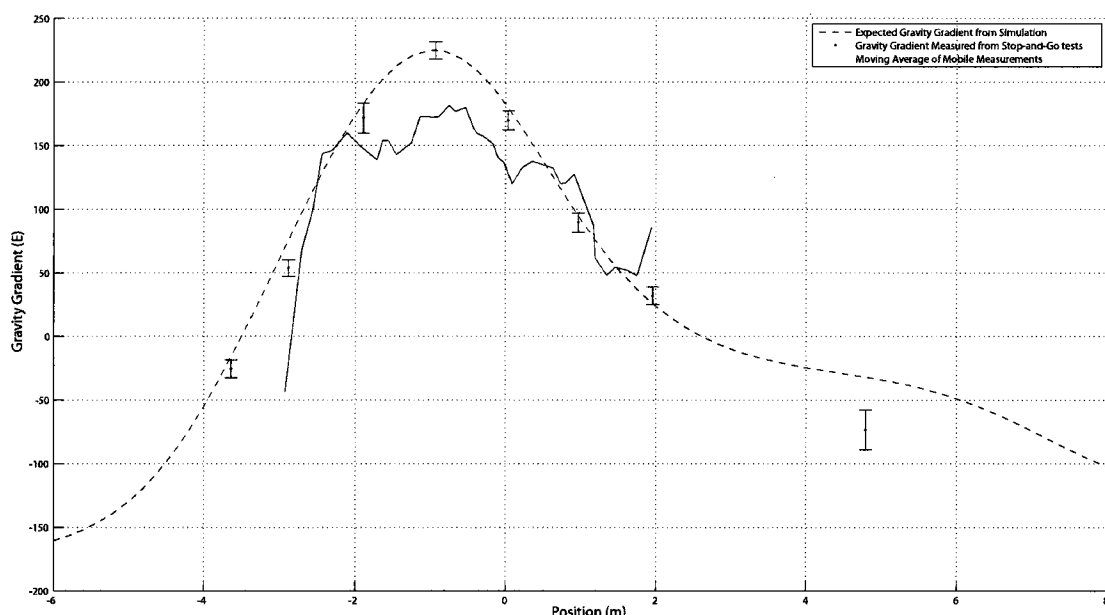


Figure 8.7: Gravity Gradient at the entrance of Hansen Experimental Physics Laboratory End Station 3 measured using mobile gradiometer. Moving average of mobile measurement (red line), static measurement (blue dots) and expected gravity gradients from simulation (dotted line) are shown.

However, the use of ellipse fitting method also introduces sign ambiguities since the extraction of phase involves \cos^{-1} function (for example, a differential phase of $\frac{\pi}{4}$ and $\frac{7\pi}{4}$) both produce the same ellipse shape as shown in Figure 8.8). If the absolute differential phase is between $(2n + 1)\pi$ to $(2n + 2)\pi$) then an increase in absolute differential phase will appear as a decrease in the phase extracted from the ellipse fitting method.

In order to determine if there is a positive or negative correlation between the absolute differential phase and the phase extracted from the ellipse, one can change T (time between the laser pulses) by a small amount and observe if the phase increases or decreases. In case of the mobile gravity gradient measurement, the phase extracted from the ellipse fitting method is decreases when the absolute phase difference increases. Hence we find that the gravity gradient anomaly produces a valley instead of a peak in the interferometer phase (as seen in figure 8.6).

8.6.2 Sources of Error

The gravity gradient measured using mobile gradiometer is shown in figure 8.7. Based on the model developed using the trajectory of the atoms and the angle of the platform (in Chapter 4), the apparent gravity gradient expected only due to platform motion is 12 E. However the noise is much higher in the mobile measurement since there is also a reduction in contrast due to the platform motion (as seen in Figure 6.14). This contrast reduction in turn produces ellipses with higher noise and during the ellipse fitting the best fit ellipse gets skewed and hence the differential phase extracted from this skewed ellipse deviates from the expected phase by as much as 10-15 mrad. Ellipse fitting can not be avoided in the present circumstance due to the presence of significant common phase noise. A model for the contrast loss due to platform motion needs to be developed and then the phase can be extracted after accounting for the phase noise due to the contrast noise.

However the errors in the measurement were small enough to be able to capture the most important aspect of the gravity gradient signature which is a peak of about 200 E in a distance of about 6 m in real time (see Figure 8.6).

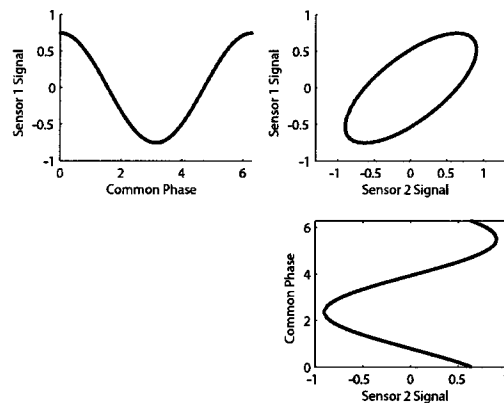
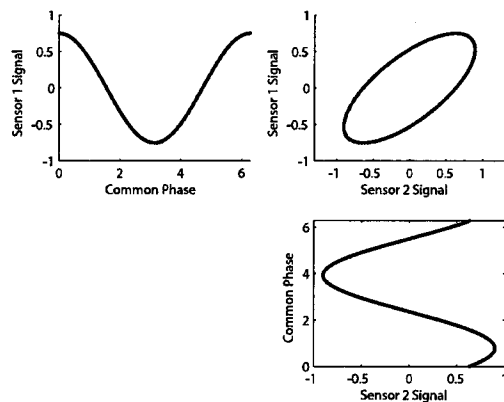
(a) Phase difference of $\pi/4$ (b) Phase difference of $7\pi/4$

Figure 8.8: Ellipse generated by plotting sinusoids with phase differences of (a) $\pi/4$ (b) $7\pi/4$.

Chapter 9

Conclusion

First ever mobile gravity gradient measurement has been made using an atom interferometric gravity gradiometer. The measured gravity gradient matched the expected gradient signature while monitoring in real time. However there were noise due to contrast reduction due to the platform motion. Contrast reduction can be modeled in the future by considering the fact that the finite size of atom clouds and the washing out of phase at large excursions of the Raman beam. This might allow us to decorrelate the phase noise due to the contrast noise from the existing data and improve the precision of the mobile measurement during post-processing.

In order to achieve this mobile gradient measurement, a number of subsystems were successfully developed. A platform for actuating the gradiometer pitch and yaw motion to experimentally measure the apparent gradient due to the platform rotational motion in order to verify the theoretical model. The same platform was also designed to actively compensate for the rotational disturbances from the truck during the mobile measurement. The truck motion was computer controlled with an electric drive that allowed low speeds and lower disturbances to capture the gravity gradient in real time while in motion.

The system could be further improved by employing an adaptive control of T (time duration between laser pulses) to suit the disturbances experienced by the truck. For example if the truck experiences a large disturbance around frequencies of $\frac{1}{2T}$ during the gradient survey then it would be possible to reduce the apparent gradient due to

platform motion by changing T so that the $\frac{1}{T}$ or an integer multiple of it matches with the frequency at which the maximum disturbance occurs.

Automation of the measurement process by controlling motion of the truck would allow multiple surveys to be conducted in a short time at the same location. This would allow for improving the accuracy by averaging multiple tests. In order to precisely locate the position and the orientation of the truck, it would be required to have two GPS antennas on the roof of the truck instead of a single receiver as in the current setup. A single GPS receiver does not allow for finding the orientation of the truck.

Airships which can fly at slow speeds and fly at low altitudes would be useful for mobile gravity gradiometry. Other than periods of turbulence, disturbances can be expected to occur at low frequencies which can be compensated using active isolation.

Appendix A

List of Symbols

Symbol	Description
α	Angular misalignment of Raman beam with the center of atom clouds
ϕ^{sensor}	Atom interferometer phase measured by sensor
$\Delta\phi$	Phase difference between two atom interferometers
k_{eff}	Effective propagation vector of the Raman beam
T	Time duration between Raman pulses
\mathbf{g}	Vector denoting acceleration due to gravity
$\hat{\mathbf{e}}_x$	Unit vector along x direction of reference system E
${}^N\omega^E$	Angular velocity of reference fram E in reference frame N
\mathbf{r}^{A_1/E_0}	Position vector of point A_1 with respect to point E_0
${}^E\mathbf{v}^{A_1}$	Velocity of point A_1 in reference frame E
$\frac{d}{dt}{}^E\mathbf{v}$	Time derivative in reference frame E of vector \mathbf{v}

Table A.1: List of symbols

Appendix B

Platform actuation parameters for pitch and roll

Rotation of stepper motor per step	1.8 degree
Number of ‘micro’ steps per step	250
Rotation of stepper motor shaft per ‘micro’ step	0.0072 degree
Number of threads per inch for lead screw	8
Linear travel of nut on lead screw per ‘micro’ step rotation of motor	$0.0635 \mu\text{m}$
Pitch rotation of the platform (with 36 inch lever arm) per ‘micro’ step rotation of motor	$3.98\mu\text{ degree (}69.4\text{ nrad)}$

Table B.1: Pitch actuation parameters

Appendix C

Expressions

C.1 Approximate Phase Calculation

$$\begin{aligned}
 \phi^{S_1} &= \sum_{i=1}^3 c_i \mathbf{k}_{eff}(t_1) \cdot \mathbf{r}^{A_1/E_0}(t_i) \\
 &= \sum_{i=1}^3 c_i k_{eff} (-\sin(\psi_i) \hat{\mathbf{e}}_x + \cos(\psi_i) \hat{\mathbf{e}}_y) \cdot (x_i \hat{\mathbf{e}}_x + y_i \hat{\mathbf{e}}_y + z_i \hat{\mathbf{e}}_z) \\
 &= \sum_{i=1}^3 c_i k_{eff} (-x_i \sin(\psi_i) + y_i \cos(\psi_i))
 \end{aligned} \tag{C.1}$$

where $c_i = 1, -2, 1$ and $t_i = t_0, t_0 + T$ and $t_0 + 2T$

Substituting $\sin(\psi_i) \approx \psi_i$, $\cos(\psi_i) \approx 1 - \frac{\psi_i^2}{2}$ and $\psi_i = \omega t_i$ we get: $\phi^{S_1} \approx \frac{1}{2}\omega^2 kLT^2$

Similarly, $\phi^{S_2} \approx -\frac{1}{2}\omega^2 kLT^2$.

Hence, $T_y y = \frac{\phi^{S_1} - \phi^{S_2}}{kLT^2} \approx \omega^2$

C.2 Gravity Gradient calculation

$$\begin{aligned}
 T_{yy} &= \frac{\partial g_y}{\partial y} \\
 &= \frac{\partial}{\partial y} \frac{Gm}{(x^2+y^2+z^2)} \frac{x \hat{\mathbf{e}}_x + y \hat{\mathbf{e}}_y + z \hat{\mathbf{e}}_z}{\sqrt{x^2+y^2+z^2}} \cdot (\hat{\mathbf{e}}_y) \\
 &= Gm \frac{(x^2-2y^2+z^2)}{(x^2+y^2+z^2)^{5/2}}
 \end{aligned} \tag{C.2}$$

Appendix D

Disturbance Levels on Truck Floor

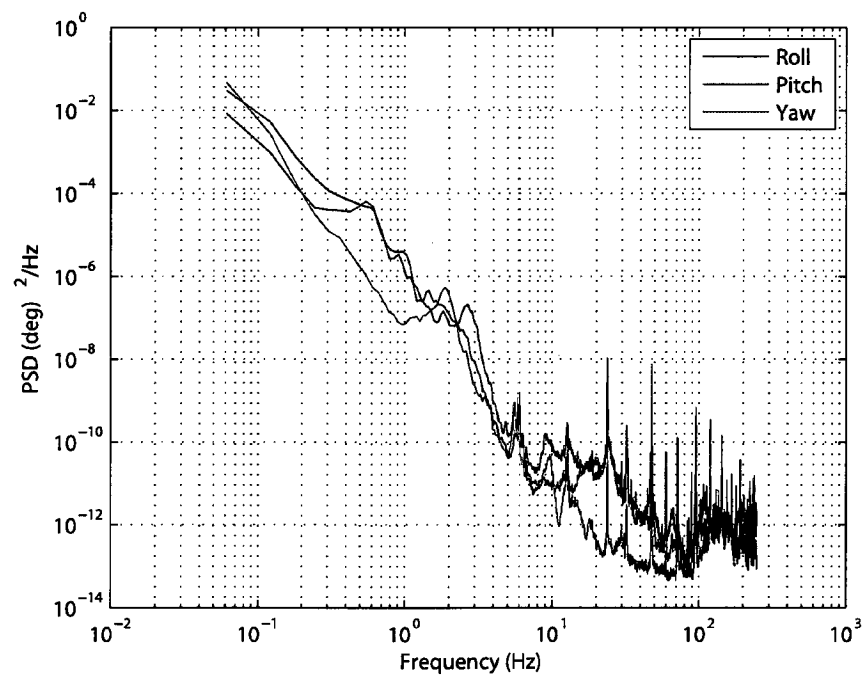


Figure D.1: Truck speed 0.4mph electric drive: Pitch, Roll and Yaw disturbance

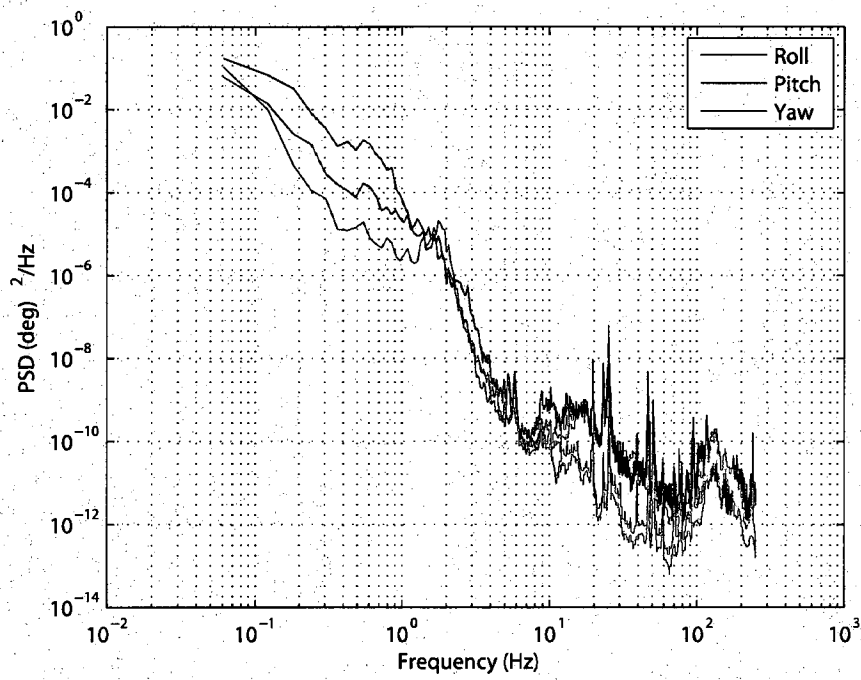


Figure D.2: Truck speed 1.5mph Engine Drive: Pitch, Roll and Yaw disturbance

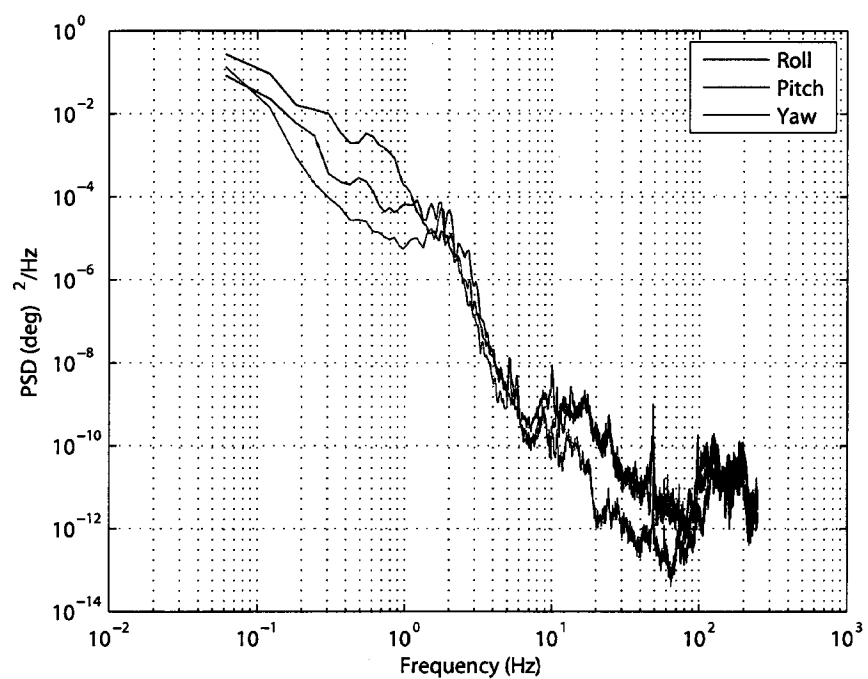


Figure D.3: Truck speed 1.5mph Electric Drive: Pitch, Roll and Yaw disturbance

Appendix E

Control system

Figures E.1 and E.2 show the control system implemented in xPCTargetTM for the overall control of the platform as well as synchronization with the atomic clock and other computers.

Figures E.3 and E.4 show control program for controlling the motion of the truck. Figure E.5 shows the stateflow diagram implemented in xPCTargetTM for timing the truck motion.

APPENDIX E. CONTROL SYSTEM

108

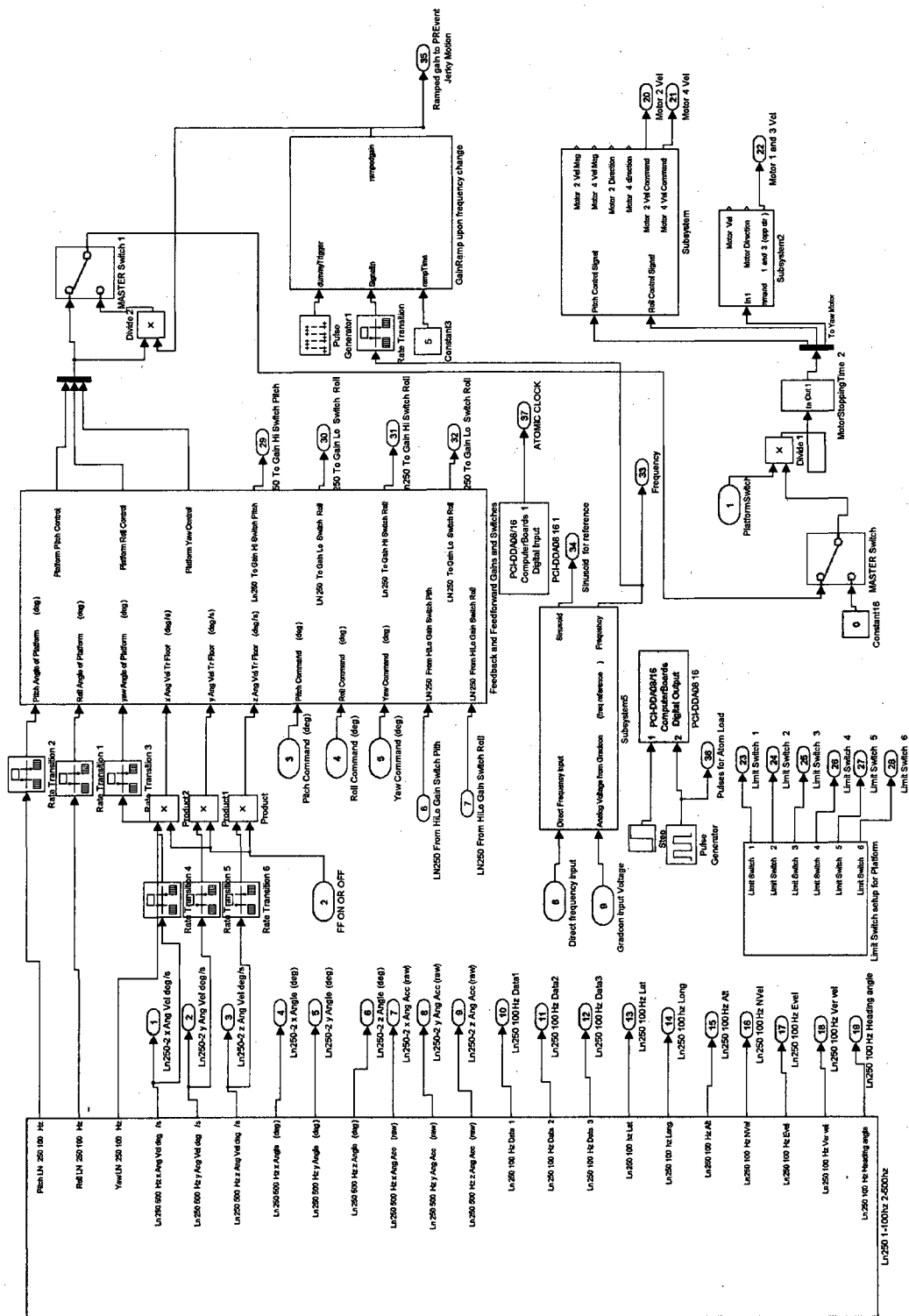


Figure E.1: Control system program implemented in xPCTargetTM for platform control

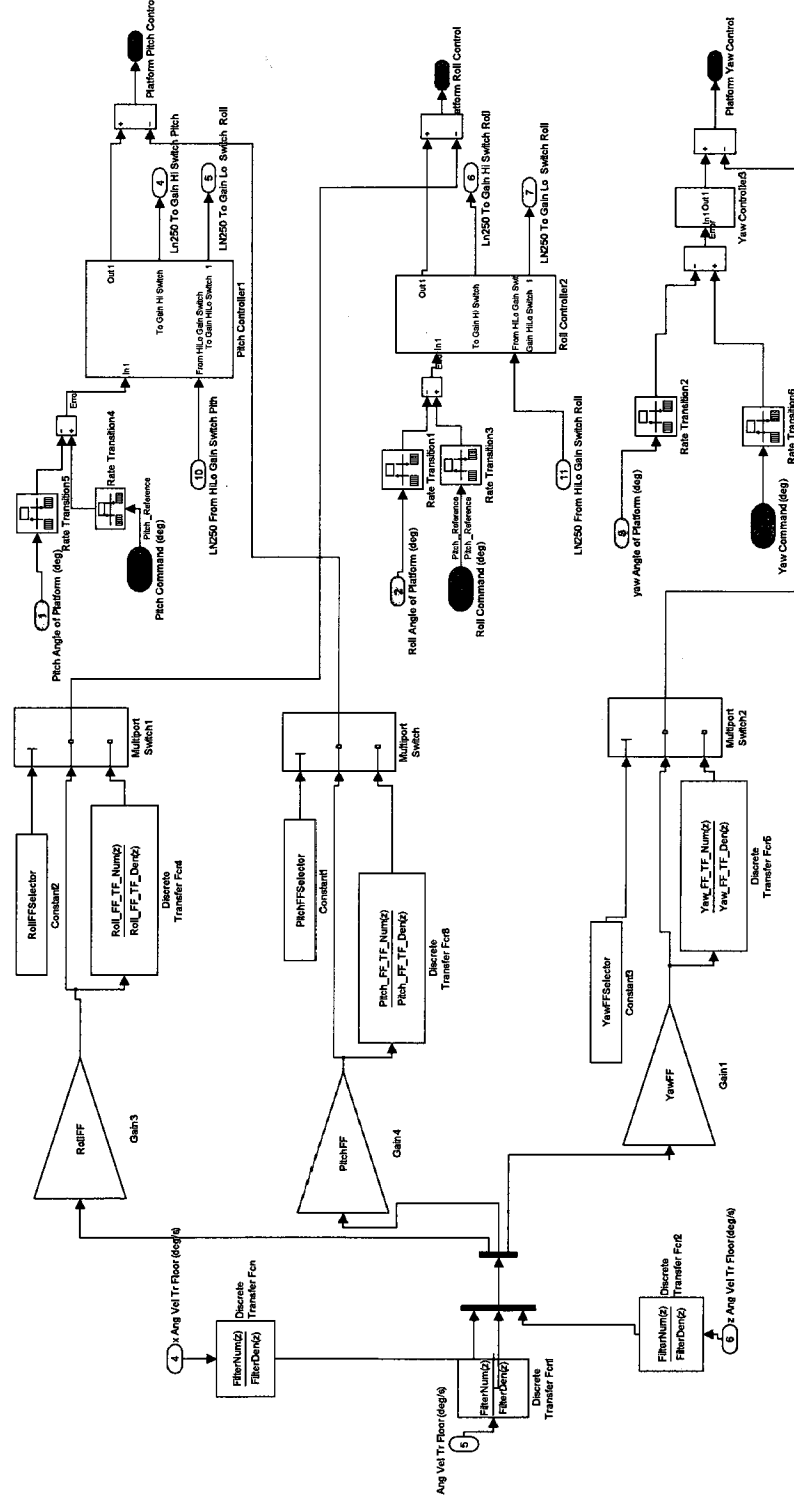


Figure E.2: Control subsystem implemented in xPCTarget™ for platform control

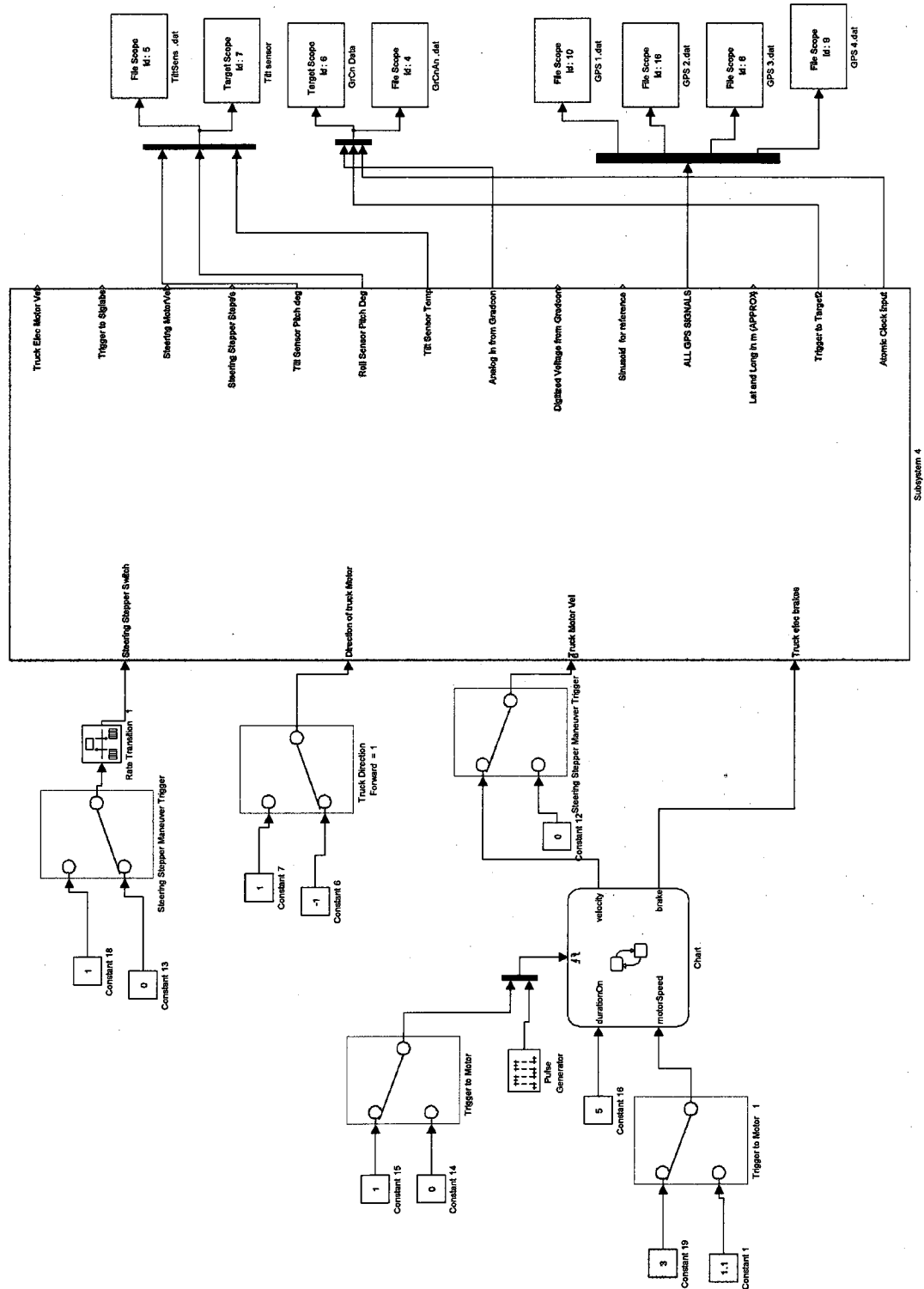


Figure E.3: Control system program implemented in xPC Target™ for truck control

APPENDIX E. CONTROL SYSTEM

111

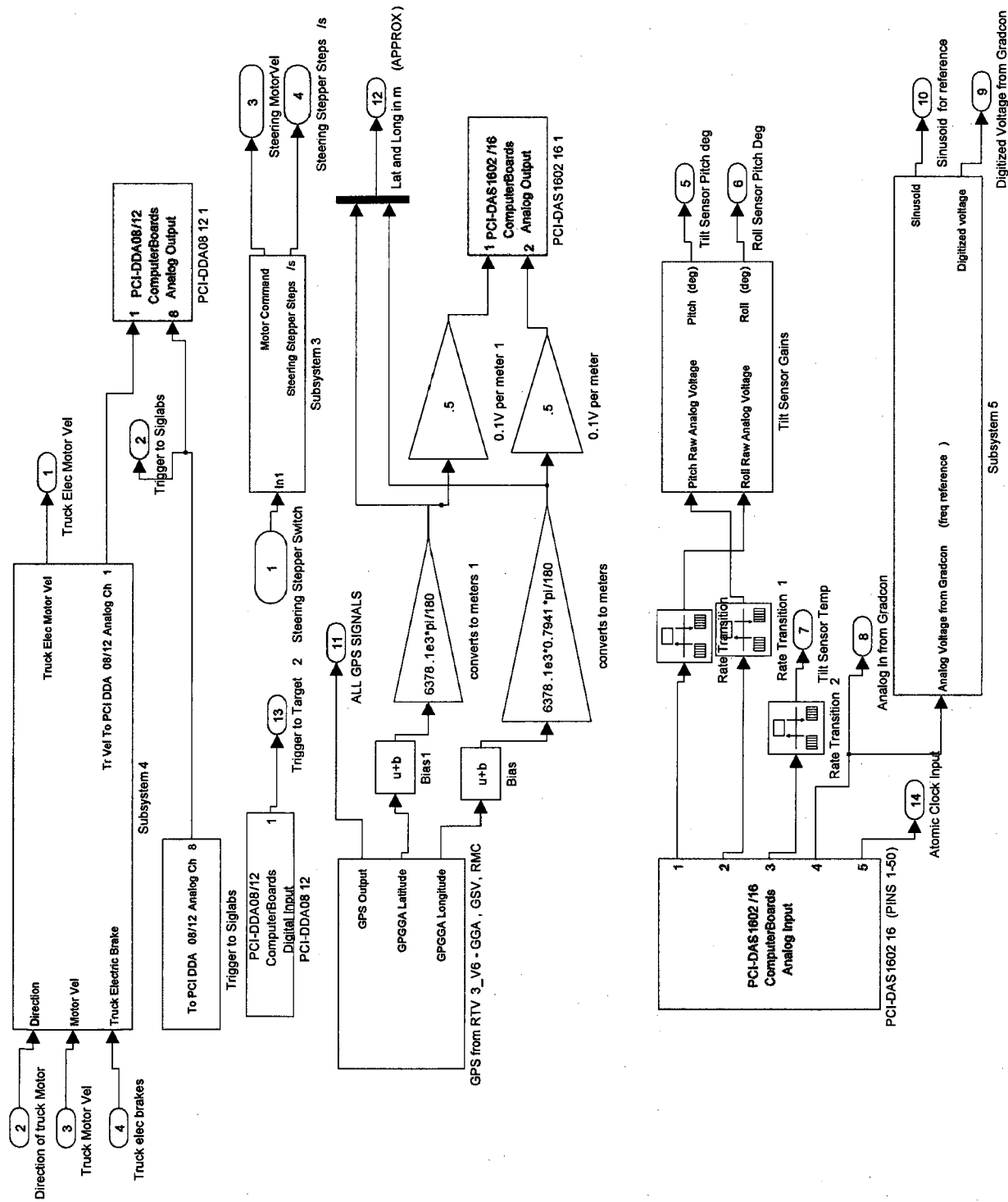


Figure E.4: Control subsystems implemented in xPCTargetTM for truck control

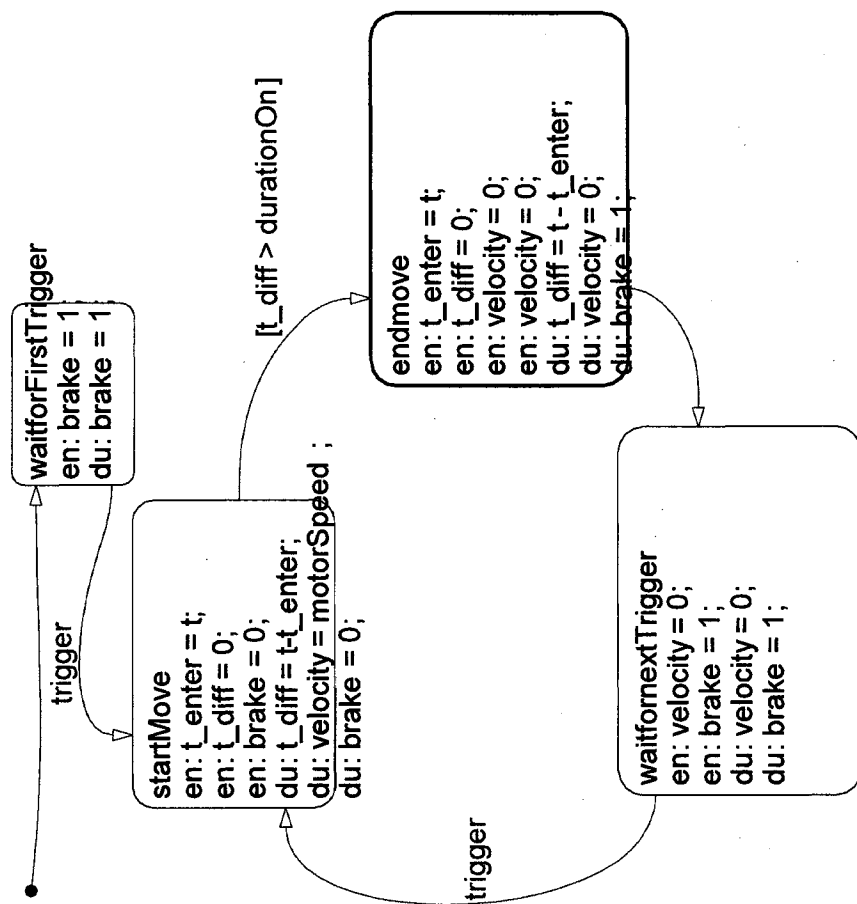


Figure E.5: Timing truck motion implemented in xPCTargetTM using a stateflow chart

Bibliography

- [1] M. A. Gerber. Gravity gradiometry - Something new in inertial navigation. *Astronautics Aeronautics*, 16:18–26, May 1978.
- [2] A.B. Chatfield. *Fundamentals of High Accuracy Inertial Navigation*. AIAA, 1997.
- [3] C. Jekeli. *Inertial navigation systems with geodetic applications*. Walter de Gruyter, 2001.
- [4] A. H. Zorn. A merging of system technologies: All-accelerometer inertial navigation and gravity gradiometry. *IEEE Position Location and Navigation Symposium (PLANS)*, 2002.
- [5] S. Vajda and A. Zorn. Survey of existing and emerging technologies for strategic submarine navigation. *Position Location and Navigation Symposium, IEEE 1998*, pages 309–315, Apr 1998.
- [6] D.B. DeBra, J.C. Harrison, and P.M. Muller. A Proposed lunar orbiting gravity gradiometer experiment. *Earth, Moon, and Planets*, 4(1):103–112, 1972.
- [7] WL Sjogren, JD Anderson, RJ Phillips, and DW Trask. Gravity fields. *IEEE Transactions on Geoscience Electronics*, 14(3):172–183, 1976.
- [8] R.L. Forward. Future lunar gravity measurements. *Earth, Moon, and Planets*, 22(4):419–433, 1980.
- [9] R. Rummel and O.L. Colombo. Gravity field determination from satellite gradiometry. *Journal of Geodesy*, 59(3):233–246, 1985.

- [10] *ESA's Gravity Mission GOCE*. <http://www.esa.int/esaLP/LPgoce.html>, 2009.
- [11] J. Wahr, S. Swenson, V. Zlotnicki, and I. Velicogna. Time-variable gravity from GRACE: First results. *Geophys. Res. Lett.*, 31(11):L11501, 2004.
- [12] R. E. Bell and R. O. Hansen. The rise and fall of early oil field technology: The torsion balance gradiometer. *The Leading Edge*, 17:81, 1998.
- [13] Edwin H. van Leeuwen. BHP develops airborne gravity gradiometer for mineral exploration. *The Leading Edge*, 19(12):1296–1297, 2000.
- [14] D. Hinks, S. McIntosh, and R. Lane. A comparison of the Falcon® and Air-FTG airborne gravity gradiometer systems at the Kokong Test Block, Botswana. *Airborne Gravity*, pages 125–134, 2004.
- [15] G. Liu, P. Diorio, P. Stone, G. Lockhart, A. Christensen, N. Fitton, and M. Dransfield. Detecting kimberlite pipes at Ekati with airborne gravity gradiometry. *Extended Abstracts, ASEG*, 15, 2001.
- [16] P. Diorio. EXAMPLES OF THE APPLICATION OF AIRBORNE GRAVITY GRADIOMETRY TO NATURAL RESOURCE EXPLORATION. In *Geophysical Research Abstracts*, volume 5, page 03996, 2003.
- [17] A. J. Romaides, J. C. Battis, R. W. Sands, A. Zorn, D. O. Benson, and D. J. DiFrancesco. A comparison of gravimetric techniques for measuring subsurface void signals. *Journal of Physics D-Applied Physics*, 34(3):433–443, 2001.
- [18] John Parmentola. The gravity gradiometer as a verification tool, 1990.
- [19] R. V. Eötvös. *Mathematische und naturwissenschaftliche berichte und ungarn*, 8:65, 1891.
- [20] R. v. Eötvös, D. Pekár, and E. Fekete. *Annalen der Physik (Leipzig)*, 68:11–66, 1922.
- [21] E Fischbach, E Sudarsky, A Szafer, C Talmadge, and S H Aronson. Reanalysis of the Eötvös experiment. *Phys. Rev. Lett.*, 56(1):3–6, Jan 1986.

- [22] L. Bod, K.F.K. Intézet, and M.T. Akadémia. *One Hundred Years of the Eötvös Experiment*. Central Research Institute for Physics, 1990.
- [23] John Hopkins. Gravity Gradiometry-A Rebirth? *Canadian Journal of Exploration Geophysics*, 11(1):34, 1975.
- [24] E Lancaster-Jones. The principles and practice of the gravity gradiometer. *Journal of Scientific Instruments*, 9(11):341–353, 1932.
- [25] M. N. Nabighian, M. E. Ander, V. J. S. Grauch, R. O. Hansen, T. R. LaFehr, Y. Li, W. C. Pearson, J. W. Peirce, J. D. Phillips, and M. E. Ruder. Historical development of the gravity method in exploration. *Geophysics*, 70(6):63ND–89ND, 2005.
- [26] C. Jekeli. The gravity gradiometer survey system (ggss). *Eos, Transactions American Geophysical Union*, 69(8):105–105, 1988.
- [27] C. Jekeli. A review of gravity gradiometer survey system data analyses. *Geophysics*, 58:508–514, 1993.
- [28] C. Jekeli. Statistical analysis of moving-base gravimetry and gravity gradiometry. *Reports of the Department of Civil and Env. Eng. and Geodetic Science, Report*, 466, 2003.
- [29] J.B. Lee. FALCON gravity gradiometer technology. *Exploration Geophysics*, 32:247–250, 2001.
- [30] H.J. Paik. Superconducting tensor gravity gradiometer. *Journal of Geodesy*, 55(4):370–381, 1981.
- [31] HA Chan, MV Moody, and HJ Paik. Superconducting gravity gradiometer for sensitive gravity measurements. II. Experiment. *Physical Review D*, 35(12):3572–3597, 1987.
- [32] M.V. Moody, H.J. Paik, and E.R. Canavan. Three-axis superconducting gravity gradiometer for sensitive gravity experiments. *Review of Scientific Instruments*, 73:3957, 2002.

- [33] M.J. Adriaans. Superconducting Gravity Gradiometers for Underground Target Recognition Final Report. 1998.
- [34] I. Marson and JE Faller. g-the acceleration of gravity: its measurement and its importance. *Journal of Physics E: Scientific Instruments*, 19:22–32, 1986.
- [35] T. M. Niebauer, G. S. Sasagawa, J. E. Faller, R. Hilt, and F. Klopping. A new generation of absolute gravimeters. *Metrologia*, 32(3):159–180, 1995.
- [36] R. Colella, AW Overhauser, and SA Werner. Observation of Gravitationally Induced Quantum Interference. *Physical Review Letters*, 34(23):1472–1474, 1975.
- [37] Ulrich Bonse and Thomas Wroblewski. Measurement of neutron quantum interference in noninertial frames. *Phys. Rev. Lett.*, 51(16):1401–1404, Oct 1983.
- [38] T.W. Hansch and A.L. Schawlow. Cooling of gases by laser radiation. *Optics Communications*, 13(1):68–69, 1975.
- [39] D. J. Wineland and Wayne M. Itano. Laser cooling of atoms. *Physical Review A*, 20(4):1521–1540, Oct 1979.
- [40] S. Chu, L. Hollberg, J. E. Bjorkholm, A. Cable, and A. Ashkin. 3-dimensional viscous confinement and cooling of atoms by resonance radiation pressure. *Physical Review Letters*, 55(1):48–51, 1985. 24.
- [41] E. L. Raab, M. Prentiss, A. Cable, S. Chu, and D. E. Pritchard. Trapping of neutral sodium atoms with radiation pressure. *Physical Review Letters*, 59(23):2631–2634, 1987. 7.
- [42] Mark Kasevich and Steven Chu. Atomic interferometry using stimulated raman transitions. *Physical Review Letters*, 67(2):181–184, Jul 1991.
- [43] F. Riehle, Th. Kisters, A. Witte, J. Helmcke, and Ch. J. Bordé. Optical ramsey spectroscopy in a rotating frame: Sagnac effect in a matter-wave interferometer. *Physical Review Letters*, 67(2):177–180, Jul 1991.
- [44] M. A. Kasevich. *Atom Interferometry in an Atomic Fountain*. PhD thesis.

- [45] M. Kasevich and S. Chu. Measurement of the gravitational acceleration of an atom with a light-pulse atom interferometer. *Applied Physics B: Lasers and Optics*, 54(5):321–332, 05/01 1992. M3: 10.1007/BF00325375.
- [46] A. Peters, K. Y. Chung, and S. Chu. Measurement of gravitational acceleration by dropping atoms. *Nature*, 400(6747):849–852, 1999. 17.
- [47] A. Peters, K Y Chung, and S Chu. High-precision gravity measurements using atom interferometry. *Metrologia*, 38(1):25–61, 2001.
- [48] M. J. Snadden, J. M. McGuirk, P. Bouyer, K. G. Haritos, and M. A. Kasevich. Measurement of the earth’s gravity gradient with an atom interferometer-based gravity gradiometer. *Physical Review Letters*, 81(5):971–974, Aug 1998.
- [49] T. L. Gustavson, P. Bouyer, and M. A. Kasevich. Precision rotation measurements with an atom interferometer gyroscope. *Physical Review Letters*, 78(11):2046–2049, Mar 1997.
- [50] T L Gustavson, A Landragin, and M A Kasevich. Rotation sensing with a dual atom-interferometer sagnac gyroscope. *Classical and Quantum Gravity*, 17(12):2385–2398, 2000.
- [51] D. S. Durfee, Y. K. Shaham, and M. A. Kasevich. Long-term stability of an area-reversible atom-interferometer sagnac gyroscope. *Physical Review Letters*, 97(24):240801, 2006.
- [52] K. Takase. *Precision Rotation Rate Measurements with a Mobile Atom Interferometer*. PhD thesis, Stanford University, 2008.
- [53] J. B. Fixler. *Atom Interferometer-Based Gravity Gradiometer Measurements*. PhD thesis, Yale University, 2003.
- [54] J. B. Fixler, G. T. Foster, J. M. McGuirk, and M. A. Kasevich. Atom interferometer measurement of the newtonian constant of gravity. *Science*, 315(5808):74–77, 2007.

- [55] A. Bertoldi, G. Lamporesi, L. Cacciapuoti, M. de Angelis, M. Fattori, T. Petelski, A. Peters, M. Prevedelli, J. Stuhler, and G. M. Tino. Atom interferometry gravity-gradiometer for the determination of the newtonian gravitational constant g. *European Physical Journal D*, 40(2):271–279, 2006.
- [56] G. W. Biedermann. *Gravity Tests, Differential Accelerometry and Interleaved Clocks with Cold Atom Interferometers*. PhD thesis, Stanford University, 2007.
- [57] K. Bongs, R. Launay, and M. A. Kasevich. High-order inertial phase shifts for time-domain atom interferometers. *Applied Physics B: Lasers and Optics*, 84(4):599–602, 09/01 2006. M3: 10.1007/s00340-006-2397-5.
- [58] X. Wu. *Gravity Gradient Survey with a Mobile Atom Interferometer*. PhD thesis, Stanford University, 2009.
- [59] MinusK Technology Inc. <http://www.minusk.com/content/technology/how-it-works.html>, 2009.
- [60] M. Pilu, AW Fitzgibbon, and RB Fisher. Ellipse-specific direct least-square fitting. In *Image Processing, 1996. Proceedings., International Conference on*, volume 3, 1996.
- [61] A. Fitzgibbon, M. Pilu, and RB Fisher. Direct least square fitting of ellipses. *IEEE Transactions on Pattern Analysis and Machine Intelligence*, 21(5):476–480, 1999.
- [62] Andrew W. J. Fitzgibbon. *Stable Segmentation of 2D Curves*. PhD thesis, University of Edinburgh.